3-2001

The Development of a Finite Element Program to Model High Cycle Fatigue in Isotropic Plates

William C. Shipman

THE DEVELOPMENT OF A FINITE ELEMENT PROGRAM TO MODEL HIGH CYCLE FATIGUE IN ISOTROPIC PLATES

THESIS

William C. Shipman, 1st Lieutenant, USAF

AFIT/GAE/ENY/01M-08

DEPARTMENT OF THE AIR FORCE
AIR UNIVERSITY

AIR FORCE INSTITUTE OF TECHNOLOGY

Wright-Patterson Air Force Base, Ohio

AFIT/GAE/ENY/01M-08

THE DEVELOPMENT OF A FINITE ELEMENT PROGRAM TO MODEL HIGH CYCLE FATIGUE IN ISOTROPIC PLATES

THESIS

Presented to the Faculty

Department of Aeronautical Engineering

Graduate School of Engineering and Management

Air Force Institute of Technology

Air University

Air Education and Training Command

In Partial Fulfillment of the Requirements for the

Degree of Master of Science in Aeronautical Engineering

William C. Shipman, B.S.

1st Lieutenant, USAF

March 2001

AFIT/GAE/ENY/01M-08

THE DEVELOPMENT OF A FINITE ELEMENT PROGRAM TO MODEL HIGH CYCLE FATIGUE IN ISOTROPIC PLATES

William C. Shipman, B.S.
1st Lieutenant, USAF

Approved:

Anthony N. Palazotto (Chairman)	3-13-01 date
Robert A. Canfield (Member)	3-13-01 date
Paul I. King (Member)	3-13-01 date

Acknowledgments

I would like to express my sincere appreciation to my faculty advisor, Dr. Palazotto for his guidance, support, direction, optimism, and patience. Thank you for always showing me things weren't as bad as they seemed and thanks for the insight you always had. I would also like to thank the joint DAGSI/AFRL team under Dr. Herman Shen for their guidance, support, and expertise.

My committee members, Dr King and Lt. Col. Canfield helped me enormously by giving extra direction. Thanks to both of you for working with me and helping me out so much. Thank you for understanding how hectic things were getting and working with me so that this research could get done.

I would also like to thank Sam and Victor for taking time out of their schedules to offer their expertise on the intricacies of DSHELL. Without y'all, I would still be trying to figure out what inputs were needed to run the program. I hope that the work I did on DSHELL will help you in the future.

Special thanks go to my parents and my in-laws for their love and support and for helping to keep motivated. Thanks for helping me see the light at the end of the tunnel and for assuring me that it wasn't the train.

I owe my wife more thanks than I have room on this page to express. You have kept me sane for this last year. When I thought the sky was falling, you would make me laugh and realize things weren't that bad. When I felt overwhelmed, you gave me the confidence to keep fighting. Your love and unwavering support made this all possible.

Finally, all credit goes to God, for He alone is worthy. Through the Lord, all things are possible.

William C. Shipman

Table of Contents

Page

List of Figures

Figure Page

List of Tables

AFIT/GAE/ENY/01M-08

Abstract

As part of a joint AFRL/DAGSI turbine blade research effort, a computer program has been developed that uses a von Karman large-deflection two-dimensional finite element approximation to determine stress levels and patterns in isotropic thin plates. The dynamic loading of various plates has been carried out in order to model a high cycle fatigue situation. The research considered the various effects of mode shapes, resident frequency, non-linear cyclic effect, endurance limits, and stress variations within a high cycle fatigue environment.

Two main initiatives were taken. First, a transient analysis tool was developed that calculates stress and displacement patterns over a period of time. This analysis also included the effects of damping. The second initiative developed a tool to calculate the eigenvalues (natural frequencies) and eigenvectors of a plate with a given geometry. The results indicated that it is possible to model fatigue at high frequencies using FE analysis and compare these findings with experimentation incorporating a shaker table.

In this research, different geometries of plates were investigated to represent turbine blade configurations. One square plate and three trapezoidal plates were investigated. It was found that a linear relationship could be found between the loading amplitude and the resulting maximum stress. This relationship allows for the prediction of the needed loading amplitude to cause high cycle fatigue. It was also determined that by altering the geometry of the plate, the needed loading frequency or loading amplitude to reach a stress level that would initiate cracks could be minimized.

THE DEVELOPMENT OF A FINITE ELEMENT PROGRAM TO MODEL HIGH CYCLE FATIGUE IN ISOTROPIC PLATES

I. Introduction

1.1 Motivation

In the past, the most common problems faced by gas-turbine engine designers involved low cycle fatigue (LCF) issues. However, with improvements in materials, inspections, and maintenance policies, LCF failures have been reduced (1). Now with the number of LCF failures decreased, the next leading cause of failures, high cycle fatigue (HFC), becomes the number one issue. With the numerous failures occurring, it was concluded that a new fatigue test method must be developed to accurately predict HCF. The use of an actual turbine blade in a test could be difficult due to the high frequencies needed to excite the correct modes. An alternative must be found that is easier to analyze but has the same high-cycle fatigue effect. One suggested test method involves exciting a plate specimen with very high cyclic base motion causing a resonant frequency response resulting in multiaxial stress states at desired locations. The first step in developing this test method is to design a topological optimization procedure to optimize the shape of the plate specimens to ensure the required stress states and patterns. This optimization procedure will be based on a dynamic von Karman nonlinear finite element code developed within this thesis that will calculate the stress and displacements of a plate with a given geometry.

1.2 High Cycle Fatigue

In this section, a general introduction to high cycle fatigue is presented. First, a description of fatigue and crack growth is presented. Some possible causes of high cycle fatigue, especially in turbomachinery, are discussed. Finally, a discussion on preventing high cycle fatigue both in design and inspection is indicated.

1.2.1 Fatigue and Crack Growth. Fatigue occurs when a load, usually less then the failure threshold, is applied in a cyclic manner over a period of time. Failure begins with micromechanical damage that eventually spreads to a small crack. At first, this crack is so minute that it is impossible to detect with the naked eye. Stress concentrations are formed in the vicinity of the crack. As the cyclic loading continues, the crack grows. After numerous cycles, the crack becomes large enough that it becomes visible to the naked eye and will eventually cause the failure of the entire structure (2). Cracks can also initiate from intrinsic defects or foreign object damage (3). Cracks propagating in this manner usually initiate earlier in the life cycle of the part and can grow to failure faster. This is a concern since it could possibly limit the life of the parts.

Fatigue failure in turbomachinery is especially important in turbine blades. The failure usually is a result of a forced response at high frequency. This forced response is generally produced by non-uniform flow causing an unsteady aerodynamic loading that can be at a frequency at or near the natural frequencies of the turbine blades. This loading must be treated as an unknown variable in the design of turbine blades since the vibration due to geometry, aerodynamics, and materials cannot be predicted with certainty (4).

High cycle fatigue is the fatigue of a part or structure occurring at these very high frequencies. For example, in a turbine assembly, flow passes by stationery stators and then by a rotating turbine blade. A single turbine blade is loaded and unloaded with an aerodynamic force each time it passes through the shock waves coming off of the trailing edge of a stator upstream. Thus it has been loaded 1 cycle passing one stator. If the turbine has 40 stators, the single blade would be loaded 40 cycles per revolution. If the turbine spool is being rotated at 15,000 rpm, then every minute the blade is being rotated through 600,000 cycles. A short sortie for the engine could be two hours. Thus, the blade would have been loaded 72,000,000 cycles. If the frequency of the loading is coincidental with the natural frequencies of the blade and the amplitude of loading was large enough, this one sortie could have already initiated a crack and caused it to propagate to failure. Of course, this loading is not enough to cause failure by itself, but as indicated above, there are numerous factors acting together to cause the actual failure. This example is indicated to show how cyclic loading can cause failure relatively quickly. An in depth discussion of the mechanics of high cycle fatigue can be found in (5).

1.2.2 Causes of High Cycle Fatigue. Though extensive research has been done to investigate the causes of high cycle fatigue, the root causes are yet unknown (4). As described by (6), there are numerous sources of HCF damage in turbomachinery that can be classified in four main areas. First, aerodynamic behavior caused by flow perturbations, as illustrated previously. Next, mechanical vibrations brought about by unbalanced rotors can cause HCF damage. Airfoil flutter, especially in blades, is the third category. Finally, acoustic fatigue can cause some HCF damage, though it normally only affects sheet metal components in the combustor, nozzle and augmentor. There are numerous other factors that effect HCF and its failure rate. These include foreign object damage (FOD), load intensity, frequency, combinations of low cycle fatigue (LCF) and HCF, fretting, and flutter (1, 5, 7, 8, 9).

1.2.3 Preventative Measures. HCF design involves either creating a condition in which the small cracks do not initiate, or a condition in which they do not grow. At present, due to inadequate understanding of the propagation of cracks under HCF conditions, current design tools deal mainly with crack initiation (10). Since it is difficult to detect the formation of the initial cracks, a very conservative route is taken that ensures the allowable stresses of a component are well below the average actual material fatigue resistance levels. This attempts to prevent crack initiation by not allowing stresses high enough to cause the cracks, but is very costly to the industry since the material is over-designed for its application (10). The Goodman diagram is the main tool used to predict the conditions that will cause crack initiation. Numerous studies have been done on the use of the Goodman diagram and have all concluded the same thing: the diagram is a good start but must be modified to accurately represent the effects of HCF (3, 4, 6, 7, 10). As illustrated by (6), there are complicating factors that modify the Goodman diagram. These include foreign object damage (FOD), fretting, and HCF/LCF interaction. HCF is extremely surface dependent, and thus is greatly affected by surface finish, coatings, shot peening, and other surface treatments. The Goodman diagram can be modified to capture these factors also as shown by Reference (7). The Goodman diagram is modified further to include manufacturing variability in geometry (4). This variation in geometry was modeled with a damping loss factor.

To ensure a condition in which cracks do not propagate, a true understanding of crack growth must be realized. Since most turbine blades are made of a titanium alloy, to predict the growth rate of cracks in turbine blades, a generalized theory of crack growth in titanium must be constructed. However, as shown by Ravichandran (11), a projection of crack growth for titanium alloys cannot be generalized. Therefore, until there is a better understanding of the influence of the microstructure of the material on the propagation of cracks (5), the design against HCF can not be focused on the propagation of existing small cracks but must focus on the prevention of these cracks.

1.3 Plate Theory.

Classical plate theory was developed to model that behavior of flat plates undergoing small displacements in an ideal elastic manner (12). However, as thickness or displacement increases, the accuracy of the theory decreases and new methods were necessary to model the plate's behavior accurately (13). According to reference (14), Cauchy and Poisson were the first to use a series expansion to solve for the general thin plate equations. Kirchhoff simplified the problem by assuming the planes normal to the mid-surface remain normal after deformation (15). The Kirchhoff theory neglects the transverse shear strains and therefore does not accurately predict deflections. Higher-order theories were developed that attempted to capture this transverse shear strain. The best-known early models were developed by E. Reissner, H. Hencky, and A. Kromm (16). The Reissner theory was shown to be accurate except for in-plane stresses (16). The Hencky theory was also shown to result in less accurate stresses without further simplifying the Reissner theory. The Kromm theory is shown to be more accurate, but fails when a harmonic load is applied (16). Other theories including Mindlin (15) and

Zienkiewicz's integration technique (17) were developed but had their limitations. Ashwell (18) continued work done by Mansfield (19) that investigated a higher-order theory based on the plate deforming to a developable surface while Kui (20) investigated a theory to account for shear locking. Srinivas (21) developed an exact solution for a simply supported homogeneous plate with unrestricted thickness. Lo (22) presented a higher-order theory and compared it to the earlier work as well as to the exact and classical plate theory. This higher-order theory also accounted for the nonlinear distribution of the in-plane displacements. Other examples of nonlinear theory can be found in (23- 28).

A higher-order nonlinear theory was developed by Palazotto and Dennis (29, 30). This theory is known as the Simplified Large Displacement, Moderately Large Rotation (SLR) theory. It has been proven for numerous loading and boundary conditions. The SLR theory is used in this research and will be discussed in more detail in Chapter 2.

1.4 Finite Element Method

The finite element method solves for, in particular, displacements, stresses, strains, and several more functions through a numerical procedure in which a structure is modeled as a series of small elements. This allows a problem that is too complicated for classical analytical methods, to be solved as a discretized model. According to (15), a finite element analysis usually involves the following steps:

1. Divide the structure into a given number of finite elements.
2. Formulate the properties of each element.
3. Assemble the elements to obtain the complete model of the structure.
4. Apply known loads.
5. Apply boundary conditions.
6. Solve simultaneous equations for nodal displacements.
7. Calculate stresses and strains.

The code used for this research follows the above steps. Step one is accomplished through a mesh generator or by specific user inputs. Step 2 is accomplished based on the user supplied material properties. Step 3 is based on the global connectivity array that is either created by the mesh generator or entered by the user. The user enters the data to accomplish steps 4 and 5. Step 6 is accomplished through the Gaussian elimination technique. Finally, step 7 is accomplished through elasticity relationships. Step 7 will be discussed more in Chapter 2.

1.5 Plate Vibrations

Since the basis of this research is the response of a plate to high frequency loading, the plate theory must be expanded upon to allow for a dynamic loading analysis. There has been a great deal of work done on the vibrations of plates including work done by Belytschko (31), Clough and Wilson (32), and Saigal and Yang (27). The method used for this research is based the work presented by Katona and Zienkiewicz (33). The method is called the beta-m method. This method is a generalization of the Newmark time marching integration scheme and can solve for a linear transient analysis. For nonlinear transient analysis, the beta-m method is combined with the Newton-Raphson iterative method (34). The details of these methods will be discussed in more detail in Chapter 2.

1.6 Eigensolutions

Another major part of this research involved finding the natural frequencies and mode shapes of flat plates. This is of particular interest since high cycle fatigue has been assumed to occur near one of these natural frequencies of turbine blades. A description of finite element eigensolutions can be found in Chapter 8 of (35). Leissa describes the free response of plates for numerous boundary conditions and geometries (36). This text was used as a comparison for eigensolutions found in this research. Srinivas, Joga Rao, and Rao present an exact analysis of eigensolutions for plates and shells(21). Reddy developed a higher-order shear deformation relationship that leads to more accurate frequencies compared to first-order theories and the classical plate theory (14). For this research however, a method known as the subspace iteration was used. This method, developed by Bathe (37), consists of the following three steps:

1. Establish starting vectors; there should be more starting vectors then the number of eigenvectors to be calculated
2. Use simultaneous inverse iterations on these vectors and the Ritz method to approximate the eigenvalues
3. After convergence, use the Sturm sequence check to verify the results.

The subspace technique is very useful since it is relatively easy to understand and can be programmed with little effort (37). This technique will be discussed in greater detail in Chapter 2.

1.7 Code Evolution.

The SLR theory developed by Palazotto and Dennis (29) was encoded in a Fortran program entitled Shell. This code was used mainly for the static analysis of shells, though it could also handle the static analysis of plates. Tsai and Palazotto (34) expanded the program to include the dynamic analysis of shells and plates through the Newton-Raphson iterative method and the beta-m time marching integration sequence mentioned previously. Gummadi and Palazotto (24) added to the program the ability to include nonlinear dynamics of shells and plates. This expanded code was entitled DSHELL. Another addition to DSHELL was made that allowed for the computation of natural frequencies and mode shapes of shells and plates using the subspace iteration method developed by Bathe (37). To allow for the eventual use of this finite element code in a larger, optimization program to be developed as part of the overall research, the shell component of DSHELL was eliminated leaving a dynamic plate analysis tool entitled DPLATE.

For this research, the code entitled DSHELL was provided. This code had the ability to calculate eigensolutions and solve linear and nonlinear transient analyses for rectangular shells and flat rectangular plates. However, this code had been modified numerous times since its original programming. Thus, extensive work was needed to debug the program and re-validate the code. When this was accomplished, the ability to use trapezoidal geometry was added. Also, the output of the program was modified to allow for quicker evaluation of results. Finally, to create an efficient program to evaluate flat plates only, the shell sections of the code were removed. The final product was entitled DPLATE.

1.8 Objective

The objective of this research is to develop a finite element program that will analyze plates under high frequency loading. This program must first be able to compute the natural frequencies and mode shapes of a plate with given geometry, material properties, and boundary conditions. Then, the program must compute stresses and displacements of this plate when a cyclic force is added. The program will compute these stresses and displacements for both linear and nonlinear cases. The effect of damping on the result will also be investigated. This code will later be used in a topological optimization program by Ohio State University as part of a DAGSI/AFRL research project.

1.9 Approach

The approach of this research is to use a finite element program to determine the stress and displacement distribution of a flat plate under a dynamic load at high frequency. This frequency is determined by first evaluating the natural frequencies and mode shapes of the plate. These mode shapes are plotted and compared. The frequency that results in a mode shape that concentrates the stress at the center of the blade tip, and thus causing the greatest opportunity for the onset of HCF, is used for the forcing frequency. With a force applied at this forcing frequency, a transient analysis of the plate is performed calculating the stress and displacement distribution. The process is done for a plate with a linear assumption and with a nonlinear assumption. The process is also run for a plate with and without damping. The results are compared to show the effects of the high-order nonlinear terms in addition to damping. A by-product of the analysis is the ability to determine the experimental requirements based on displacement or acceleration at the frequency levels associated with high cycle fatigue failure.

II. Theory

To fully understand the results of a project, the theory used to arrive at these results must be understood. The analysis was based primarily on the SLR finite element theory introduced in Chapter 1. The analysis was further simplified by applying the von Karman large-deflection two-dimensional finite element approximation. The dynamic aspect of the analysis was accomplished through the use of a Newton-Raphson iterative method and beta-m time marching integration sequence. Finally, the subspace iteration method was used to solve for the natural frequencies and mode shapes of the different plates.

2.1 Simplified Large Displacement Moderately Large Rotation Theory

The SLR theory approaches the solution using two-dimensionality with the most important three-dimensional influence, transverse shear flexibility, being approximated. The SLR theory is explained in its entirety in (29), but the main assumptions and basic principles will be discussed here.

2.1.1 Assumptions. The SLR theory is based on the following assumptions: 1) The plate's three-dimensional aspects can be modeled using a two-dimensional theory based on the thickness being much smaller than the in-plane dimensions. 2) Transverse shear stresses are equal to zero on the top and bottom surfaces and parabolic through the thickness. For transversely isotropic materials, the transverse shear strains are also equal to zero on the top and bottom surfaces and parabolic through the thickness. 3) Since the plate is thin, it can be assumed to be in a state of plane stress, or σ_3 is equal to zero. 4) The in-plane strains are represented using all Green strain nonlinear terms while the out-of-plane strains are approximated with only the linear displacement terms.

2.1.2 Formulation. Since the theory is designed for shell elements, the coordinate system used is curvilinear. However, this system can be easily converted to a flat plate by setting any radius term to large values (exact would be a value equal to infinity). The coordinate system used for this analysis is shown in Figure 2.1.

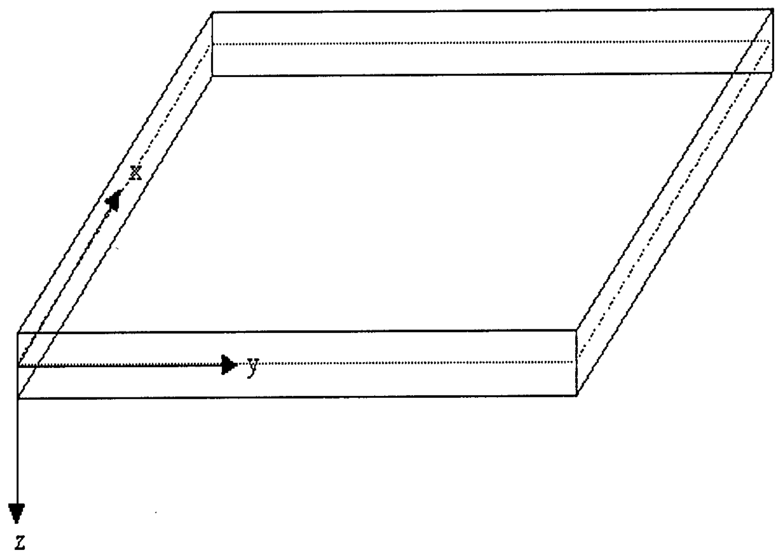

Figure 2.1 Plate Coordinate System

Throughout this thesis, a shorthand tensor notation will be used. Table 2.1 illustrates the shorthand notation.

Table 2.1 Shorthand Tensor Notation

STRESS	STRAIN	COORDINATES
$\sigma_{11}=\sigma_1$	$\varepsilon_{11}=\varepsilon_1$	X=1
$\sigma_{22}=\sigma_2$	$\varepsilon_{22}=\varepsilon_2$	Y=2
$\sigma_{33}=\sigma_3$	$\varepsilon_{33}=\varepsilon_3$	Z=3
$\sigma_{23}=\sigma_4$	$\varepsilon_{23}=1/2\varepsilon_4$	YZ=4
$\sigma_{13}=\sigma_5$	$\varepsilon_{13}=1/2\varepsilon_5$	XZ=5
$\sigma_{12}=\sigma_6$	$\varepsilon_{12}=1/2\varepsilon_6$	XY=6

The complete Green's strain tensor is developed in (29:22-26). The SLR theory modifies these strains by first assuming ε_3 is equal to zero. This is valid since the thickness of the plate is small. The second assumption assumes the in-plane stresses and strains are more dominant then the transverse stresses and strains. Therefore, the full Green strain representation is used for the in-plane strains (ε_1, ε_2, and ε_6), but the transverse shear strains (ε_4 and ε_5) are approximated by using only the linear terms. Though this approximation leads to a failure in continuity, Palazotto and Dennis (29) show that for moderate rotations, the continuity equations are approximately met. The need for transverse shear strain is required when composite materials are considered in the analysis. This thesis only considers isotropic materials and thus the transverse shear strain's importance is limited.

The transverse strains assume a parabolic through the thickness relationship. This representation accounts for an internal transverse shear but still allows it to reduce to zero on the upper and lower surfaces. In order to develop these strains in the plate, it is important to capture the proper kinematics through the displacement terms. The SLR kinematics for a flat plate are:

$$
\begin{aligned}
u_1 &= u + \zeta\psi_1 - \frac{4}{3h^2}\zeta^3(\psi_1 + w,_1) \\
u_2 &= v + \zeta\psi_2 - \frac{4}{3h^2}\zeta^3(\psi_2 + w,_2) \\
u_3 &= w
\end{aligned}
\tag{2.1}
$$

where h is the plate thickness, u and v are measured at the midplane, ζ is the distance from the midplane, ψ_1 and ψ_2 are the rotations of the cross-sections and $w,_1$ and $w,_2$ are the slopes of the plate in the x and s direction. The degrees of freedom u, v, w, ψ_1, ψ_2, $w,_1$ and $w,_2$ are discussed later. The kinematics for the plate can be derived from a Taylor's series expansion of the ζ-direction about the midplane. The differences in many of the plate theories depend on the chosen truncation of this infinite series.

Shear locking is a problem in Reissner-Mindlin (RM) kinematics. As the thickness decreases bending dominates over the shear. In RM theories, the shear and bending terms are the same order, which results in a disproportionate representation (15). This over-constrains the finite element analysis, causing it to "lock." In the SLR theory, there is a higher order representation of the shear terms, which reduce to zero as the thickness decreases. Therefore, the bending terms are allowed to dominate for a thin model and shear locking is avoided.

The physical strains ε_{ij} are found from:

$$\varepsilon_{ij} = \frac{\gamma_{ij}}{h_i h_j} \tag{2.2}$$

where γ_{ij} is the Green's strain tensor in curvilinear coordinates shown in (29, Equation 2.10) and the h_i terms are known as "scale factors." These scale factors are needed when curvilinear coordinates are used in the analysis. For flat plates, the scale factors are set equal to one. Equation (2.1) is applied to Equation (2.2). As previously stated, the in-plane strains are represented with the full Green strain representation so all terms remain. The in-plane strains become:

$$\begin{aligned}
\varepsilon_1 &= \underline{\varepsilon}_1^0 + \zeta\kappa_1 + \zeta^2\kappa_1^2 + \zeta^3\kappa_1^3 + \zeta^4\kappa_1^4 + \zeta^6\kappa_1^6 \\
\varepsilon_2 &= \underline{\varepsilon}_1^0 + \zeta\kappa_2 + \zeta^2\kappa_2^2 + \zeta^3\kappa_2^3 + \zeta^4\kappa_2^4 + \zeta^6\kappa_2^6 \\
\varepsilon_6 &= \underline{\varepsilon}_6^0 + \zeta\kappa_6 + \zeta^2\kappa_6^2 + \zeta^3\kappa_6^3 + \zeta^4\kappa_6^4 + \zeta^6\kappa_6^6
\end{aligned} \tag{2.3}$$

where $\underline{\varepsilon}^0_J$ and κ^I_J (J=1,2,6, I= 1,2,3,4,6) are functions of displacement. These expressions can be written in short hand as:

$$\begin{aligned}
&\varepsilon_i = \varepsilon_i^0 + \zeta^p \kappa_{ip} \\
&i = 1,2,6 \\
&p = sum \quad 1 \quad to \quad 7
\end{aligned} \tag{2.4}$$

The full expressions for ε_i^0 and κ_i^p can be found in Appendix A of (29) by setting α_γ=1 and $R_\gamma=\infty$. The transverse shearing strains are approximated by using only the linear terms:

$$\varepsilon_4 = (w_{,2} + \psi_2)(1 - \frac{4\zeta^2}{h^2})$$
$$\varepsilon_5 = (w_{,1} + \psi_1)(1 - \frac{4\zeta^2}{h^2}) \qquad (2.5)$$

where h is the thickness of the plate and ζ is the distance from the midplane. Note that the transverse shearing strains are represented by a parabolic function that equals zero at $\pm h/2$. This illustrates the earlier comments of a parabolic through-the-thickness strain equal to zero at the top and bottom surfaces.

The analysis can be simplified through the use of a von Karman plate. The von Karman strain displacement relations are:

$$\varepsilon_1 = u_{1,1} + \frac{1}{2} w_{,1}^2$$
$$\varepsilon_2 = u_{2,2} + \frac{1}{2} w_{,2}^2 \qquad (2.6)$$
$$\varepsilon_6 = u_{1,2} + u_{2,1} + w_{,1} w_{,2}$$

where u_1 and u_2 are given by Equation (2.1). When Equations (2.1) and (2.6) are combined, the full expressions for ε_i^0 and κ_i^p in Equation (2.4) are easier to use and are:

$$
\begin{aligned}
\varepsilon_1^0 &= u_{,1} + \frac{1}{2} w_{,1}^2 \\
\kappa_{11} &= \psi_{1,1} \\
\kappa_{13} &= -\frac{4}{3} h^2 (w_{,11} + \psi_{1,1}) \\
\kappa_{1p} &= 0, (p = 2,4,5,6,7) \\
\varepsilon_2^0 &= v_{,1} + \frac{1}{2} w_{,2}^2 \\
\kappa_{21} &= \psi_{2,2} \\
\kappa_{23} &= -\frac{4}{3} h^2 (w_{,22} + \psi_{2,2}) \\
\kappa_{2p} &= 0, (p = 2,4,5,6,7)
\end{aligned}
\tag{2.7}
$$

$$
\begin{aligned}
\varepsilon_6^0 &= u_{,2} + v_{,1} + w_{,1}\, w_{,2} \\
\kappa_{61} &= \psi_{1,2} + \psi_{2,1} \\
\kappa_{63} &= -\frac{4}{3} h^2 (2w_{,12} + \psi_{1,2} + \psi_{2,1}) \\
\kappa_{6p} &= 0, (p = 2,4,5,6,7)
\end{aligned}
$$

For more efficient analysis, the degrees of freedom are transformed from the global coordinate system to a localized coordinate system through the use of shape functions at each node of the element.

$$
\begin{Bmatrix} u(\xi,\eta) \\ v(\xi,\eta) \\ w(\xi,\eta) \\ w(\xi,\eta)_{,1} \\ w(\xi,\eta)_{,2} \\ \psi(\xi,\eta)_1 \\ \psi(\xi,\eta)_2 \end{Bmatrix} = [N]\left\{U_j^{(0)}\right\} \tag{2.8}
$$

where

$$
\left\{U_j^{(0)}\right\}^T = \left\{u(x,y) \quad v(x,y) \quad w(x,y) \quad w(x,y)_{,1} \quad w(x,y)_{,2} \quad \psi(x,y)_1 \quad \psi(x,y)_2\right\}
$$

where [N] is a matrix of shape functions and j=1,2,3,4. The definitions of the degrees of freedom are shown in Table 2.2 and graphically displayed in Figure 2.2.

Table 2.2 Degrees of Freedom Definitions

u	displacement in the x direction
v	displacement in the y direction
w	displacement in the z direction
w,1	slope δw/δx at the node
w,2	slope δw/δy at the node
ψ1	rotation of the normal to the plate midsurface in the x direction
ψ2	rotation of the normal to the plate midsurface in the y direction

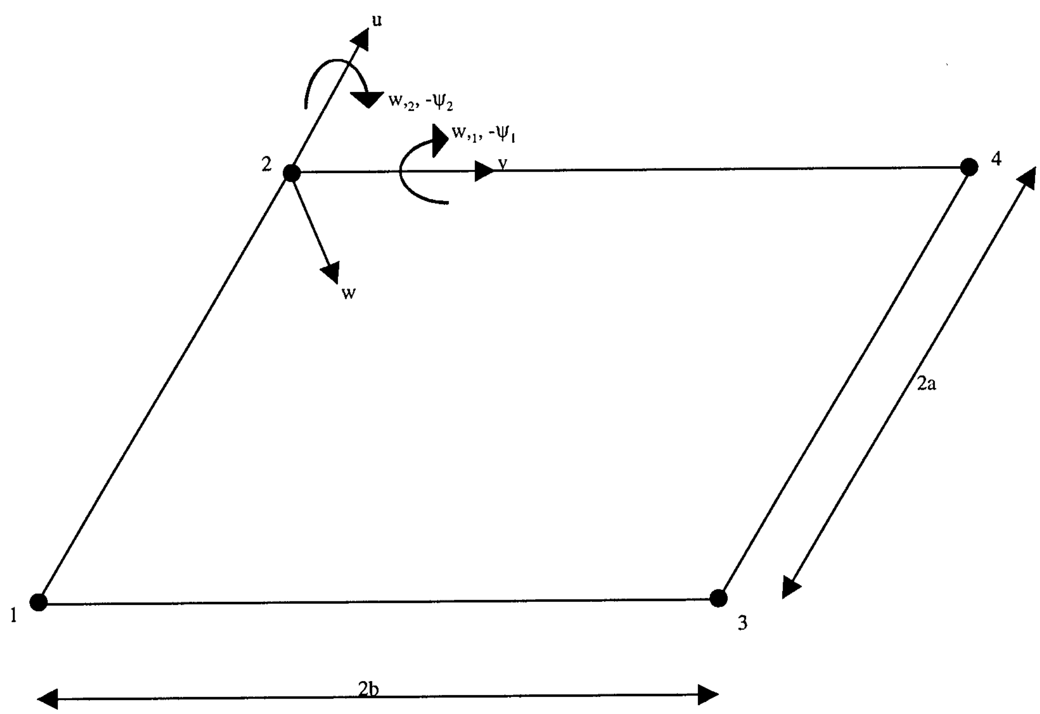

Figure 2.2 Degrees of Freedom of Plate at One Node

There are two types of shape functions used to form the [N] matrix. Linear Lagragian shape functions are used to relate the functions $u(\xi,\eta)$ and $v(\xi,\eta)$ to values of u and v, and $\psi(\xi,\eta)_1$ and $\psi(\xi,\eta)_2$ to values of ψ_1 and ψ_2 at each node. At the four corner nodes, Hermitian shape functions are used to relate $w(\xi,\eta)$ to values of w, $w,_1$, and $w,_2$ at the nodes.

The displacement field of the element can be represented as

$$\begin{Bmatrix} u_1(\xi,\eta,\zeta) \\ u_2(\xi,\eta,\zeta) \\ u_3(\xi,\eta,\zeta) \end{Bmatrix} = [R]\{U\} \tag{2.9}$$

where

$$[R] = \begin{bmatrix} 1 & 0 & 0 & k\zeta^3 & 0 & k\zeta^3+\zeta & 0 \\ 0 & 1 & 0 & 0 & k\zeta^3 & 0 & k\zeta^3+\zeta \\ 0 & 0 & 1 & 0 & 0 & 0 & 0 \end{bmatrix}$$

and

$$\{U\} = \begin{Bmatrix} u(\xi,\eta) \\ v(\xi,\eta) \\ w(\xi,\eta) \\ w(\xi,\eta)_{,1} \\ w(\xi,\eta)_{,2} \\ \psi(\xi,\eta)_1 \\ \psi(\xi,\eta)_2 \end{Bmatrix}$$

where k=-4/3h^2 and h is the plate thickness. The natural coordinates are defined as ξ=x/a and η=y/b where a and b are shown in Figure 2.2.

The equation of motion is derived through the use of the Hamilton principal. This is done by setting the variation of the time integral of the total energy equal to zero.

$$\delta\int_{t_1}^{t_2} (E - T - W_e) = 0 \tag{2.10}$$

E is defined as the internal strain energy of conservative or body forces. T is the kinetic energy and W_e is the external work including nonconservative forces. From Equation (2.10), the dynamic Equation of motion can be derived to be:

$$[M]\{\ddot{U}\}+[C]\{\dot{U}\}+[K]\{U\}=P(t) \tag{2.11}$$

where $\{\ddot{U}\},\{\dot{U}\}$, and {U} are the acceleration, velocity, and displacement vectors respectively. The consistent mass matrix [M] is found by using Equation (2.12) where ρ is the mass density, [R] is the transformation as shown in Equation (2.9), [N] is a matrix of the shape functions, and Ω is the domain of the neutral surface.

$$[M]=\int_{\Omega}\int_{\zeta}\rho[N]^T[R]^T[R][N]d\zeta d\Omega \tag{2.12}$$

The damping matrix [C] has a similar formulation as the mass matrix except for a damping coefficient c being substituted for ρ as shown in Equation (2.13). Damping will be discussed in more detail in section 2.4.

$$[C]=\int_{\Omega}\int_{\zeta}c[N]^T[R]^T[R][N]d\zeta d\Omega \tag{2.13}$$

The stiffness matrix [K] is defined for large displacement moderately large rotations of plates in Equation (2.14),

$$[K]=[K_0]+\frac{1}{2}[N_1]+\frac{1}{3}[N_2] \tag{2.14}$$

where $[K_0]$ is a constant stiffness matrix, $[N_1]$ is a stiffness matrix which includes linear displacement, and $[N_2]$ is a stiffness matrix as a function of quadratic displacement.

2.2 Beta-m Method and Newton-Raphson

The beta-m method is a generalization of the Newmark time marching integration scheme (33). The advantage of this method is the ability to choose the method order *m* and *m* integration parameters, $\beta_0, \beta_1, \ldots, \beta_m$. The integration parameters control accuracy and stability of the chosen method order. Other advantages include general single step algorithms that simplify programming and the fact that the finite difference scheme is not required.

The beta-m method is an implicit time integration method and is defined as

$$U_{n+1}^{(k)} = q_k + b_k \Delta U^{(m)} \tag{2.15}$$

where

$$q_k = \sum_{j=k}^{m} \frac{U_n^{(j)} \Delta t^{j-k}}{(j-k)!} \tag{2.16}$$

and

$$b_k = \frac{\beta_k \Delta t^{m-k}}{(m-k)!} \tag{2.17}$$

The variable k is equal to 0,1,..., m and β_m is equal to one. In Equations (2.16) and (2.17), Δt is the time increment. For this research, *m* was set equal to 2. Therefore, $\Delta U^{(m)}$ is the small change in the second derivative of the displacement vector, or the acceleration. Note that for a method order of 2 (m=2), that the beta-m method is the Newmark time marching integration scheme.

As shown in (24 and 34), substituting Equation (2.15) into Equation (2.11) at time t_{n+1}, the Equation becomes:

$$\begin{aligned} &[b_2[M] + b_1[C] + b_0[K](q_0 + b_0 \Delta U^{(m)}]\Delta U^{(m)} \\ &= P_{n+1} - \{[M]q_2 + [C]q_1 + [K](q_0 + b_0 \Delta U^{(m)})q_0\} \end{aligned} \tag{2.18}$$

where P_{n+1} is the applied load at t_{n+1}. From Equation (2.17) it can be seen that the b_0, b_1, and b_2 are scalars dependent upon the integration parameters and from Equation (2.16) it can be seen that the q_0, q_1, q_2 variables are history vectors known at time t_n.

The result of Equation (2.18) is a set of algebraic Equations. If a linear analysis is done, then the mass, damping, and stiffness matrices (N_1 and N_2 are discarded) are all constant and the set of Equations can be solved directly. However, if a nonlinear analysis is done, the stiffness matrix is a function of displacement (N_1 and N_2) and therefore is no longer constant. To solve these Equations, a Newton-Raphson iterative method is used. This method assumes that at t_{n+1}, $U^{(m)}$ is simply $U^{(m)}$ at t_n plus a small change. This is shown in Equation (2.19).

$$\Delta U_{i+1}^{(m)} = \Delta U_i^{(m)} + \delta U_i^{(m)} \tag{2.19}$$

where i is the iteration number. Equation (2.19) is applied to Equation (2.18) giving the following result as shown in (24 and 34):

$$\begin{aligned}[b_2[M] + b_1[C] + b_0[K_T](q_0 + b_0 \Delta U_i^{(m)}]\delta U_i^{(m)} &= P_{n+1} - [M]\{q_2 + b_2 \Delta U_i^{(m)}\} \\ -[C]\{q_1 + b_1 \Delta U_i^{(m)}\} - [K](q_0 + b_0 \Delta U_i^{(m)})\{q_0 + b_0 \Delta U_i^{(m)}\}\end{aligned} \tag{2.20}$$

where

$$[K_T] = [K_0] + [N_1] + [N_2] \tag{2.21}$$

Equation (2.19) is solved by the following algorithm:

1) Given $U_n^{(0)}$, $U_n^{(1)}$, …, $U_n^{(m)}$ at time t_n, we seek t_{n+1}
2) Calculate $q_0, q_1, \ldots, q_m$ from Equation (2.16)
3) Given $\Delta U_i^{(m)}$ and $\Delta U_{n+1}^{(0)}$ from the i^{th} iteration, we obtain the right-hand side of Equation (2.20)
4) Update the $[K_T]$ matrix recalling $[K_1]$ and $[K_2]$ are functions of displacement so they need to be updated by the $\Delta U_{n+1}^{(0)}$ term
5) Solve for the unknown $\delta U_I^{(m)}$ from Equation (2.20)
6) Calculate the updated solution vector $U_{i+1}^{(m)}$ from Equation (2.19)
7) Update $U_{n+1}^{(0)}$, $U_{n+1}^{(1)}$, …, $U_{n+1}^{(m)}$ for the i+1 iteration from Equation (2.15)
8) Check for convergence using Equation (2.22) where ε is a set tolerance value, l is the degree of freedom number and L is the total number of degrees of

freedom for the entire mesh. If the criteria is met, return to step 1 for the next time step. If the criterion is not met, return to step 3 for the next iteration.

$$\frac{\left\{\sqrt{\sum_{l=1}^{L}(U_{n+1}^{(0)})_l^2}\right\}_{i+1} - \left\{\sqrt{\sum_{l=1}^{L}(U_{n+1}^{(0)})_l^2}\right\}_{i}}{\left\{\sqrt{\sum_{l=1}^{L}(U_{n+1}^{(0)})_l^2}\right\}_{i}} \leq \varepsilon \tag{2.22}$$

2.3 Natural Frequencies

To find the natural frequencies of the plate, Equation (2.11) is modified for free response. That is, the forcing function is set equal to zero. Also, the damping term is eliminated, leaving Equation (2.23).

$$[M]\ddot{U} + [K]U = 0 \tag{2.23}$$

It assumed that the response will be harmonic and the displacement vector, U, can be written as:

$$U = U_0 e^{i\omega t} \tag{2.24}$$

Substituting Equation (2.24) into (2.23) and rearranging terms results in the following expression:

$$\left([K] - \lambda_i [M]\right)\{\phi_i\} = 0 \tag{2.25}$$

where λ_i is equal to the natural frequencies squared ($\lambda_i=\omega_i^2$) and ϕ_i is the eigenvector (mode shape) for the ith mode. If we define a modal matrix Φ as in Equation 2.26 and Λ as a diagonal matrix of the eigenvalues, then Equation (2.25) can be re-written as Equation (2.26).

$$\Phi=[\ \{\phi_1\}\ \{\phi_2\}\ \ldots\ \{\phi_n\}] \tag{2.26}$$

$$[K]\Phi=[M]\Phi\Lambda \tag{2.27}$$

To solve this equation for the "p" lowest eigenvalues, a method developed by Bathe (37) known as the subspace iteration method is used. The solution is named the subspace iteration method because the iteration is equivalent to iterating with a q-dimensional subspace and should not be regarded as a simultaneous iteration with q individual iteration vectors. This method is used due to its efficiency in memory storage and time to converge to a solution. The method not only solves for a solution to Equation (2.27) but also satisfies the orthogonality conditions:

$$\Phi^T[K]\Phi=\Lambda \quad \text{and} \quad \Phi^T[M]\Phi=[I] \tag{2.28}$$

where [I] is the identity matrix. To solve for the eigenvalues and vectors that satisfy Equations (2.27) and (2.28), the subspace iteration method follows three steps as shown in 2.3.1-2.3.2.

2.3.1 Establish q Starting Iteration Vectors. For the analysis, q is greater then the number of required eigenvalues to be calculated. The starting iteration vectors, $\mathbf{X}_i$, are chosen to excite the degrees of freedom with a relatively large mass and small stiffness. To accomplish this, the first column of MX_1 is set equal to the diagonal of the M matrix. The remaining columns, except for the last column, have a value of +1 in the location corresponding to the degrees of freedom with the smallest stiffness to mass ratio and a value of 0 at the remaining locations. The last column of MX_1 is set as a random vector.

2.3.2 Simultaneous Inverse Iteration. This iteration is performed on the q vectors and then a Rayleigh-Ritz analysis is used to extract the "best" eigensolution approximation from the q iteration vectors. This step finds an orthogonal basis of vectors in the subspace E_{k+1}. These vectors are the eigenvectors when E_{k+1} converges to E_∞. The algorithm is as follows:

1) For k=1,2,... iterate from E_k to E_{k+1}:

$$K\overline{X}_{k+1} = MX_k \tag{2.29}$$

2) Find the projections of the matricies K and M onto E_{k+1}:

$$\begin{aligned} K_{k+1} &= \overline{X}_{k+1}^T K \overline{X}_{k+1} \\ M_{k+1} &= \overline{X}_{k+1}^T M \overline{X}_{k+1} \end{aligned} \tag{2.30}$$

3) Solve for the eigensystem of the projected matricies:

$$K_{k+1} Q_{k+1} = M_{k+1} Q_{k+1} \Lambda_{k+1} \tag{2.31}$$

4) Find an improved approximation to the eigenvectors:

$$X_{k+1} = \overline{X}_{k+1} Q_{k+1} \tag{2.32}$$

As long as the vectors X_1 are not orthogonal to one of the required eigenvectors, the following is true:

$$\Lambda_{k+1} \rightarrow \Lambda \text{ and } X_{k+1} \rightarrow \Phi \text{ as } k \rightarrow \infty \tag{2.33}$$

The last step involves checking for convergence based on a set tolerance value tol. The check is accomplished through use of Equation (2.34).

$$\left[1 - \frac{\left(\lambda_i^{(k)}\right)^2}{\left(q_i^{(k)}\right)^T q_i^{(k)}}\right]^{\frac{1}{2}} \leq tol, \quad i-1,\ldots,p \tag{2.34}$$

If Equation (2.34) is met, the eigensolution is the eigensolution for the plate to within the accuracy of *tol.*

2.3.3 Sturm Sequence Check. After iteration convergence, the Sturm sequence check is used to verify the eigensolution. The Sturm sequence check determines a shift value μ such that μ is slightly larger than the largest eigenvalue calculated. The Sturm sequence property along with Gauss factorization can determine the number of eigenvalues that are smaller then μ (37). If this number does not match the number of eigenvalues calculated, then the correct eigenvalues have not been found and another iteration is accomplished.

2.4 Damping

The damping used in this research is Rayleigh or proportional damping for homogeneous materials. The damping matrix [C] is a linear combination of the mass matrix [M] and stiffness matrix [K] as shown in Equation (2.35).

$$[C] = \alpha[K] + \beta[M] \tag{2.35}$$

where α and β are the stiffness and mass proportional damping constants respectively. It was assumed for this research that the stiffness damping would have negligible effect compared to the mass damping. Thus α was set equal to zero. The values of β are limited to a maximum less then 0.1 to ensure that the mass-proportional damping is not excessive. This is especially important if rigid body motion could be possible (15). With α set equal to zero, Equation (2.35) reduces to Equation (2.36).

$$[C] = \beta[M] \tag{2.36}$$

Equation (2.37) is developed by substituting Equation (2.12) for [M] into (2.36).

$$[C] = \beta\int_{\Omega}\int_{\zeta} \rho[N]^T[R]^T[R][N]d\zeta d\Omega \tag{2.37}$$

Since β is a constant, it can be moved inside the integration. Then Equation (2.13) can be derived by setting $c=\beta\rho$.

2.5 Convergence Criteria

The theory used in this research is not exact, but rather is dependent upon converging to solutions within a prescribed error. There are three values that must be set to prescribe these error tolerances. The first is the value of *tol* used in Equation (2.34) for the eigensolution. According to (37),

$$tol = 10^{-2s} \tag{2.38}$$

where the desired accuracy of the largest eigenvalue is 2s digits. For this research, it was decided to have the eigenvaules accurate to at least the 6th digit. Therefore, *tol* was set equal to 1e-6 or *s* is set equal to 3.

The second variable is the convergence criteria ε from Equation (2.22) used to terminate the Newton-Raphson inner-loop iteration. This value should be small enough to ensure needed accuracy in the transient analysis, but not so small that the time needed for the solution to converge is too extreme. A value of 0.01% was chosen for this research based on past experience.

The final parameter that must be set is the Δt value from Equations (2.16-2.17). This is the time increment between steps for the transient analysis. This proved to be the most sensitive parameter in this research. It was hypothesized that the response will have sinusoidal form for a given node point. Based on experience and common practice, a time increment to properly represent a sinusoid should be equal to or smaller then one-twentieth of the period of the response frequency. A study was done to see the effect of the time increment on the solution. The results of this study showed that the time increment should be set to one-fortieth of the period of the expected response frequency.

III. Results and Discussion

The main objective of this research is to show trend data, which will later allow for an optimization program to be designed to achieve specified high cycle fatigue scenarios. To show these trends, two main shapes were investigated, square and trapezoidal. The square plate investigated was 0.1143m X 0.1143m titanium plate with a thickness of 0.001016m. These dimensions were chosen based on on-going experiments being performed in a Ohio State University thesis to allow for eventual comparisons. Three trapezoids were investigated where all three had the same in-plane area as the square and the same material. The first trapezoid had a hub to tip ratio of 0.3. The second trapezoid had a hub to tip ratio of 0.7. The third trapezoid was the inverse of the first with a hub to tip ratio of 3.33. The basic geometries of the plates are shown in Figure 3.1.

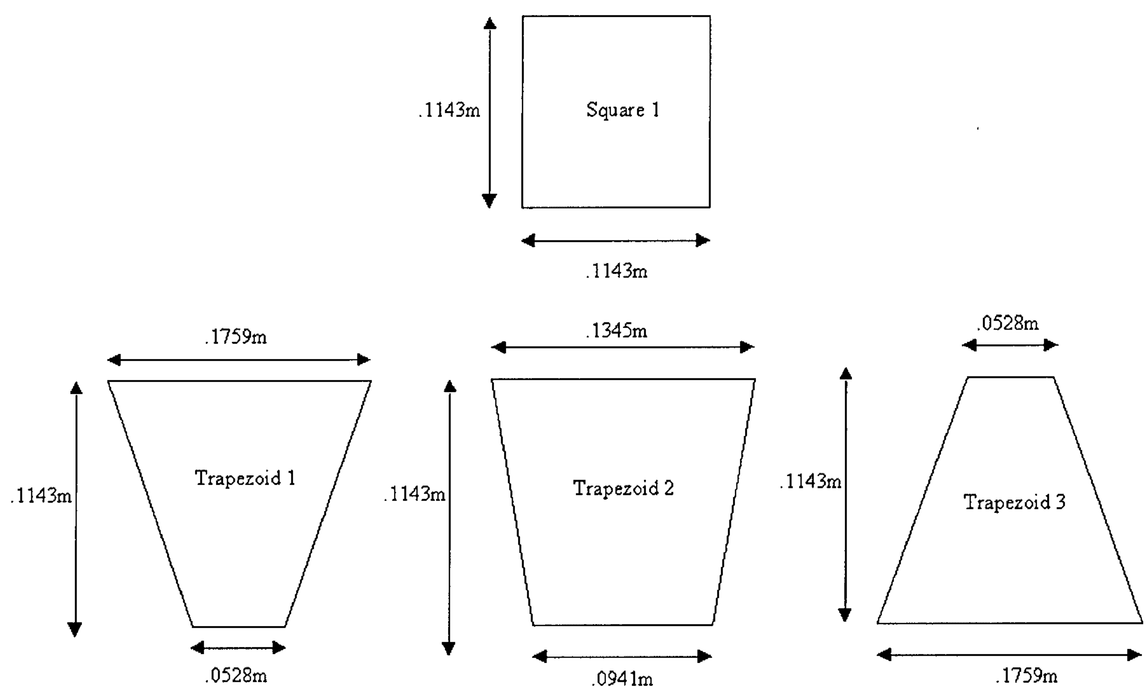

Figure 3.1 Plate Geometries

For each of these four cases, an eigensolution was found that included the first six natural frequencies and mode shapes. A transient analysis was then accomplished for each case with a sinusoidal forcing function applied at the center of the plate. The frequency of this forcing function was based on the natural frequencies of the plate. The mode shapes were examined to determine the one that concentrated the most energy in the center of the tip of the plate. The stress at this point can be predicted and compared to the estimated value needed to initiate cracks in the material, and thus it can be determined when the correct stress levels are reached to cause fatigue. The amplitude of the forcing function was set at two different values thus allowing a trend to be developed that could then predict the amplitude of the force needed to raise the stress high enough to initiate cracks based on the Goodman diagram. The plates were then loaded with this large forcing function. Numerical factors that could affect the outcome were also examined. These factors included nonlinearity, damping, and the von Karman assumption.

The material used for all four cases was a titanium alloy (Ti-6Al-4V). This material has numerous applications in the aerospace industry, particularly turbine blades. Therefore, the response of this material to high cycle fatigue is very critical to the future development of turbomachinery. The material properties for Ti-6Al-4V are shown in Table 3.1.

Table 3.1 Material Properties

Property	Symbol	Value
Young's Modulus	E	114 Gpa
Poisson's Ratio	ν	0.33
Thickness	t	1.016 mm

3.1 Code Validation

Before the cases can be investigated, the code used must be verified. The actual code used for this research is a subset of a code entitled DSHELL. This code can do linear/nonlinear dynamic analysis for plates and shells. The code was first run and compared to published results for shell elements. The first case, as presented in (34), involved the static response of a shell to a uniformly distributed half-sinusoidal wave loading applied in the center of the shell with a peak intensity of 90 psf as shown in Figure 3.2.

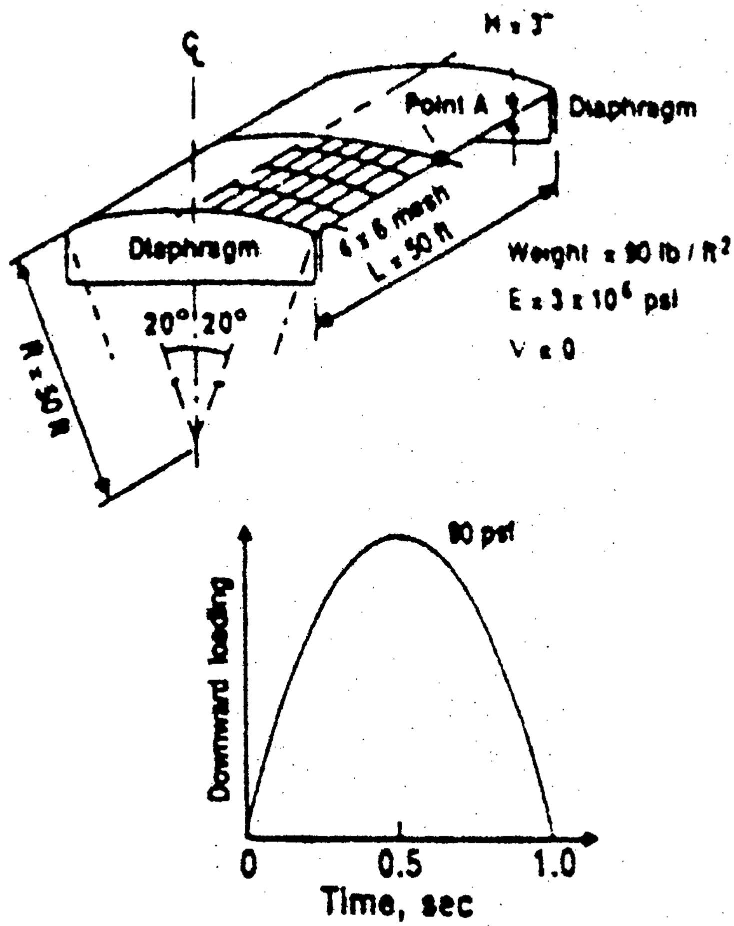

Figure 3.2 Distributed Half-Sinusodial Impulse Load

The shell is an isotropic shell with a Young's Modulus E=3 X 10^6 psi, a Poisson ratio of 0, and a weight density of 90 psf or mass density of 2.795 slugs/ft. In DSHELL, a static solution is accomplished by setting the mass density equal to 0, thus eliminating the mass and damping matrices from the equation of motion. The displacement of point A over time is calculated. The results of DSHELL compared to Clough and Wilson's results can be seen in Figure 3.3.

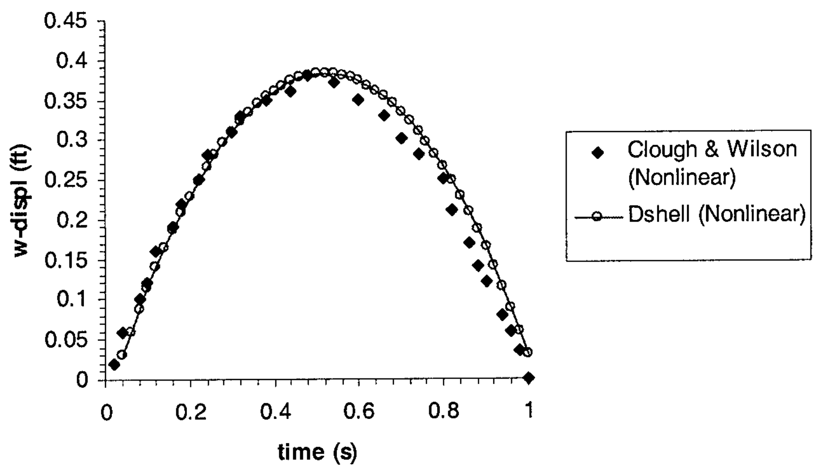

Figure 3.3 Static Response of Shell with Distributed Half-Sinusodial Impulse Load

The graph shows the displacement of point A with respect to time. DSHELL's result indicates that the code is adequate for static solutions. For validation of a dynamic solution, another case done by Clough and Wilson was tested. The same shell and loading were used as above, but a dynamic solution was sought (34). The result of this analysis is shown in Figure 3.4.

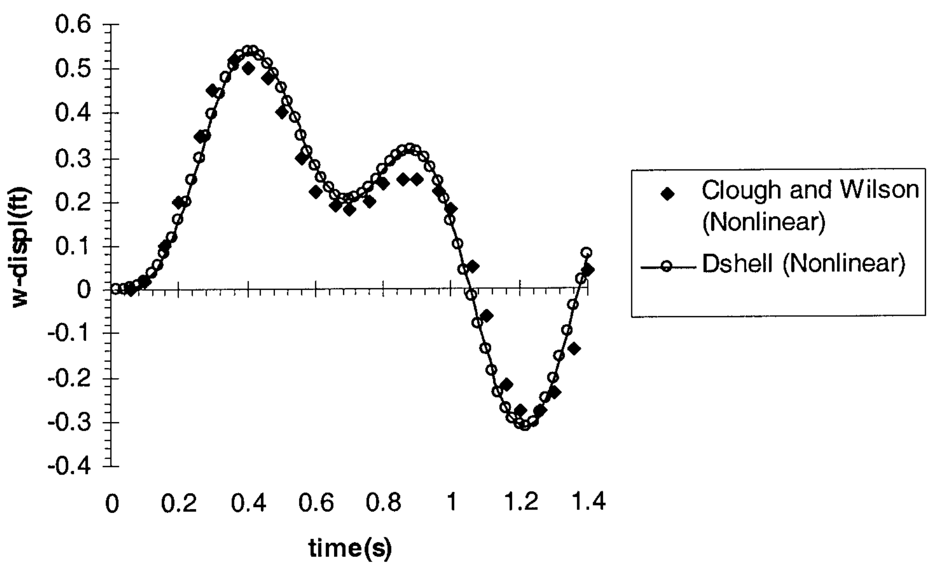

Figure 3.4 Dynamic Response of Shell with Distributed Half-Sinusodial Impulse Load

Once again DSHELL results are approxiamtely the same as the results presented by Clough and Wilson. A third case is presented for validation from (38). This case involved a step load applied at the center of an arch that reaches its maximum value at 0.002 seconds as shown in Figure 3.5.

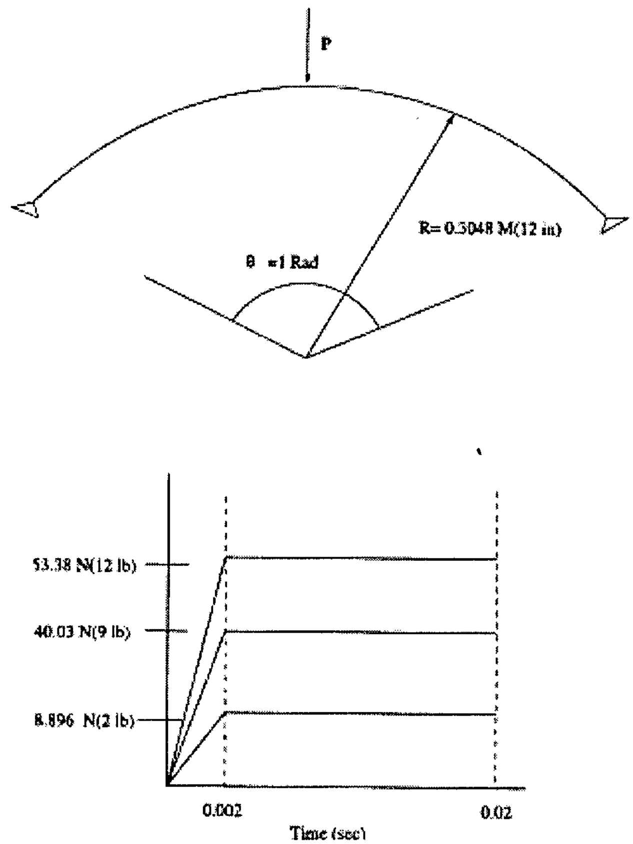

Figure 3.5 Concentrated Step Load

The arch is simply supported at the ends. The results for the max loading amplitude of 8.896 N from DSHELL as well as from (38) are shown in Figure 3.6. DSHELL's results are approxiamtely the same as those presented by the reference.

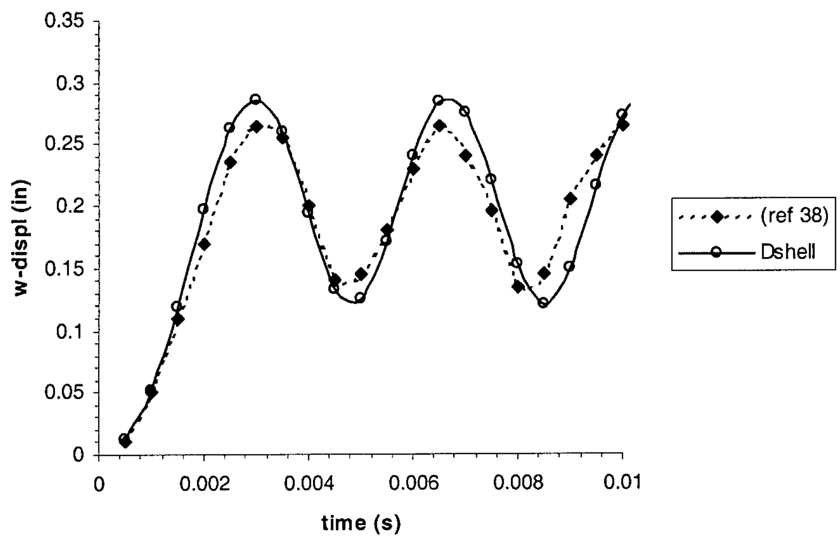

Figure 3.6 Dynamic Response of Arch with Concentrated Step Load

The difference between a flat plate and a shell is the radial dimension used. A flat plate is a shell with a radius that approaches infinity. A shell analyis and a plate analysis are both done with the same material properties, boundary conditions, geometries, and loading conditions. The shell has a radius set equal to a very large value (100,000m). The results of the two analyses are identical. This leads to the conclusion that since the shell analysis was verified, and that the plate analysis matches the reults of this shell analysis, the plate anlsysis has also been verified.

3.2 Time Increment Investigation

As mentioned in Chapter 2, an investigation was done on the sensitivity of the results to the time increment incorporated. Since the forcing function has a sinusoidal shape, the response is expected to be sinusoidal. From past experience, to accurately represent a sinusoid there should usually be at least 10 data points per cycle but 20 is sometimes required depending upon the frequency of the sine wave. To investigate how many points were needed to accurately capture the data for this analysis, four cases were run, 10 data points per cycle, 20 data points per cycle, 40 data points per cycle, and 100 data points per cycle. A 20x20 mesh was used based on the results of the convergence study discussed in the next section. The time increment investigation and mesh convergence investigation had to be done simultaneously since one causes change in the other. The time increment investigation was done first. The results were then used in the mesh convergene test. The results from the mesh convergence test were used to update the time increment investigation. This process was continued until the results from one test did not change the other test. The results for the final time increment investigation are shown in Figures 3.7. The results are shown for comparison only. The details of the analysis will be discussed later.

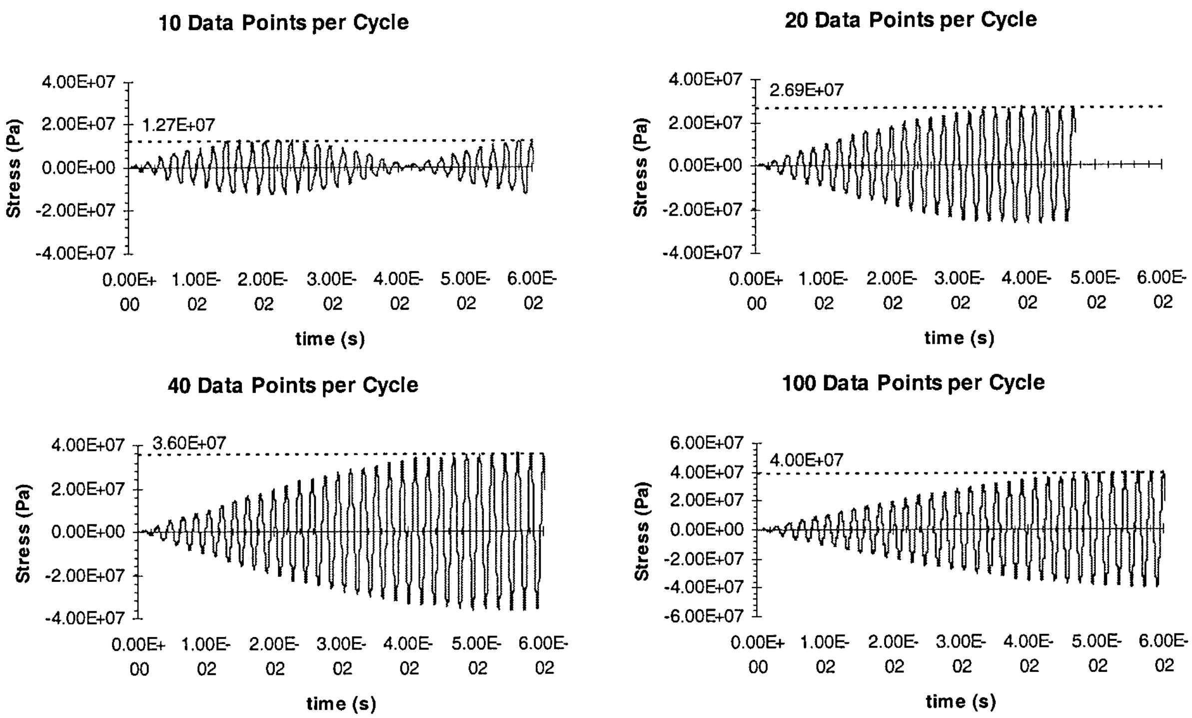

Figure 3.7 Graphical Results of Time Increment Study

There is an obvious shape difference between 10 data points per cycle and the remaining cases. There is also a difference in the maximum values of stress between the four cases. These differences are illustrated in Table 3.2 where τ is the period of the expected response. Therefore, 10 data points per cycle can be written as $\tau/10$.

Table 3.2 Error Analysis of Results of Time Increment Study

	Max Stress (Pa)	% error based on next	% error based on $\tau/100$
$\tau/10$	1.27E+07	53%	68%
$\tau/20$	2.69E+07	25%	33%
$\tau/40$	3.60E+07	10%	10%
$\tau/100$	4.00E+07	-----------	----------

The results of an error analysis that assumes the next level of accuracy is the true solution is shown in the column titled "% error based on next". The results of an error analysis that assumes the result using 100 data points per cycle as the true solution is shown in the column titled "% error based on $\tau/100$". Based on the error calculations, it can be assumed that if the data points were doubled again, the result for 100 data points per cycle would be less then 10%. The error for 40 data points per cycle will be slightly over 10%. Though the analysis using 100 data points per cycle would be slightly more accurate, it would be much more costly in computational time. Therefore, for this analysis, it was decided to use an analysis with 40 data points per cycle. This assumption is valid for this research since the trends are being investigated, not the precise response of the plates.

3.3 Geometry Investigation

In this section, each geometry will be discussed and the results given. For each geometry, the eigensoultion will first be presented. Next the transient analysis will be presented where the frequency of the loading function is based on the eigensolution. A linear analysis is done for three geometries (square and first two trapezoids). A nonlinear analysis is accomplished on the square only to show its effect on the analysis. With this analysis, a loading amplitude will be approximated that will result in a stress field that will lead to high cycle fatigue. An analysis will be done with this loading amplitude to verify the predicted stress values. After the four geometries have been discussed, the results from the four cases will be compared and the trends indicated.

3.3.1 Square Plate. The first geometry examined was the square plate. The mesh used for this plate is shown in Figure 3.8. For this research, displacements will be measured at node 66. This point is at the center of the plate's side opposite of the loading conditions. Stress values will be at a Gaussian point near this node. The program outputs stress at four Gaussian points at five different thickness locations, or 20 Gaussian points. The Gaussian point chosen to track data for this research is on the upper surface of the plate in the corner of the element near node 66. The boundary conditions used for all four geometries was a cantilever system in which all seven of one side's degrees of freedom are fixed and held at a constant value of zero. The initial conditions for all four geometries were zero displacement, zero velocity, and zero acceleration at all node points.

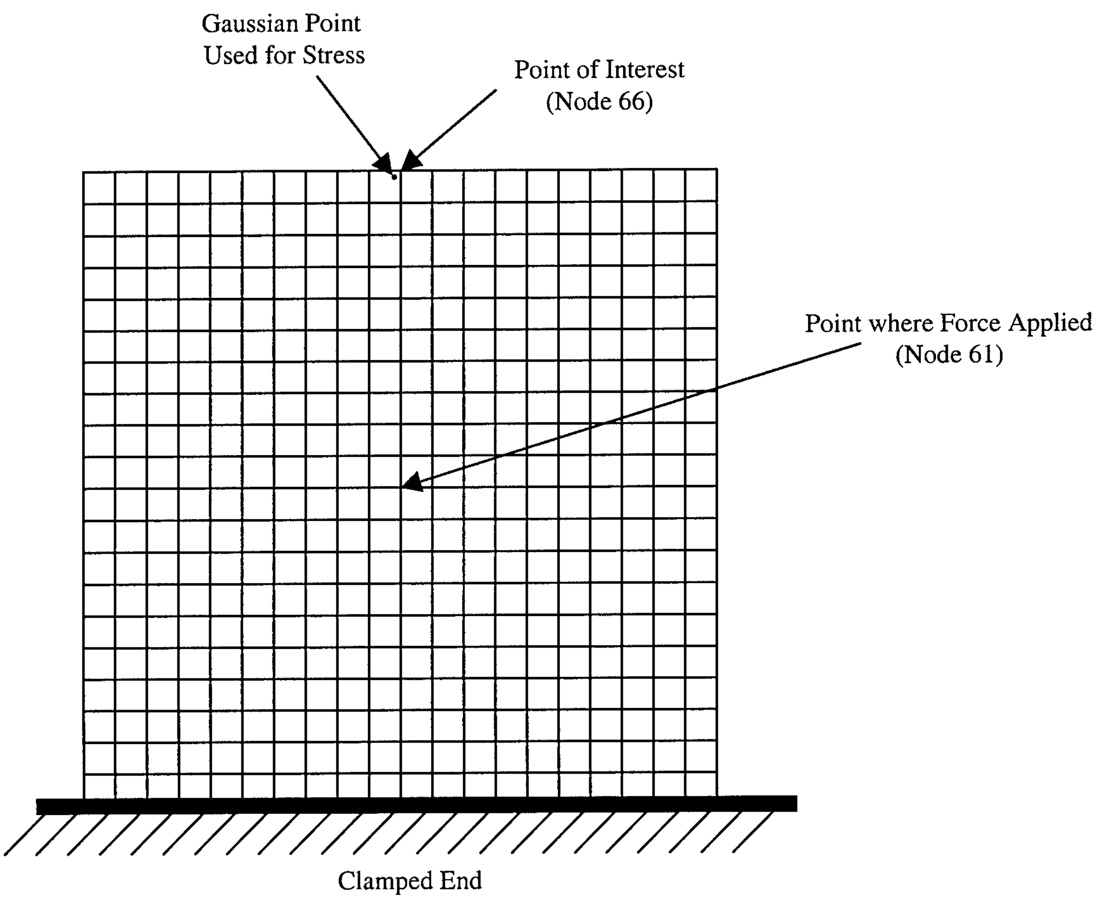

Figure 3.8 20x20 Mesh Illustration

It was determined after a convergence study that a 20x20 mesh would be best. Table 3.3 shows the errors of three different mesh sizes. The same error criteria as discussed in the time increment study is used.

Table 3.3 Converegence Error Analysis

Mesh	Max Stress	% error based on next	% error based on 20X20
6x6	2.51E+07	21%	22%
10x10	3.19E+07	1%	1%
20x20	3.22E+07	-----	-----

It can be assumed based on the data that the 20x20 mesh will have less then 1% error since as the mesh is refined, the solution approaches the true solution. Normally, the 10x10 mesh would be adequate for this research. However, due to the coupling between the mesh size and time increment, it was decided to use the 20x20 mesh to ensure accuracy.

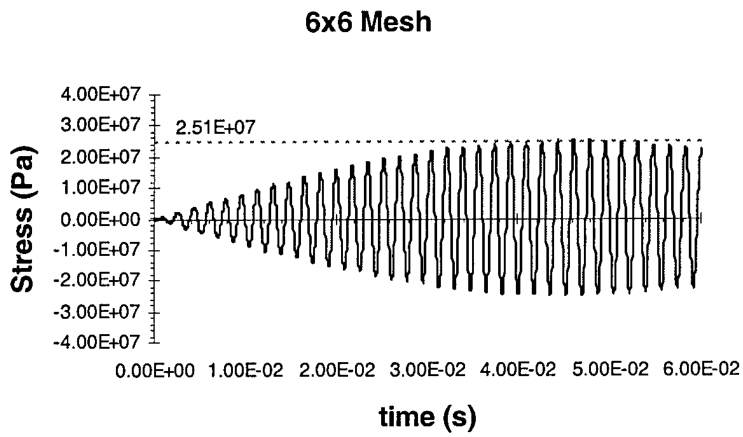

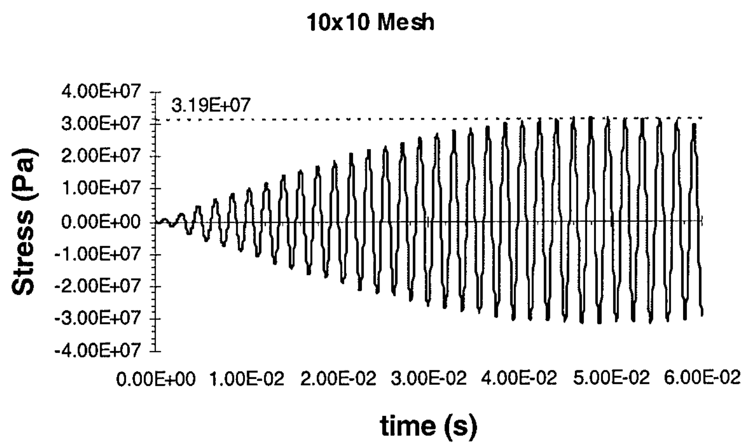

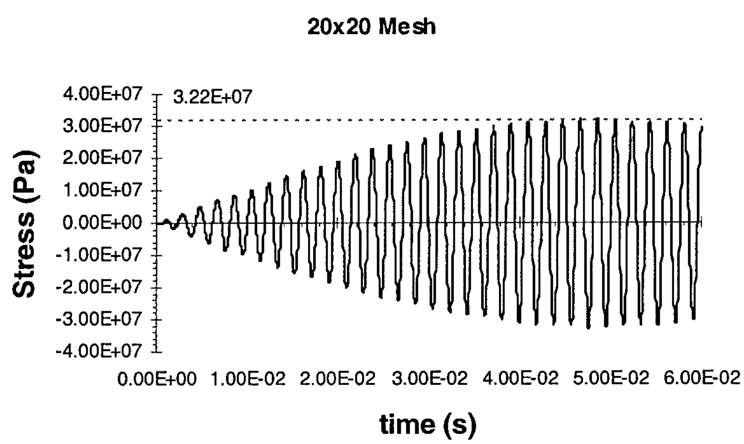

Figure 3.9 Graphical Results of Convergence Study

3.3.1.1 Eigensolution. An eigensolution is found for the square plate in order to determine the frequency of the loading function to use in the transient analysis. By examining the mode shapes of the plate, it can be hypothesized which mode will concentrate the most energy at the point of interest (node 66). Knowing that stress is a function of displacement, a mode will be chosen that shows the greatest rate of change of relative displacement of the plate near node 66. The results of the eigensolution for the square plate are shown in Figure 3.10. Mode 4 is selected as the mode that will concentrate the most energy at the center point of the tip of the plate. Modes 1 and 2 will impart little to no energy at the desired point since the edge is undeformed. Mode 3 will impart some energy, but very little since the relative displacement is so small. Mode 5 shows that most of the energy will be concentrated on the sides of the plate. Mode 6 will concentrate the energy both on the sides and in the center of the tip, but the difference in relative displacement will not be as great as mode 4, and thus impart a smaller amount of energy at the center-point.

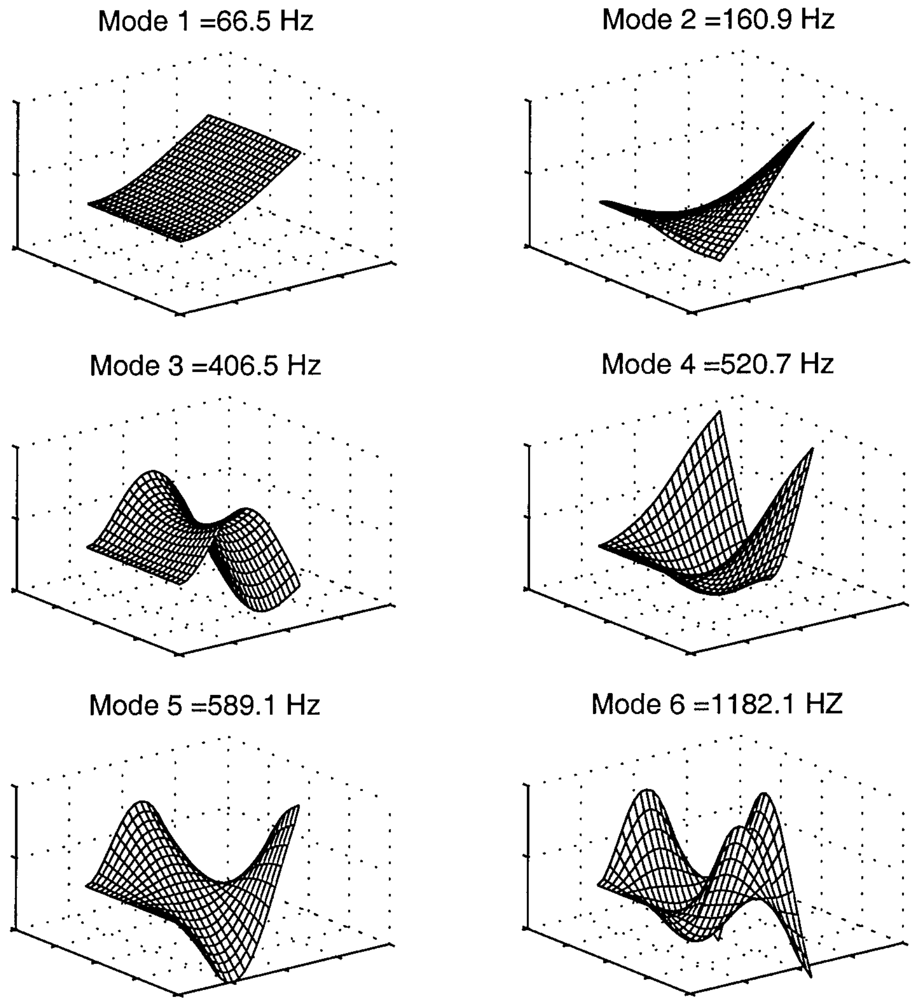

Figure 3.10 Square Plate Mode Shapes

<u>3.3.1.2 Transient Analsysis.</u> The square plate is loaded with a forcing function as shown in Equation 3.1.

$$\mathbf{F} = \overline{F}\sin(\varpi t) \tag{3.1}$$

From the eigensolution, the frequency of the applied load, $\varpi/(2\pi)$, should be 520.7 Hz. However, loading at this frequency will lead to resonance. Therefore, the actual frequency used is 528.9 Hz. This is slightly larger then the actual natural frequency allowing for the correct mode to be excited, but resonance will not occur. The amplitude of the function, $\overline{F}$, will be determined later. The forcing function with an amplitude of 1 is shown in Figure 3.11.

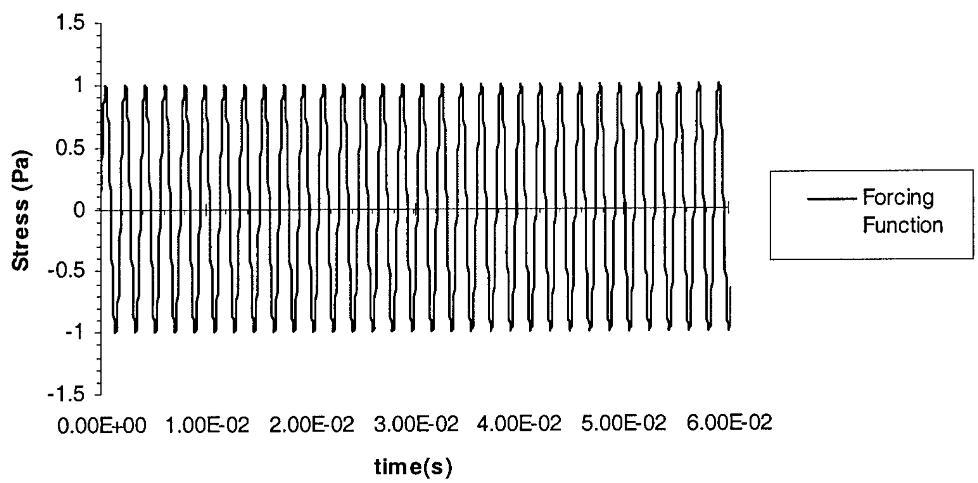

Figure 3.11 Square Plate Forcing Function

A linear analysis is done for a forcing function with an amplitude of 1. The stress of the Gaussian point near node 66 (as discussed previously) is shown in Figure 3.12. It is noted that the response is a repetitive pattern in which the stress rises to a maximum value, then lowers again in a cyclic fashion. This pattern is the result of the beat phenomenon that occurs when the loading frequency is near but not at one of the natural frequencies of the plate. For convience, only the first half of the response of the plate, up to the maximum stress, will be shown in following graphs.

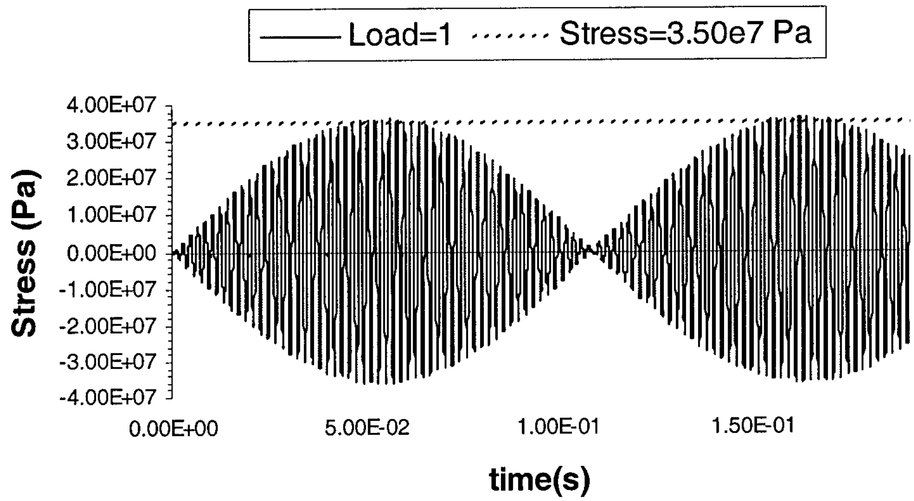

Figure 3.12 Stress at $\overline{F}=1$

The analysis is repeated for an amplitude of 3. This allows the comparison of the response to different amplitudes. The results of the two analyses are shown in Figure 3.13.

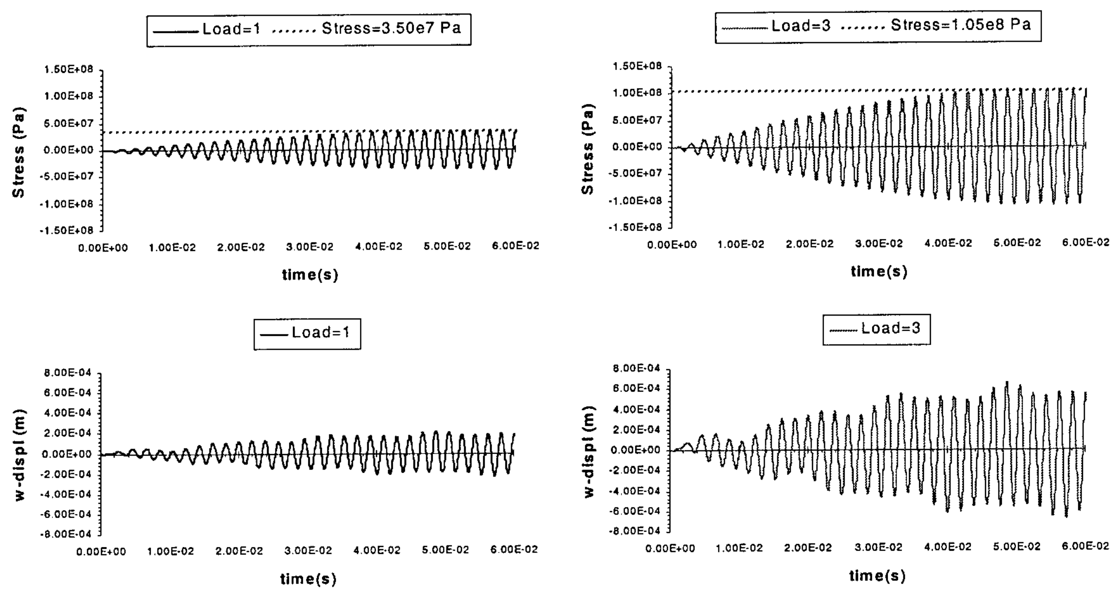

Figure 3.13 Linear Response of Square Plate

As indicated in Figure 3.13, a maximum stress value of 35 MPa is reached when the forcing function has an amplitude of 1. When the amplitude is tripled, the resulting maximum stress is also shown to triple. This allows the prediction through a linear function of what amplitude would be needed to arrive at a certain stress. To determine what the stress should be to initiate cracks the Goodman diagram in Figure 3.14 is used. The mean stress is zero for this case since the stress is approximately symmetric about the x-axis. The chart indicates that an alternating stress of at least 500 MPa is needed to initiate a crack. Based on the linear relationship above, the forcing amplitude needed to arrive at this stress is approximately 14.3. (500MPa / 35MPa = 14.3)

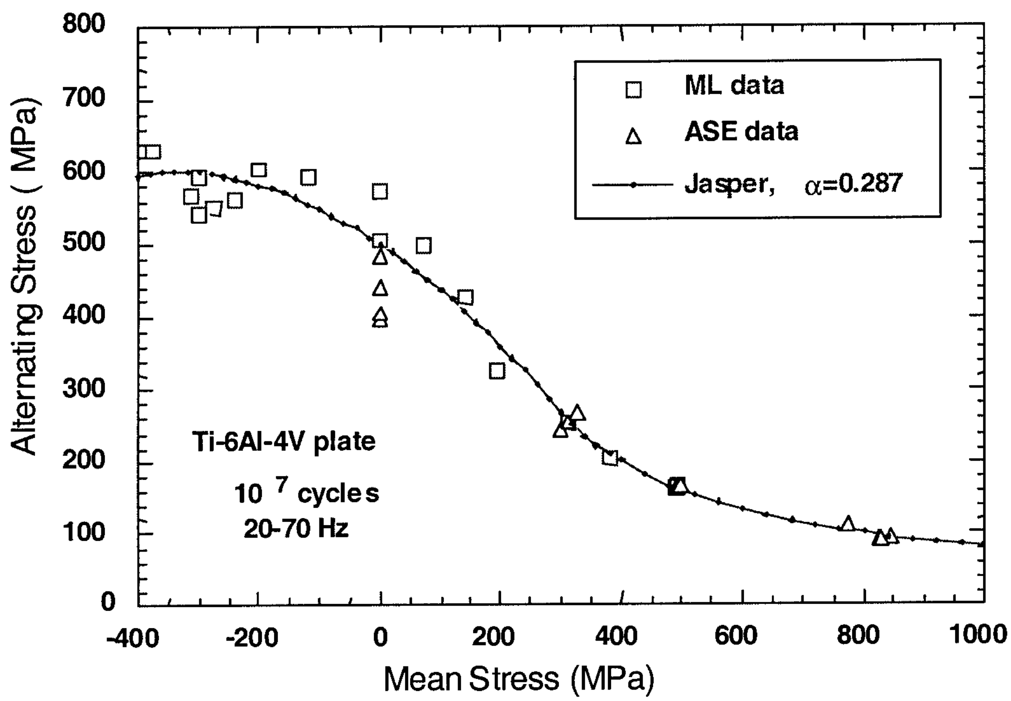

Figure 3.14 Goodman Diagram for Ti-6Al-4V

A linear transient analysis was then done with a frequency still at 528.9 Hz and an amplitude of 14.3 based on the above analysis. The result of this analysis is shown in Figure 3.15. The results show that the sought after stress of 500 MPa was realized and that the linear model for predicting the needed loading amplitude is accurate for the linear analysis.

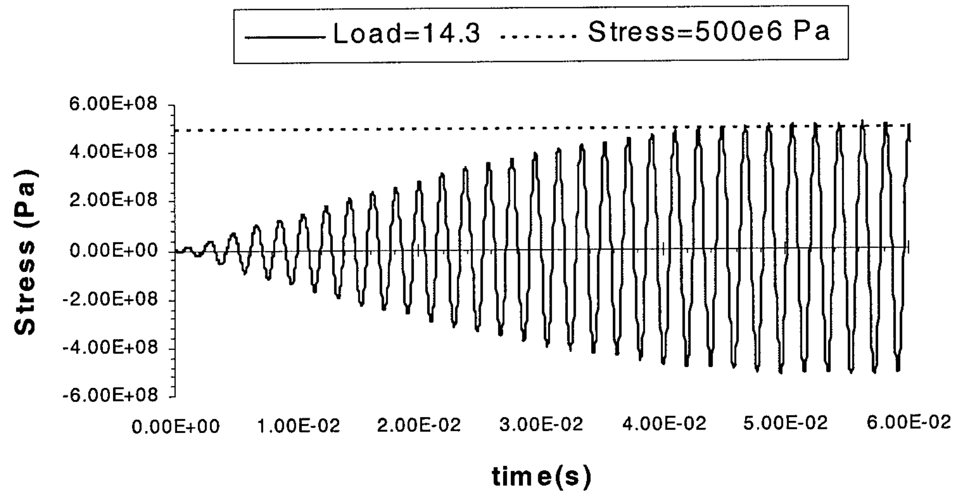

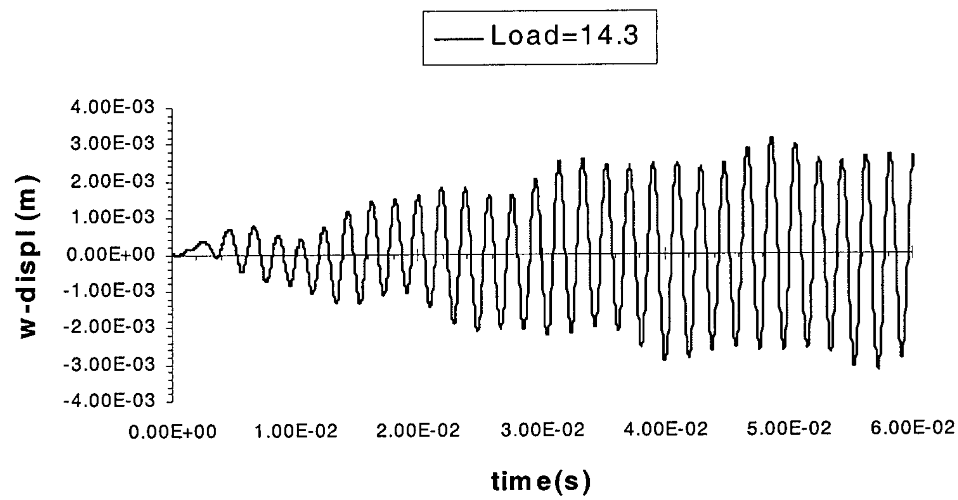

Figure 3.15 Linear Response of Square Plate with $\overline{F}$ =14.3

It is interesting to note that the displacement profile for all cases, and later for all geometries, is approximately the same shape with only the amplitude and frequency of the response differing. This is due to the same basic mode shape being excited in all cases. Since the same mode shape is being excited, the shape of the curve representing the displacement of a single point should be the same for all of the cases with only the amplitude changing.

3.3.1.3 Other Numerical Factors Possibly Affecting Solution. The analysis above models an amplitude multiplier that allows a simple method for a high cycle fatigue experiment. The experiment would first determine the stress state at a low loading amplitude. The multiplier would be used to determine the needed amplitude to cause HCF failure. The specimen would then be run at the needed frequency and loading amplitude based on the analysis in the previous section. However, there were assumptions made in the code that simplified the analysis and could have introduced unacceptable error. One assumption was that the analysis was a linear analysis where the stiffness matrix is independent of displacement. Another assumption used was the von Karman assumption to simplify the nonlinear analysis. Also, damping was assumed to be negligible. The effect of these assumptions on the expected solution is discussed in this section.

A nonlinear analysis was done to test the accuracy of the linear analysis. As in the linear analysis, the amplitude of the forcing function was set equal to 1. The result of this analysis is shown in Figure 3.16. The results are indistinguishable from the results found in the linear analysis previously discussed.

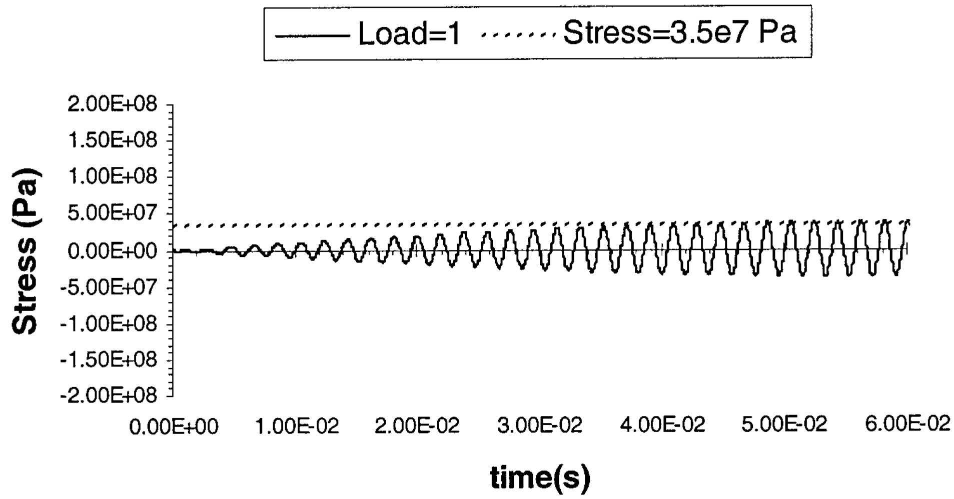

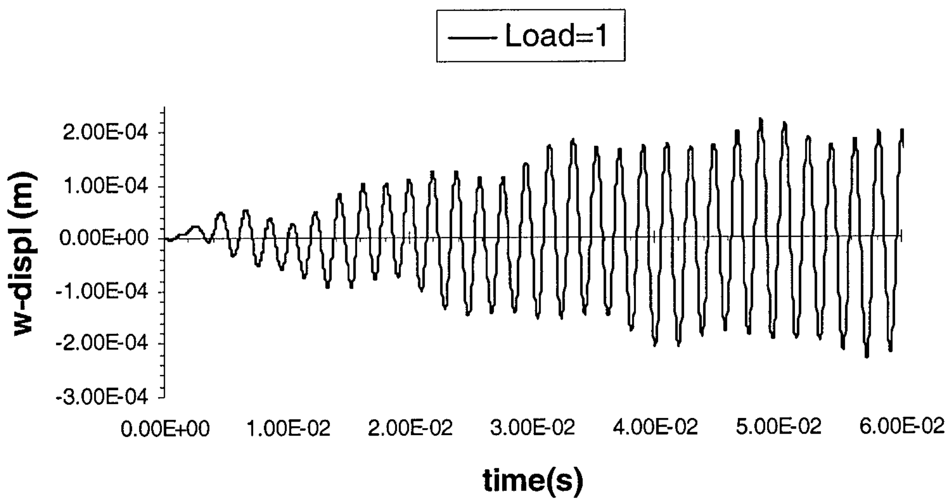

Figure 3.16 Nonlinear Response of Square Plate with $\overline{F}=1$

It is hypothesized that the same relationship exists between the loading amplitude and stress. Thus, a nonlinear analysis is done with the load amplitude set equal to 14.3 as in the linear analysis. The result of this analysis is shown in Figure 3.17.

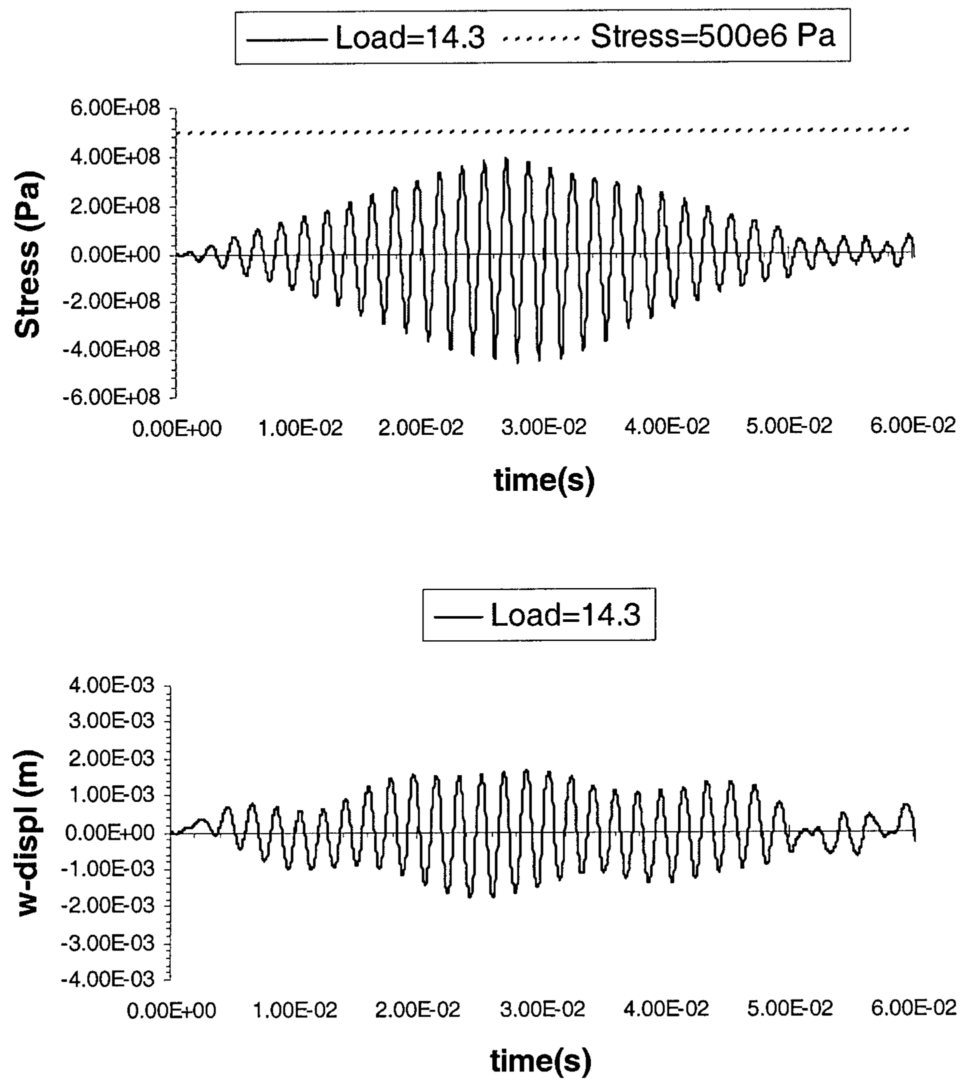

Figure 3.17 Nonlinear Response of Square Plate with $\overline{F}$ =14.3

The results indicate that the nonlinear analysis does not result in the sought after stress of 500 MPa. The explanation for this is based on the difference between the linear and nonlinear analyses. The linear and nonlinear analyses are approximately the same when the displacement is much smaller then the thickness. However, as the displacement approaches the thickness of the plate, the nonlinear and linear analyses lead to different solutions. The error in the linear solution becomes much larger and leads to an incorrect solution.

To try and attain a stress of 500Mpa, a case is run where the amplitude is set equal to 19.74. This value is based on a linear relationship between the maximum stress at an amplitude of 1 and the maximum stress at an amplitude of 14.3. It is assumed that there still is a linear load relationship as found in the linear analysis, but with a different slope. The result is shown in Figure 3.18.

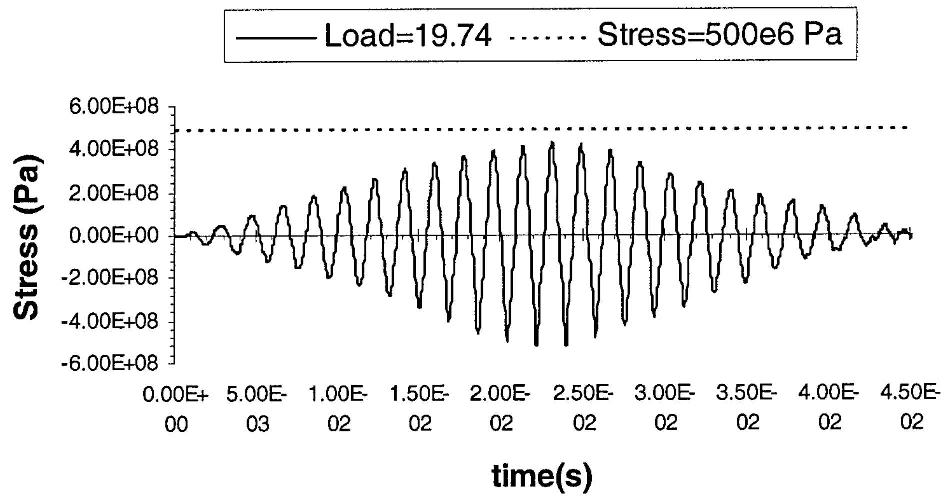

Figure 3.18 Nonlinear Response of Square Plate with Load=19.74

The result indicates that there is not a linear relationship between the amplitude of the loading function and the resulting maximum stress. To accurately represent the relationship between the loading function amplitude and the resulting maximum stress, a study must be accomplished where numerous loading amplitudes are used and the resulting maximum stresses are calculated. In Figure 3.19, the results of a nonlinear analysis with the amplitude set equal to 6,9, and 15 are shown. These results and the results from Figures 3.16-3.18 are plotted in Figure 3.20. This figure shows the possibility of a higher-order function that could relate the amplitude of loading function to the max stress. Further investigation is needed to truly capture this function.

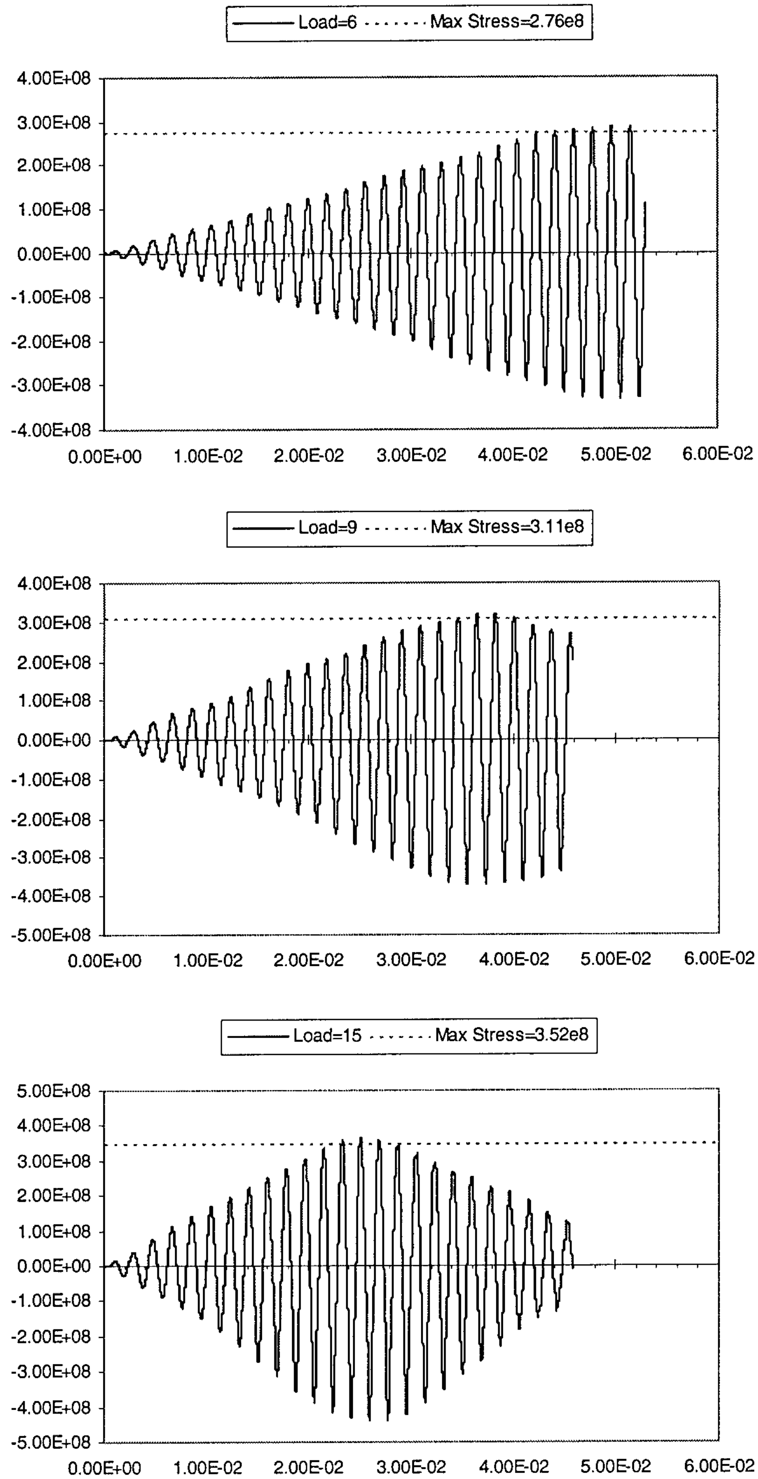

Figure 3.19 Nonlinear Response of Square Plate with Load=6,9,&15

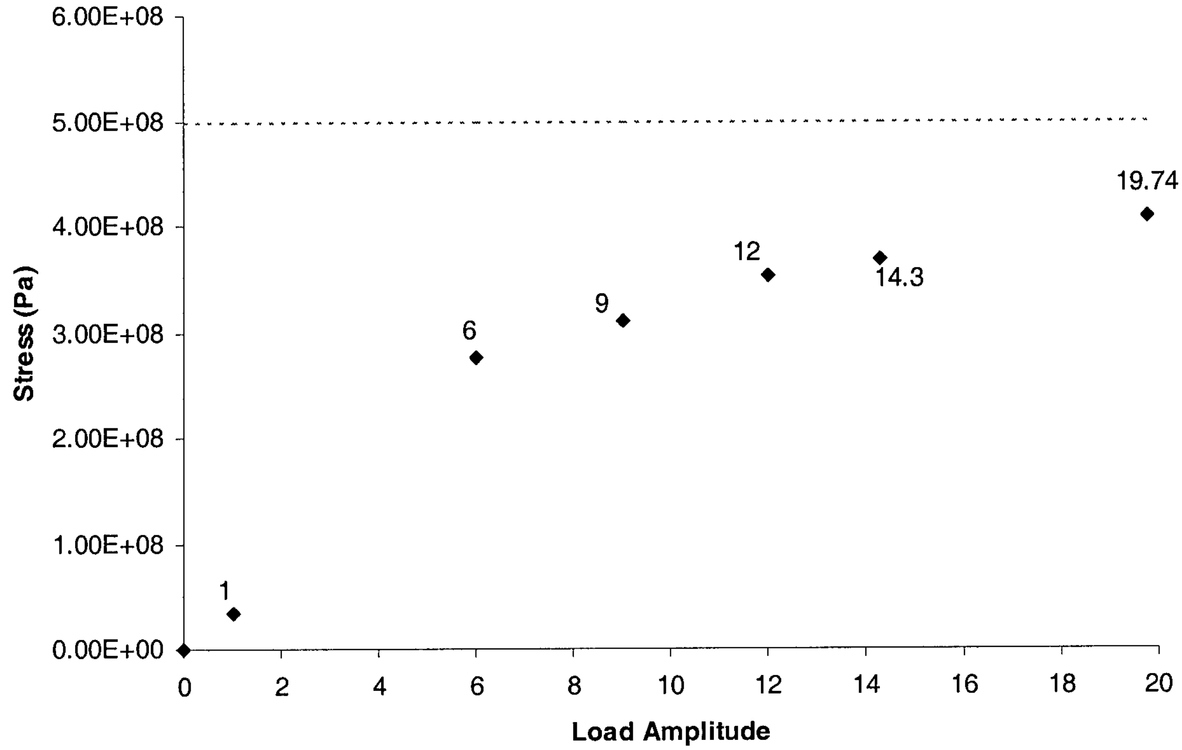

Figure 3.20 Results of Nonlinear Response Study

Recalling from Chapter 2, the von Karman assumption simplified the nonlinear analysis by eliminating certain terms. These terms were mainly rotation terms and terms related to the higher order dependency on in-plane displacements. Anytime terms are eliminated, error is introduced into the results. However, this error is sometimes accepted due to the benefit of the assumption. To accomplish a cost-benefit analysis of the von Karman assumption, a case must be run with the original terms included in the calculation. Figure 3.21 shows the results from analyses done with and without the von Karman assumption at load amplitudes of 1 and 14.3. The graphs on the left are the results using the von Karman assumption. These are compared to the corresponding nonlinear analysis graph on the right where the von Karman assumption is not utilized (full SLR theory).

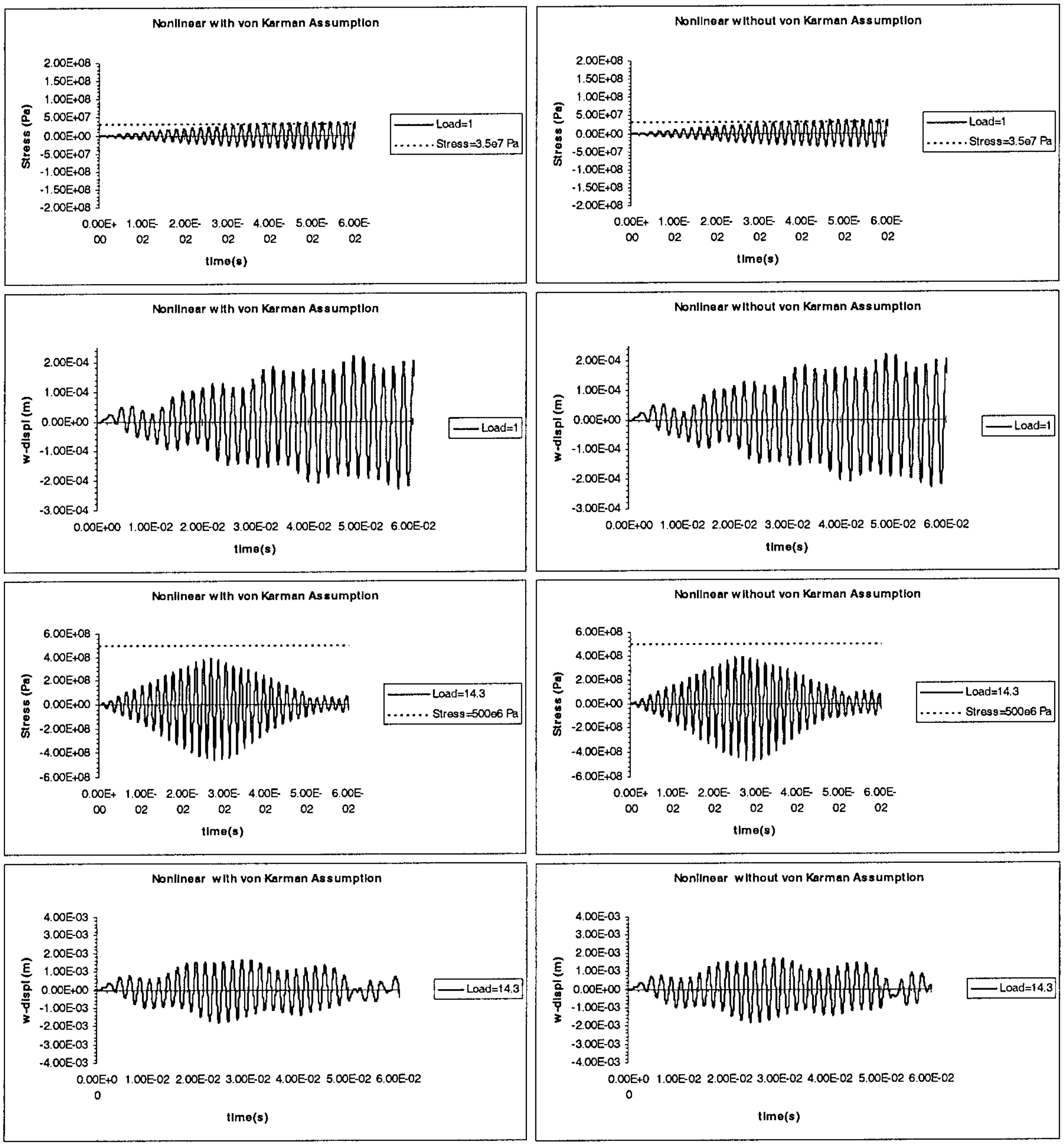

Figure 3.21 von Karman Affect on Analysis

The results are almost the same. Thus, the error cost of using the von Karman assumption is nearly zero. The benefit is found in computational time. With the von Karman assumption, the runs were taking approximately 24 hours. Without the von Karman assumption, the runs were taking almost 32 hours. Therefore, a cost-benefit analysis of the von Karman assumption indicates that the assumption should be used.

Since the analysis indicates a vibratory response, damping could be a very important factor. To illustrate the effect of damping on a solution, a dynamic analysis was done in which an impulse was applied to a plate and then suddenly stopped as shown in Figure 3.5. The response of the plate after the force is stopped is shown in Figure 3.22 for a mass proportional damping constant, β, of 0.09 (see chapter 2).

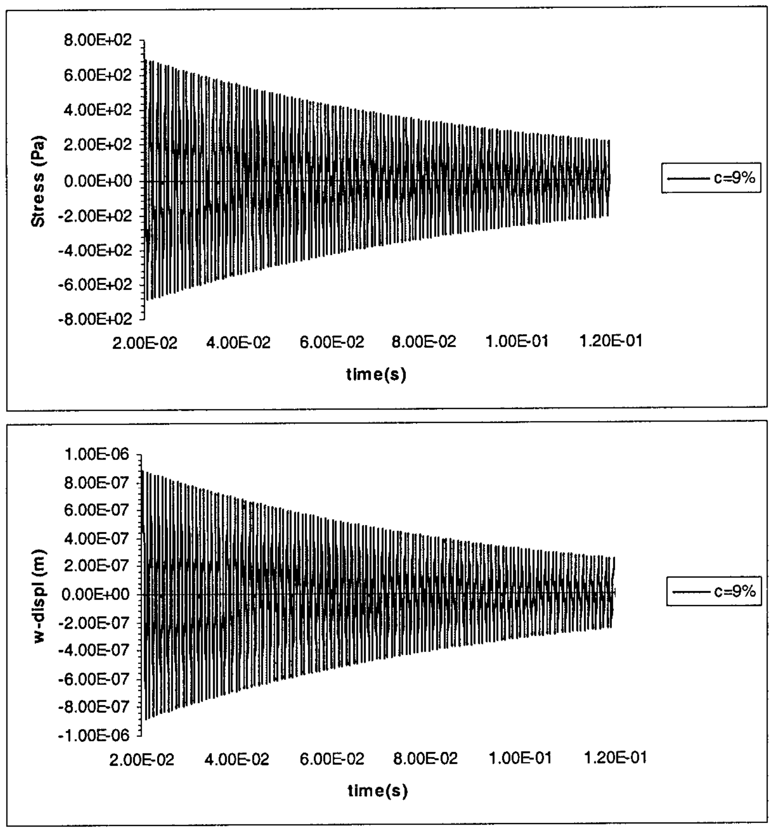

Figure 3.22 Dynamic Response of Square Plate to Stopped Impulse Load with β=9%

The analysis was repeated for a β value of 0.05. The result is shown in Figure 3.23.

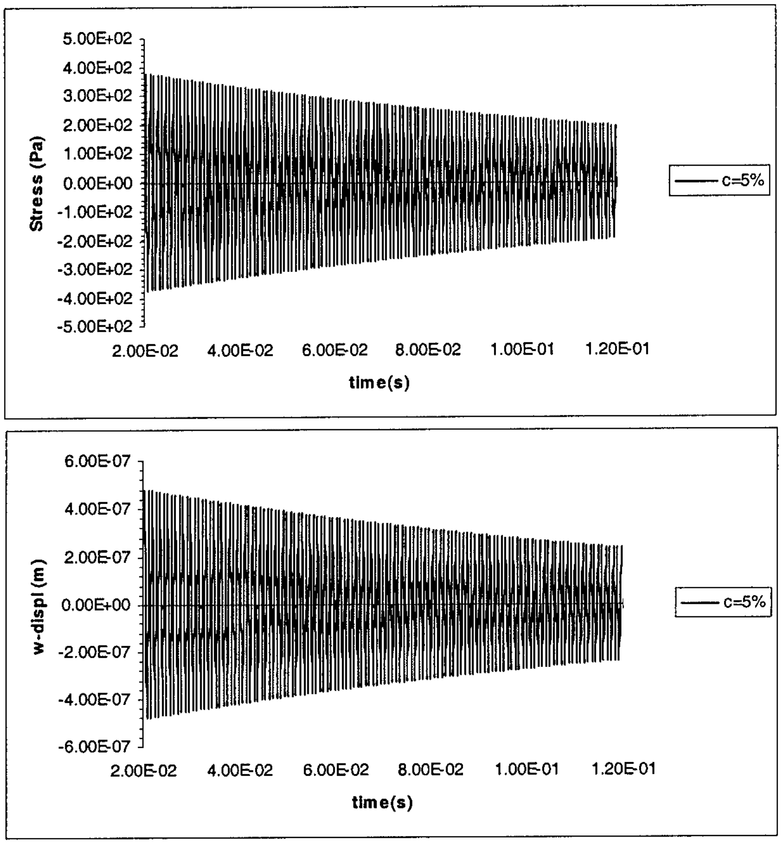

Figure 3.23 Dynamic Response of Square Plate to Stopped Impulse Load with β=5%

The damping diminishes the displacement and stress amplitudes over time. The higher the damping, the quicker the displacement and stress amplitudes are decreased. The effect of damping on the transient sinusoidal loading function analysis done previously is shown in Figure 3.24 for β values of 9% and 5%. When these results are compared to the previously discussed results, it becomes evident that damping does not have a noticeable effect on the analysis. The analysis, with or without damping, results in the same solutions with only a small error (less then 1 % difference). This is due to the fact that the loading function is sinusoidal and continual. The effect of the loading function dominates the reaction of the plate so the small damping contributions are negligible. It can be assumed that as long as β is less the 10%, the effects of damping are insignificant for this research. If β is larger then 10% (which is not very practical),

practical), its effects must be investigated since this is larger then the basic assumption made in Chapter 2, and could start to affect the solution both physically and/or numerically.

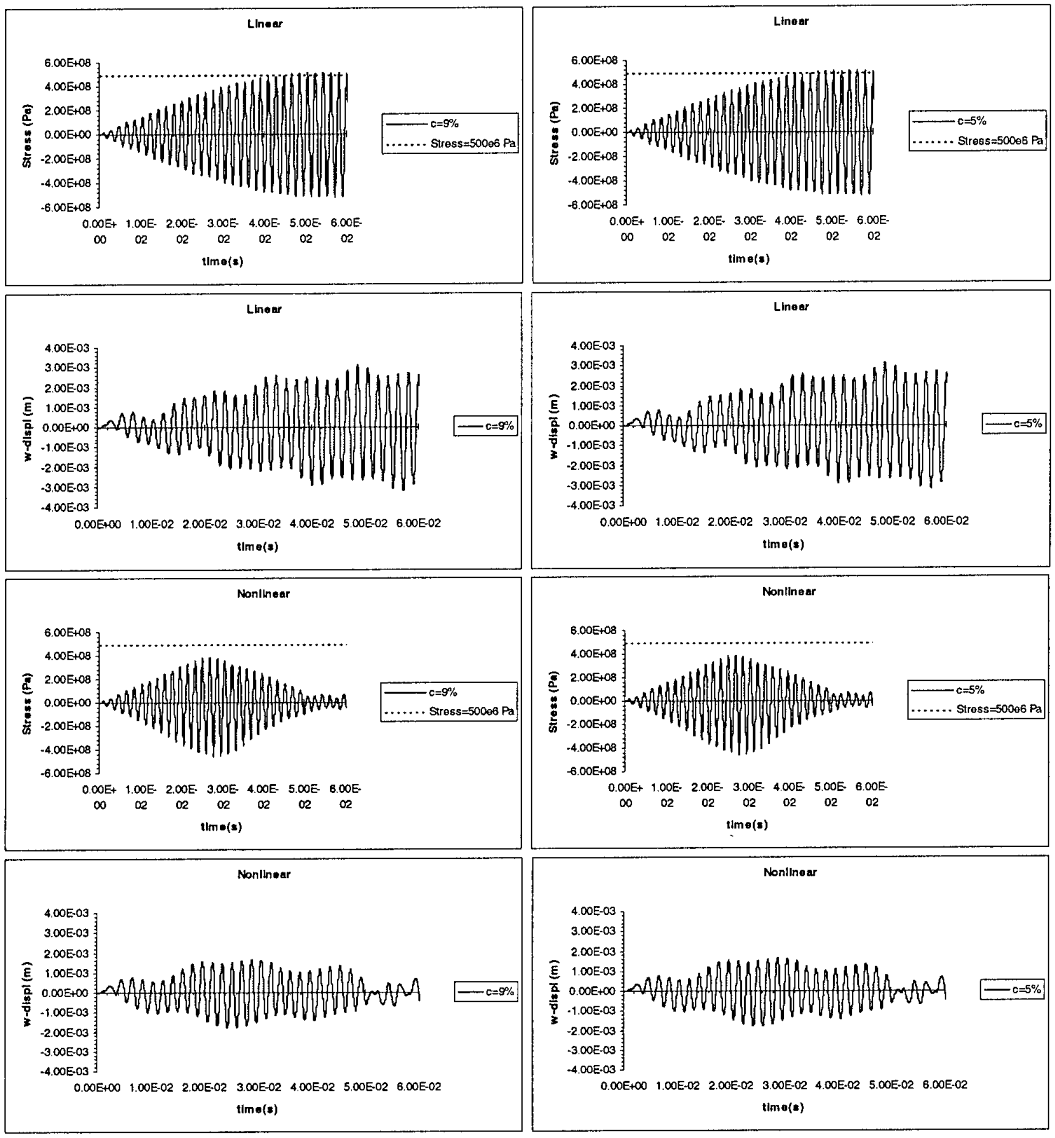

Figure 3.24 Dynamic Response of Square Plate including Damping

3.3.2 Trapezoid 1. The second geometry investigated was a trapezoid with a hub to tip ratio of 0.3 as shown in Figure 3.1. The mesh used for the trapezoid is shown in Figure 3.25. As previously shown in the mesh for the square plate, stress values are calculated at the Gaussian point, and displacement values are at the node in the center of the plate far from the boundary condition. The same boundary condition as earlier is used in which all seven degrees of freedom at the clamped end are fixed and held constant at zero. The initial conditions are also the same with zero initial displacement, velocity, and acceleration.

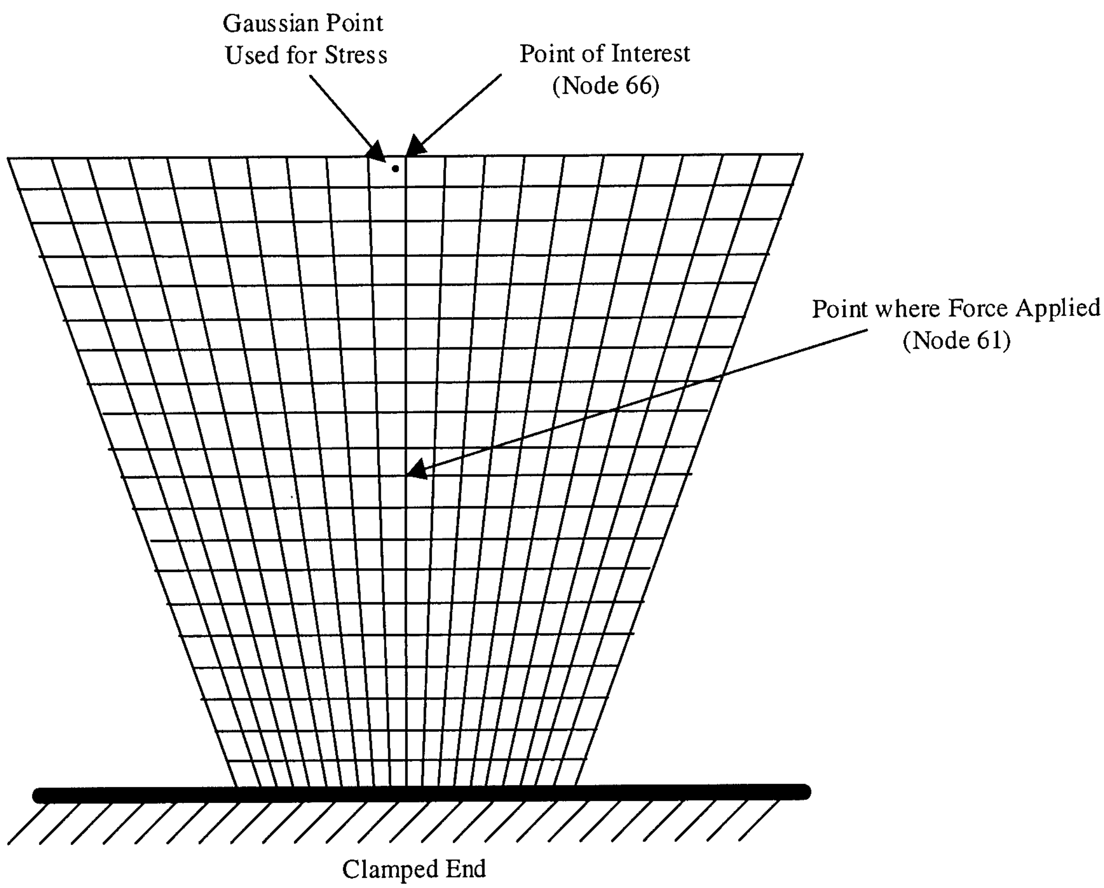

Figure 3.25 20x20 Mesh for Trapezoid 1

Before the trapezoid could be investigated, the code must be validated for this geometry. To accomplish this, a test case was run that modeled results given in (39). The same geometry was used as presented in Figure 3.25 except all four sides were clamped. This geometry is the most severe deviation from normal rectangular plates and therefore if proven to be correct, then trapezoid 2 and trapezoid 3 can also be investigeated with the code. The material properties for titanium were still used. A single point load in the center of the plate was applied and the static maximum displacement was calculated. DPLATE calculated the maximum displacement to be 0.0114mm. The results from (39) calculated the maximum displacement to be 0.0121mm. This leads to a 5% error in DPLATE's solution. This error can easily be explained by the fact that (39) does not take tranverse strain through the thickness into account but instead uses a lower-order theory. This leads to the conclusion that the code is adequate for trapezoidal shapes.

3.3.2.1 Eigensolution. An eigensolution is found for trapezoid 1. The mode shapes are examined and the frequency resulting in the mode shape concentrating the most energy at the center of the tip of the blade is chosen. The results of this eigensolution are shown in Figure 3.26. As in the square plate, mode 4 is chosen since it will concentrate the most energy at node 66. The results are very similar to the square plate, but the frequencies are much lower. The frequency needed to excite mode 4 is only 419.2 Hz, compared to the 528.9 Hz for the square plate. This can be explained by realizing that in the trapezoid, more mass has been concentrated far from the clamped end. Therefore, the inertia forces here are greater and cause the flapping reaction to come about much easier.

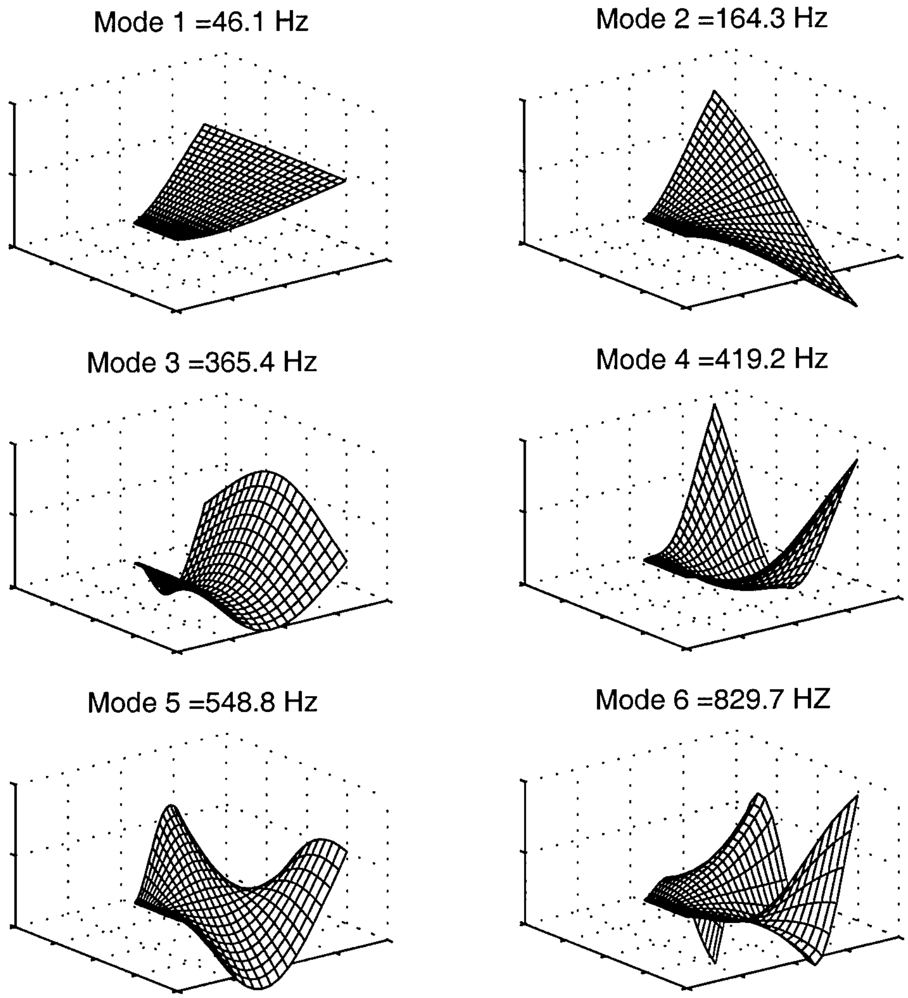

Figure 3.26 Trapezoid 1 Mode Shapes

<u>3.3.2.2 Transient Analysis.</u> A transient analysis similar to the one performed on the square plate is accomplished for trapezoid 1. The frequency used for this analysis according to the eigensolution should be 419.2 Hz. However, as in the square plate, when this frequency is used, resonance occurs. The frequency is exactly at the natural frequency of the plate. It is decided to increase the forcing frequency slightly to 430 Hz to allow the response to remain near the natural frequency, but far enough away so the resonance is not a problem.

The first case run with trapezoid 1 is with a loading amplitude equal to 1. A graphical representation of the forcing function is shown in Figure 3.27.

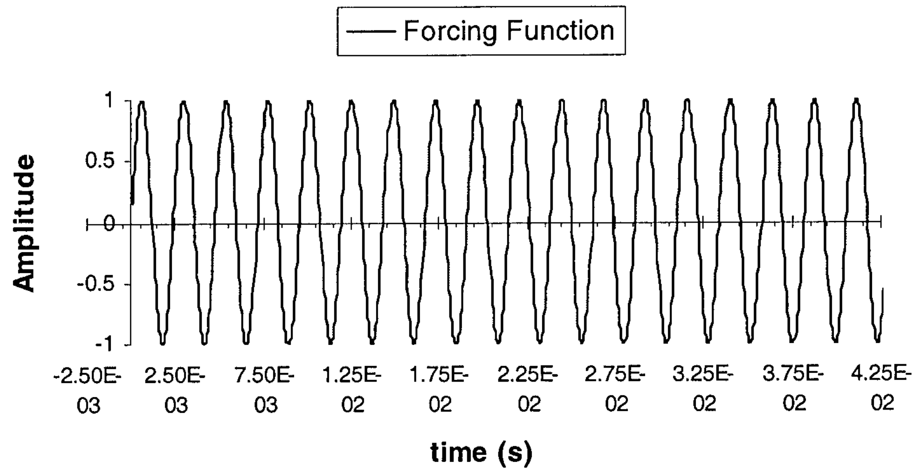

Figure 3.27 Trapezoid 1 Forcing Function

A linear analysis is done with this forcing function. The stress is calculated for the Gaussian point nearest to node 66 as shown earlier in Figure 3.25. The resulting stress of trapezoid 1 is shown in Figure 3.28. The same repeating pattern as seen for the square plate is seen again. Figure 3.28 shows the resulting stress for trapezoid up to 0.2 seconds. Though there appears to be two curves, there is actually only one curve. The rate at which the data is sampled and the printing ability of the printer are causing the appearance of a phantom curve of smaller amplitude. For convenience, the remaining graphs will only present data up to one half of the first cycle.

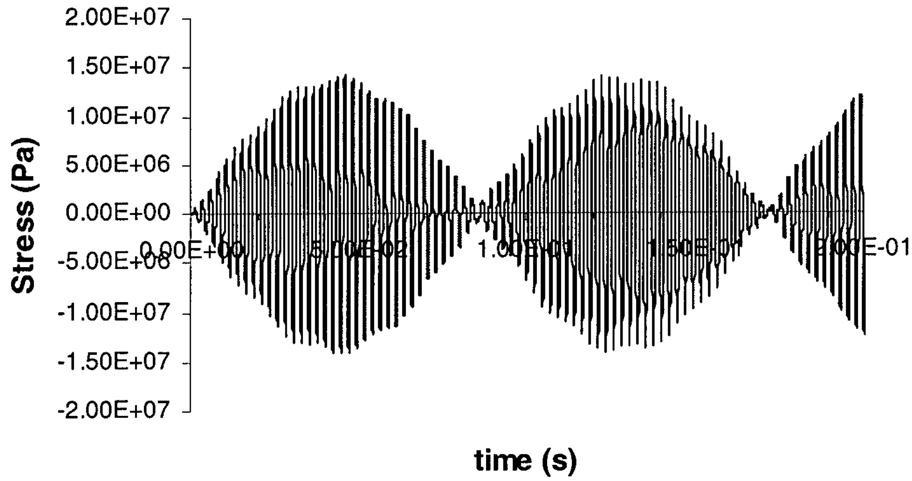

Figure 3.28 Stress at $\overline{F}=1$

The analysis is repeated for a forcing function amplitude of 3. The results for the two analyses are shown in Figure 3.29 allowing for their comparison.

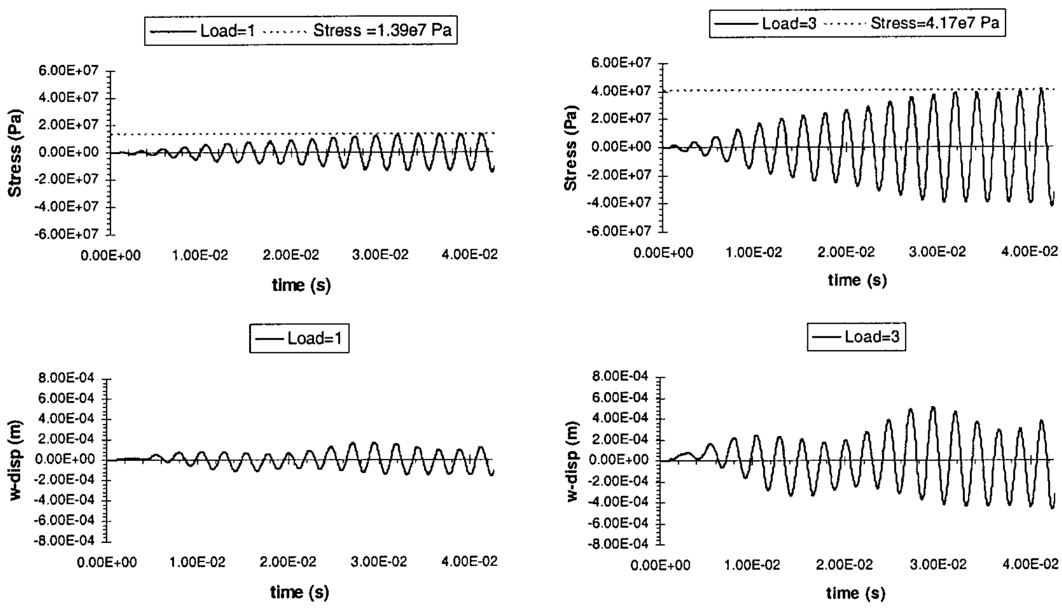

Figure 3.29 Linear Response of Trapezoid 1

As found in the square plate, a linear relationship exists between the loading function's amplitude and the maximum stress. When the loading amplitude was tripled, the resulting maximum stress was also tripled. Therefore, to arrive at the stress needed to initiate a crack, a loading amplitude is calculated. The stress needed is 500 MPa based on the Goodman diagram shown in Figure 3.14. The analysis leads to a predicted loading amplitude of 35.97 to initiate a crack. The result of the linear analysis with this predicted loading amplitude of 35.97 is shown in Figure 3.30. The sought after value of 500 MPa for maximum stress is realized, and thus the linear relationship between the loading amplitude and resulting maximum stress is accurate.

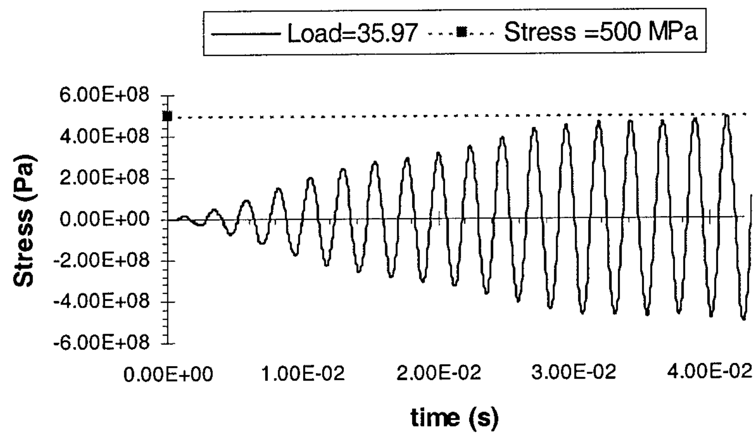

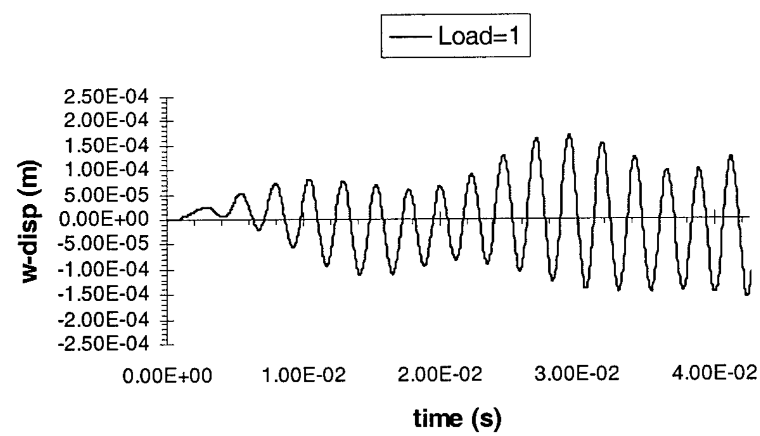

Figure 3.30 Linear Response of Trapezoid 1 with $\overline{F}$ =35.97

3.3.3 Trapezoid 2. The third geometry investigated was a trapezoid with a hub to tip ratio of 0.7 as shown in Figure 3.1. The mesh used for the trapezoid is shown in Figure 3.31. As previously shown, stress values are calculated at the Gaussian point, and displacement values are at the node in the center of the plate far from the boundary condition. The same boundary condition as earlier is used in which all seven degrees of freedom at the clamped end are fixed and held constant at zero. The initial conditions are also the same with zero initial displacement, velocity, and acceleration.

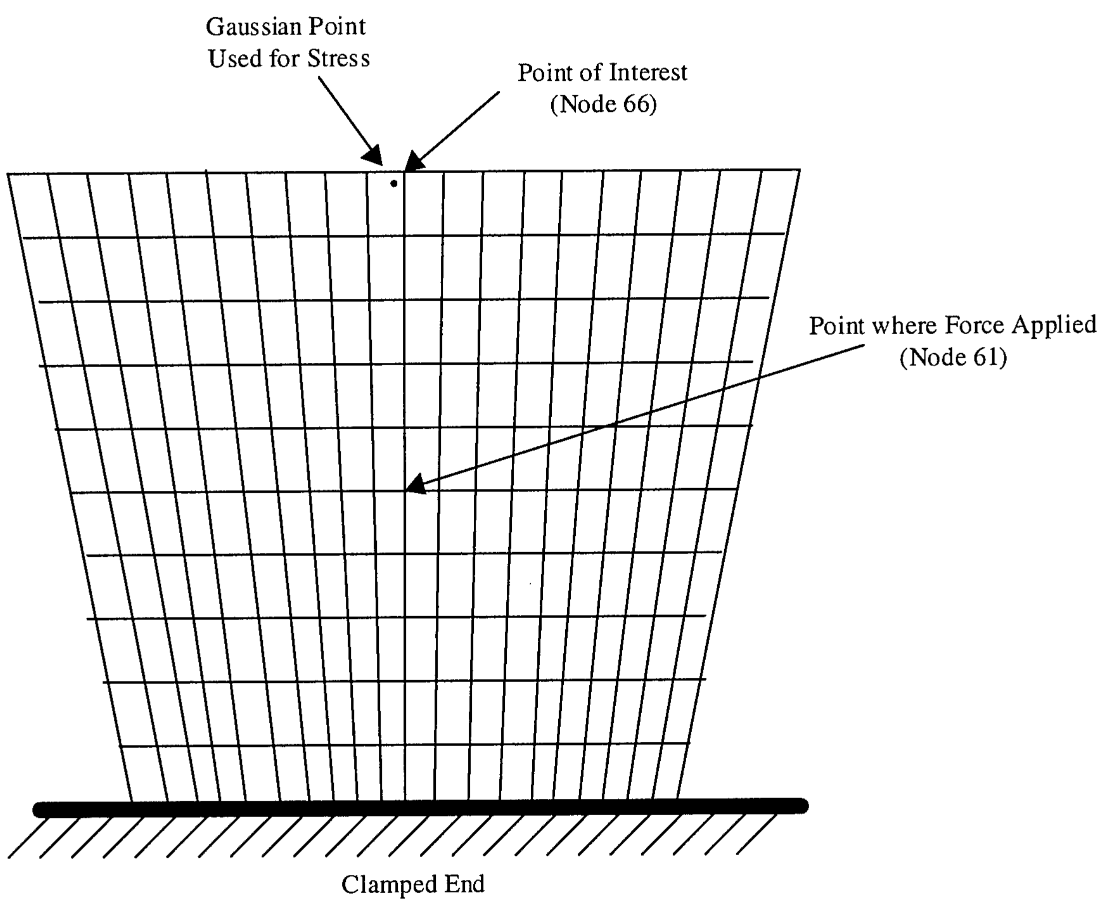

Figure 3.31 20x20 Mesh for Trapezoid 2

<u>3.3.3.1 Eigensolution.</u> An eigensolution is found for trapezoid 2. The mode shapes are examined and the frequency resulting in the mode shape predicted to concentrate the most

energy at the center of the tip of the blade is chosen. The results of this eigensolution are shown in Figure 3.32. As in the previous geometries, mode 4 is chosen since it will concentrate the most energy at node 66. The results are in between the results of the square plate and trapezoid 1 as expected since the geometry is in between the two. The frequency needed to excite mode 4 is only 467.6 Hz.

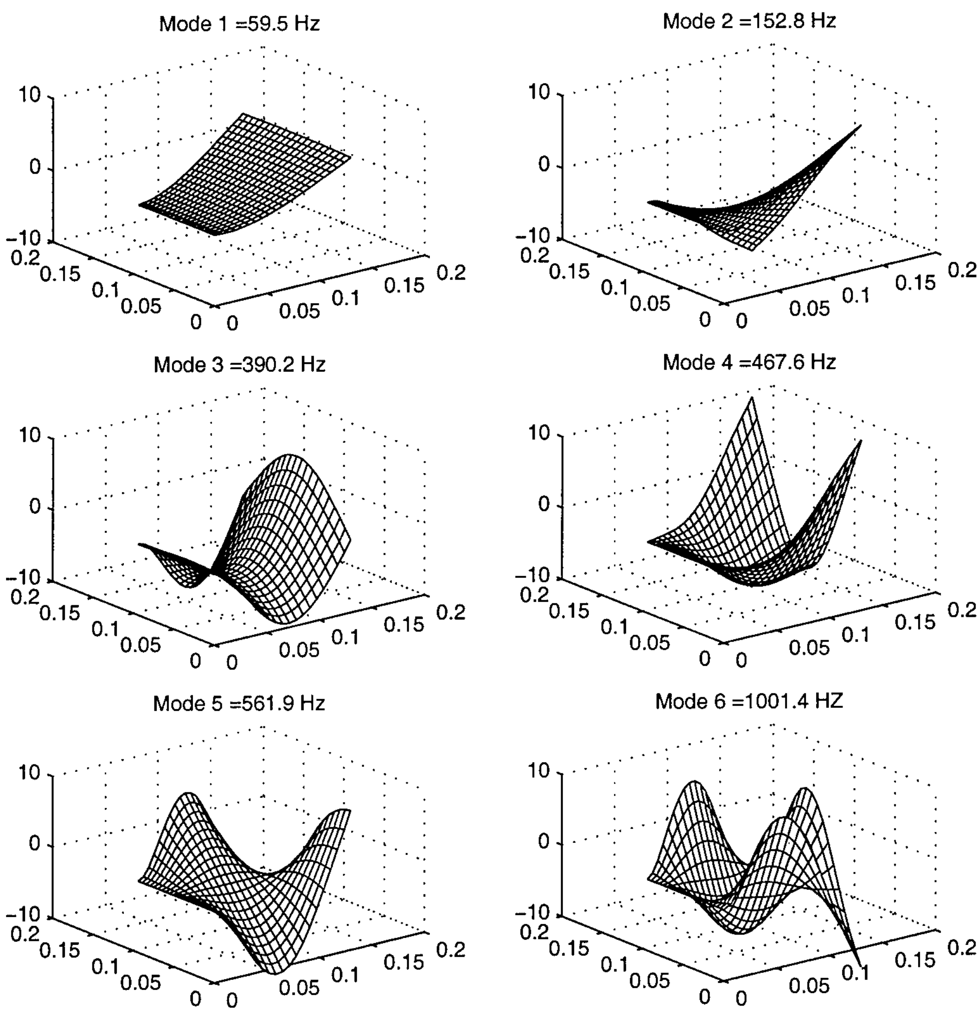

Figure 3.32 Trapezoid 2 Mode Shapes

3.3.3.2 Transient Analysis. A transient analysis similar to the one before is accomplished for trapezoid 2. The frequency used for this analysis according to the eigensolution should be 467.6

Hz. However, when this frequency is used, resonance occurs in this trapezoid like it did in the square plate and trapezoid 1. The frequency is exactly at the natural frequency of the plate. It is decided to increase the forcing frequency slightly to 478 Hz to allow the response to remain near the natural frequency, but far enough away the resonance is not a problem.

The first case run with trapezoid 2 is with a loading amplitude equal to 1. A graphical representation of the forcing function is shown in Figure 3.33.

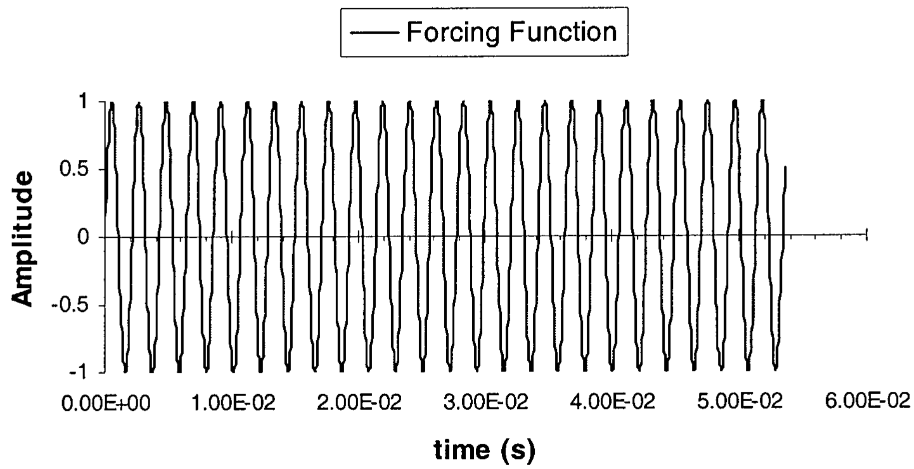

Figure 3.33 Trapezoid 2 Forcing Function

A linear analysis is done with this forcing function. The stress is calculated for the Gaussian point nearest to node 66 as shown earlier in Figure 3.31. Also, a linear analysis with a loading amplitude equal to 3. The results of these analyses for trapezoid 2 are shown in Figure 3.34. The same repeating pattern as seen before is seen again and therefore only the first half of the first cycle will be graphed.

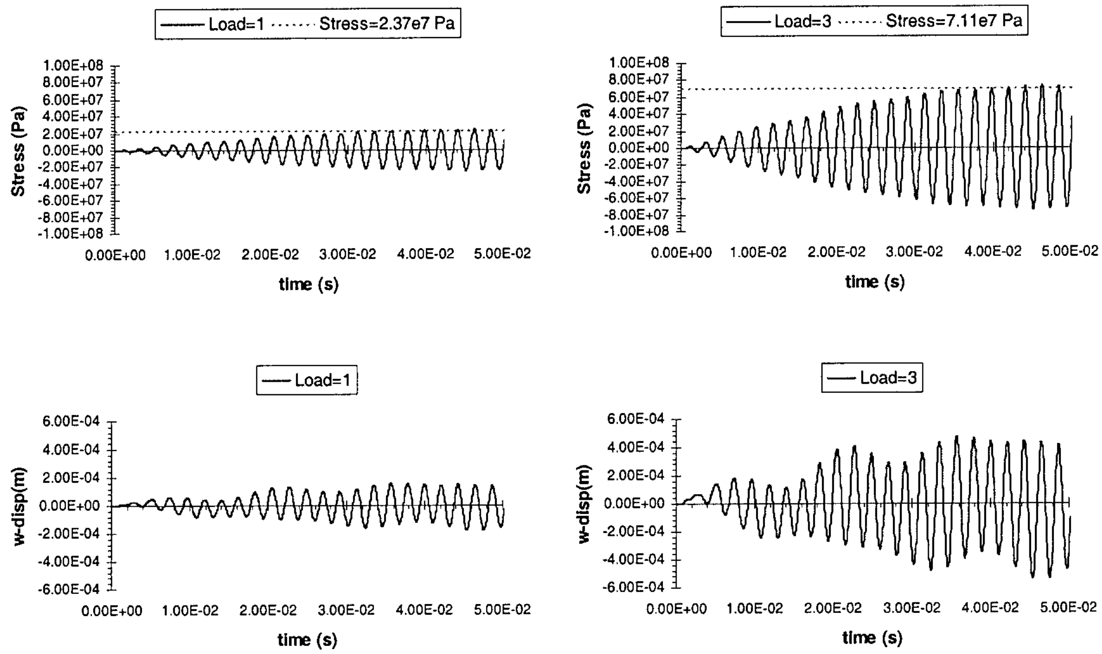

Figure 3.34 Linear Response of Trapezoid 2

As found in before, a linear relationship exists between the loading function's amplitude and the maximum stress. When the loading amplitude was 1, the maximum stress was 23.7 MPa. When the amplitude is tripled, the resulting is also tripled to 71.1 MPa. With this relationship and knowing what stress level is needed to initiate cracking, the loading amplitude needed to initiate cracks can be determined. The stress needed is 500 MPa based on the Goodman diagram shown in Figure 3.14. The analysis leads to a predicted loading amplitude of 21.1 to initiate a crack. The result of the linear analysis with this predicted loading amplitude of 21.1 is shown in Figure 3.35. Once again, the sought after value of 500 MPa for maximum stress is realized, and thus the linear relationship between the loading amplitude and resulting maximum stress is accurate.

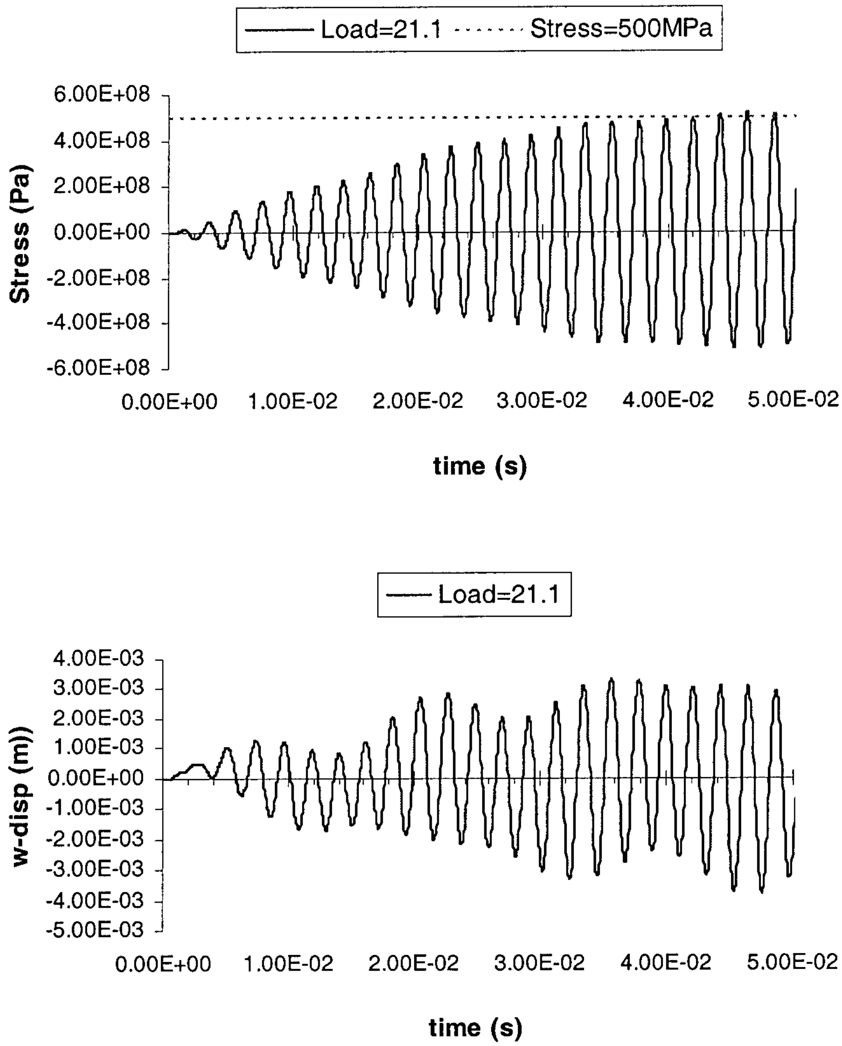

Figure 3.35 Linear Response of Trapezoid 2 with $\overline{F}$ =21.1

3.3.4 Trapezoid 3. The final geometry investigated is the inverse of trapezoid 1. This geometry was investigated to illustrate why it is better to have the longer length away from the clamped edge. The dimensions of the geometry can be found in Figure 3.1. The mesh used for this trapezoid is shown in Figure 3.36.

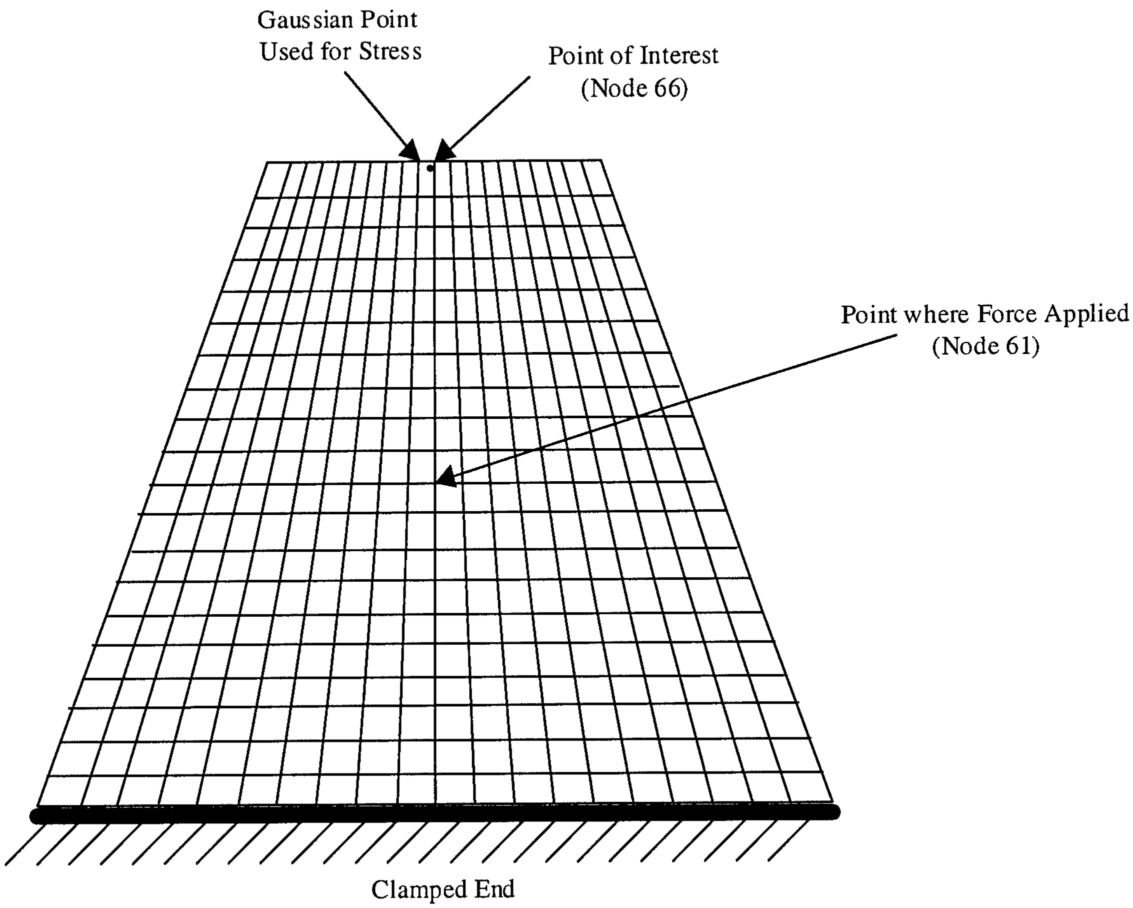

Figure 3.36 20x20 Mesh for Trapezoid 3

The eigensolution of this trapezoid indicates why this geometry would be a bad choice if the desired result was a shape that would have cracks initiating at the center of the tip. The mode shapes and frequencies are shown in Figure 3.37.

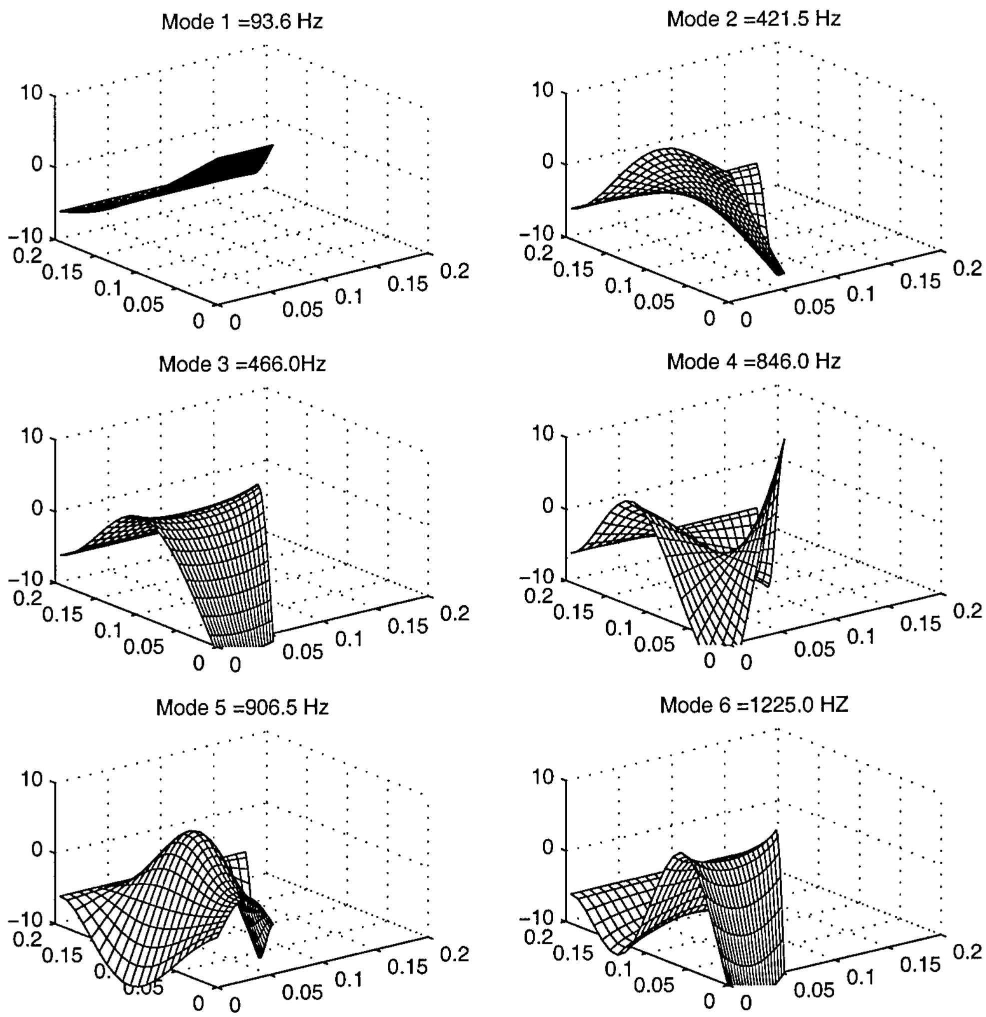

Figure 3.37 Trapezoid 3 Mode Shapes

The mode seen in the previous geometries that concentrated the energy at the point of interest is not brought about in the first six modes. Also, the frequencies are much higher. For example, Mode 2 for the square plate was 163.4 Hz. The 2nd mode for trapezoid 3 is 421.5 Hz. This is over a 250% increase in frequency for the same mode shape. Also, it is noted that the desired flapping mode shape does not occur. Mode 5 is similar, but will not result in the concentrated stress like before because some of the energy is being concentrated on the sides of the trapezoid as well as the tip. Because of the increase in frequencies and lack of the desired mode shape within the first 6 modes, this geometry was not investigated further.

3.3.5 Comparison of Results. With the results of the first three geometries, a comparison can be made and a trend developed to guide the optimization of the best shape to use in an experiment. Experiments are limited by the amount of loading amplitude as well as by the frequency it can operate at. Table 3.4 shows the frequency and load amplitude for the three geometries needed to cause a maximum stress large enough to initiate cracking.

Table 3.4 Comparison of Results for Three Geometries

Geometry	Frequency	Load Amplitude
Square 1	528.9	14.3
Trapezoid 1	419.2	35.97
Trapezoid 2	467.6	21.1

If the square plate is considered the reference condition, a %-change can be found by altering the geometry. This will indicate the trends and allow for a better choice of the proper geometry to be made. Table 3.5 shows the %-change of frequency and loading amplitude for trapezoid 1 and trapezoid 2. Trapezoid 1 decreases the needed frequency by 21%, but increases the needed loading amplitude by 152%. Trapezoid 2 decreases the frequency by 12%, but only increases the loading amplitude by 48%.

Table 3.5 %-Change in Frequency and Loading Amplitude

Geometry	Frequency % Change	Load Amplitude % Change
Trapezoid 1	-20.741161	151.5384615
Trapezoid 2	-11.590093	47.55244755

If frequency is the only factor being optimized, then the trend indicates that a trapezoid with the smallest hub-to-tip ratio should be used. If the loading amplitude is the only factor, then the results indicate the square plate should be used. Since an experiment is actually limited by both, a factor needs to be assigned to each based on their relative importance. As an example, it is decided that the frequency should drive 75% of the decision and the load amplitude should only drive 25%. This would indicate that the frequency is three times more crucial then the loading amplitude. A reference condition is chosen where the frequency is set at 100 Hz and the amplitude is set at 10. The results from the analyses for the different geometries are normalized based on this reference condition. Then the normalized values are multiplied by the factors of for frequency and for load amplitude. The result can be considered the weighted comparison value for the given geometry. Since the lowest frequency and loading amplitude is desired, the lowest weighted comparison value indicates the most ideal geometry. Table 3.6 shows the weighted comparison values for the three geometries for three different sets of factor schemes. The first case is the same as the example above where the frequency is three times as important as the loading amplitude. The second is when the two are equally important. Finally, the third case is when the loading amplitude is three times as important as the frequency.

Table 3.6 Weighted Comparison Values

Geometry	Normalized Frequency	Normalized Load Amplitude	Weighted Comparison Value		
			Case 1	Case 2	Case 3
Square 1	5.289	1.43	4.32425	3.3595	2.39475
Trapezoid 1	4.192	3.597	4.04325	3.8945	3.74575
Trapezoid 2	4.676	2.11	4.0345	3.393	2.7515

From Table 3.6, for case 1, trapezoid 2 would be the best choice, though trapezoid 1 is a very close second. For case 2, the best choice would be the square plate though trapezoid 2 is very close. For the final case, the square plate is the obvious choice by a much larger margin than the two previous cases. The actual factors for the analysis should be chosen based on the actual limitations of the experiment. These factors were chosen as an illustration.

IV. Conclusions

This research developed a tool that is useful to analyzing flat, isotropic plates for a high cycle fatigue analysis. The approach was based on numerous proven concepts including the SLR theory, beta-m method, Newton-Raphson iterative method, and the subspace iteration method. Some key conclusions can be drawn from this research:

1. Finite Element Methods are a useful tool to analyze the response of isotropic thin plates due to their ability to calculate displacement and stress at almost any point in the structure based on the mesh for any time during the loading. This is important to this research since the goal is to concentrate the stress at or near a single point. With the stress and displacement at this point known, an experiment can be done to confirm the results and test the accuracy of the model.
2. The code DPLATE is a working code that has been verified and is capable of an eigensolution analysis and a transient analysis. The transient analysis can be static or dynamic as well as linear or nonlinear.
3. When a nonlinear analysis is done, the result indicates that the plate is less stiff then a linear analysis, thus reducing the resulting maximum stress. This is extremely important to this research. Most finite element tools currently being used to predict maximum stress only use a linear analysis. This analysis over-predicts the maximum stress. If an experiment is set-up based on the results from a linear analysis, the loading amplitude may be too low and the plate stress needed to initiate cracks will never be realized.
4. A multiplier can be determined that describes the relationship between the loading amplitude and the resulting maximum stress. This multiplier would allow the loading

amplitude needed to initiate cracks to be determined and thereby allowing an experiment to be conducted at a proper amplitude to initiate cracks. This multiplier is linear if only a linear analysis in considered. However, it becomes a higher-order relationship for the nonlinear analysis.

5. This multiplier is not affected by the von Karman assumption that is utilized to shorten computation time. This is important since one goal of this research was to develop a tool that could be included in a topological optimization program. To accomplish this goal, the code must be as efficient as possible.
6. The multiplier is unaffected by damping if the damping matrix is limited to 10% of the mass matrix. If an experiment is run correctly (no extra wires or unnecessary connections), the material damping should be of greatest interest. This damping would be negligible as shown in this research.
7. It is possible to get a response with a displacement distribution that resembles a mode shape by modeling the plate with a point force that has a frequency near the natural frequency associated with the desired mode shape.
8. For a desired maximum stress, changing the geometry of the plate can alter the needed frequency and loading amplitude of a forcing function. To decrease the frequency, the bulk of the mass should be moved away from the clamped end. This was seen in trapezoid 1. However, this causes the loading amplitude to increase. To minimize the loading amplitude, an even distribution of the mass should be used as illustrated by the square plate. To optimize both of these parameters (frequency and loading amplitude) a weighting function must be determined that accounts for the relative importance of the parameters.

It would be beneficial to compare these results with results from experimentation. Also, more research is needed for the nonlinear multiplier. Other possible areas that can be examined include adding the ability to have a base motion loading condition in which the clamped end of the plate is vibrated at a certain frequency over a certain distance. This would better model an experiment. The results from this analysis could be compared to the results from the concentrated forcing function used in this research. Also, the addition of a graphical post-processor to the code would be beneficial by allowing for a faster analysis of the results. Finally, a study should be done on the effects of the thickness of the plates on the results. The trend from this research would be beneficial to the design of an optimization program.

It is recommended that this code be inserted into a topological optimization program that will try different geometries to find the best combination to minimize the required frequency and loading amplitude for a needed stress level. Then, the results from the program could be used to determine an experiment that will help give insight to the behavior of high cycle fatigue.

Appendix A: DPLATE Users Guide

The program used in this research is titled DPLATE. It is a Fortran 77 code. The code is run by initiating the executable file titled a.out. The program will ask for the name of the input file to be used. This input file is either created before or created by using a question/answer scenario. Enter the name of the input file. The computer will then ask if this is a new file. If the file exists, enter a 0 and the code will execute. If you want to create the file using the question/answer subroutine, enter a 1. The computer will ask for certain inputs. If you make a mistake, proceed and when the code begins to run, stop the computer. Open the input file and edit the mistake manually. The format of the input file is shown on the next page as Table A-1. The definition of the variables used is shown in Table A-2. The program outputs the information to three files. First is the OUTPUT.filename where filename is the name of the input file. This file echos your input. The next file is Billy.filename. This file outputs the displacement vectors. Finally, STRESS.filename output the stresses at the Gaussian points. The output can be modified to output only the desired data. For this research, the displacement of node 231 was of interest and the stress at the Gaussian point in element 200 nearest node 231 was needed. Therefore, the output was modified to show only these values. A sample input file is shown starting on pages A-6 and A-7. The OUTPUT.filename file is shown on pages A-8 to A-21. The Billy.filename file is shown on page A-22. Finally, the STRESS.filename is shown on page A-23.

Table A-1 Input File Format

Card1		TITLE							
Card2		MKXUNV	ISYMM	UXLIMT	MBXMAX	NOXPRT	UXDISP	UXVEL	UXACC
		UXSTRS	UXSTRN						
Card3		IEL	NPE	NANAL(1)	NANAL(2)	NANAL(3)	IMESH	NPRNT	NCUT
		MORD	NTIMES	NEIGN	DELT	NPRINT	NIMAX	NRESTR	NSTORE
Card4		THOUGH	CDAMP	METHOD	BETA0(1)	BETA0(2)	BETA0(3)		
Card5	if NANAL(1)=2	RSTEP							
	if NANAL(1)=0 or 1	INTYP	NINC	IMAX	IRES	TOL	RTOL		
Card6	if NANAL(1)=0 & INTYP=1	TABLE(1)	TABLE(2)	...	TABLE(NINC)				
	Else skip card								
Card7a	If IMESH=0	NEM	NNM	NX	NY				
Card8a	If IMESH=0	NOD(1,1)	NOD(1,2)	NOD(1,3)	NOD(1,4)	NOD(1,5)	NOD(1,6)	NOD(1,7)	NOD(1,8)
		NOD(2,1)	NOD(2,2)	NOD(2,3)	NOD(2,4)	NOD(2,5)	NOD(2,6)	NOD(2,7)	NOD(2,8)
		.	.	.	.	.	.	.	.
		.	.	.	.	.	.	.	.
		.	.	.	.	.	.	.	.
		NOD(NEM,1)	NOD(NEM,2)	NOD(NEM,3)	NOD(NEM,4)	NOD(NEM,5)	NOD(NEM,6)	NOD(NEM,7)	NOD(NEM,8)
Card9a	If IMESH=0	X(1)	Y(1)	X(2)	Y(2)	...	X(NNM)	Y(NNM)	
Card7b	If IMESH=1	NX	NY						
Card8b	If IMESH=1	DX(1)	DX(2)	...	DX(NPE*NX/4)				
Card9b	If IMESH=1	DY(1)	DY(2)	...	DY(NPE*NY/4)				
Card10	If NCUT>0	ICUT(1)	ICUT(2)	...	ICUT(NCUT)				
	If NCUT=0 Skip Card								
Card11		LD	PO						
Card12	If LD=3	NEDGE							
	Else skip card								
Card13	If LD=3	IEDGE(1)	IEDGE(2)	...	IEDGE(NEDGE)				
	Else skip card								
Card14		NBDY1							
Card15		NBOUND(1,1)	NBOUND(1,2)	NBOUND(1,3)	NBOUND(1,4)	NBOUND(1,5)	NBOUND(1,6)	NBOUND(1,7)	NBOUND(1,8)
		NBOUND(2,1)	NBOUND(2,2)	NBOUND(2,3)	NBOUND(2,4)	NBOUND(2,5)	NBOUND(2,6)	NBOUND(2,7)	NBOUND(2,8)
		.	.	.	.	.	.	.	.
		.	.	.	.	.	.	.	.
		.	.	.	.	.	.	.	.
		NBOUND(NBDY1,1)	NBOUND(NBDY1,2)	NBOUND(NBDY1,3)	NBOUND(NBDY1,4)	NBOUND(NBDY1,5)	NBOUND(NBDY1,6)	NBOUND(NBDY1,7)	NBOUND(NBDY1,8)
Card16		VBDY(1)	VBDY(2)	...	VBDY(NBDY)				
Card17		NBSF							
Card18	If NBSF>0	BSF(1)	BSF(2)	...	IBSF(NBSF)				
	IF NBSF=0 Skip Card								
Card19	If NBSF>0	VBSF(1)	VBSF(2)	...	VBSF(NBSF)				
	IF NBSF=0 Skip Card								
Card20	If NANAL(2)=1	EY	NU	HT					
	If NANAL(2)=0 or 2	E1	E2	G12	NU12	G13	G23		
Card21		IREST	INDIS	INVEL					
Card22		NFOR							
Card23	If NFOR>0	IFOR(1)	IFOR(2)		IFOR(NFOR)				
	If NFOR=0 Skip Card								
Card24		NSTRES							
Card25	If NSTRES>0	ISTRES(1)	ISTRES(2)		ISTRES(NFOR)				
	If NSTES=0 Skip Card								
Card26	If NTIMES=0	ILOAD	TIM1	TIM2	TIM3	TIM4			
	If NTIMES<>0	DLFACT(ii)							

Table A-2 Input Variables

Variable Names	Description
TITLE	Descriptive title that will appear as the first line on your data input file.
MKXUNV	=0 no universal file =1 universal file created
ISYMM	Used only for universal file =0 no symmetry, keep mesh as is =1 bilaterally symmetric mesh will be created
UXLIMT	=0 no limit to the size of the universal file =1 limit the size of the universal file to MBXMAX megabytes
MBXMAX	The maximum size of the universal file in megabytes
NOXPRT	=0 Stress data will be written to the output file =1 Stress data will not be written to the output file
UXDISP	=0 Displacement data will not be written to universal file =1 Displacement data will be written to the universal file
UXVEL	=0 Velocity data will not be written to universal file =1 Velocity data will be written to the universal file
UXACC	=0 Acceleration data will not be written to universal file =1 Acceleration data will be written to the universal file
UXSTRS	=0 Stress data will not be written to universal file =1 Stress data will be written to the universal file
UXSTRN	=0 Strain data will not be written to universal file =1 Strain data will be written to the universal file
IEL	=1 Plate elements =2 Shell elements
NPE	=4 Four-noded elements (4 corners) =8 Eight-noded elements (4 corners + 4 midside nodes)
NANAL(1)	=0 Nonlinear analysis =1 Linear analysis =2 Bifurcation analysis
NANAL(2)	=0 Arbitrary laminate =1 Isotropic material =2 Symmetric laminate
NANAL(3)	=0 von Karman Plate/ Donnell Shell Assumptions will not be used =1 von Karman Plate/ Donnell Shell Assumptions will be used
IMESH	=0 User defined mesh =1 Computer generated mesh (Preferred method)
NPRNT	=0 Elasticity arrays will not be printed to output file =1 Elasticity arrays will be printed to output file
NCUT	Number of elements eliminated to model a cutout in the structure. If there are no cutouts, then enter 0
MORD	Beta-m method order. Set equal to 2.
NTIMES	=0 Load factor will be based on a function (sine, step, multistep) (preferred) =1 Load factor will be based on discrete data points entered by user(AVOID)
NEIGN	Number of natural frequencies to calculate. If transient analysis is wanted, set equal to 0.
DELT	The time increment.
NPRINT	=0 The elemental stiffness matricies will not be printed to output file =1 The elemental stiffness matricies will be printed to output file

NIMAX	Set equal to 0
NRESTR	=0 No restart option =1 Restart option
NSTORE	Number of steps to store for restart
THOUGH	Mass density in consistent units (BE CAREFUL ON UNITS!!!)
CDAMP	Damping factor
METHOD	Set equal to 0. Only option.
BETA0(1)	Set equal to 0.5
BETA0(2)	Set equal to 0.5
BETA0(3)	Set equal to 1.0
RSTEP	Step used for Bifurcation analysis
INTYP	=0 Load Control =1 Displacement Control
NINC	Number of load or displacement increments
IMAX	Maximum iterations performed to try and reach convergence before the program halts.
IRES	=0 Update stiffness matrix after each iterations =1 Update stiffness matrix after each increment
TOL	Convergence criteria in percentage (I.e. 0.1 = .1% = .001)
RTOL	Convergence tolerance on eigenvalues (1.00e-6 or smaller)
TABLE(m)	Table of multipliers for displacement specified input where m=1..NINC
NEM	Total number of elements
NNM	Total number of nodes
NX	Number of elements in the x-direction
NY	Number of elements in the y-direction
NOD(m,n)	Connectivity array where m=1..NEM and n=1..NPE These values should be entered by starting at the corner node with the smallest x,y coordinate. Then go to the remaining three corner nodes in a clockwise rotation. If there are midside nodes, start with the midside node with the smallest y coord, and then go clockwise to the remaining three nodes.
X(m)	X-coordinate of node m where m=1..NNM
Y(m)	Y-coordinate of node m where m=1..NNM
DX(m)	Distance between nodes in x direction where m=1..(NPE*NX/4)
DY(m)	Distance between nodes in y direction where m=1..(NPE*NY/4)
ICUT(m)	Array of element numbers deleted to model cutout where m=1..NCUT
LD	Structural Load Parameter =0 No Load =1 Transverse or normal load =2 Dead weight =3 Axial load
PO	Distributed load intensity. Enter 0.0 if there is no distributed load.
NEDGE	Number of nodes with in-plane loading
IEDGE(m)	Array of nodes where there in-plane loading is applied where m=1..NEDGE
NBDY1	Number of nodes with specified degrees of freedom

NBOUND(ii,jj)	Specifies which degrees of freedom are fixed. _ii=1..NBDY1 jj=1..8 where the first value is the node number. Then comes the degrees of freedom u v w w,x w,y psi,x psi,y A 1 is entered if the degree of freedom is fixed and a 0 is entered if the degree of freedom is free. Remember, midside nodes can only have u and v fixed, all other must be entered as zeros.
VBDY(m)	The prescribed displacement values for the degrees of freedom called out in NBOUND. Usually, this is just an array with a 0.0 for every 1 entered into NBOUND
NBSF	Number of degrees of freedom with specified loads
IBSF(m)	Array of degree of freedom numbers with specified loads where m=1..NBSF
VBSF(m)	Array of the values of the specified loads applied to the degree of freedoms where m=1.. NBSF
EY	Youngs Modulus (for isotropic material)
NU	Poisson's Ratio (for isotropic material)
HT	Thickness of plate/shell (for isotropic material)
E1	Young's Modulus in fiber direction (composite materials)
E2	Young's Modulus perpendicular to fiber direction (composite materials)
G12	Shear Modulus in 12-plane (composite materials)
NU12	Poisson's Ration in 12-plane (composite materials)
G13	Shear Modulus in 13-plane (composite materials)
G23	Shear Modulus in 23-plane (composite materials)
IREST	=0 Zero initial displacement and velocity =1 Nonzero initial displacement and velocity
INDIS	=0 Uniform initial displacement =1 non-uniform initial displacement =2 initial displacement input by continuous function
INVEL	=0 Uniform initial velocity =1 non-uniform initial velocity =2 initial velocity input by continuous function
NFOR	Number of nodal forces to be calculated at end of each increment
IFOR(m)	Array of degrees of freedom numbers to calculate the nodal forces where m=1..NFOR
NSTRES	Number of elements to calculate stress/strain data at the at end of each increment.
ISTRES(m)	Array of element numbers to calculate stress/strain data at the end of each increment where m=1..NSTRES
ILOAD	=1 Single step loading =2 Sinusoidal loading =3 Multi-Step Loading
TIM1	If ILOAD=1 Time to reach max loading If ILOAD=2 Time for half sine wave If ILOAD=3 Time to reach max loading for first step
TIM2	If ILOAD=1 or 2 Time when loading ends If ILOAD=3 Time to reach max loading for second step
TIM3	If ILOAD=1 or 2 Dummy variable, set equal to zero If ILOAD=3 Time to reach max loading for third step
TIM4	If ILOAD=1 or 2 Dummy variable, set equal to zero If ILOAD=3 Time to reach max loading for fourth step
DLFACT(ii)	Loading factor in discrete data points where ii=1 (AVOID USING THIS)

```
Square Titanium Plate, Linear, No Damping, 4 Noded, Von Karman
0,0,0,1,0,0,0,0,0,0
1,4,1,1,1,1,0,0,2,0,0,4.73e-5,0,0,0,0
4430,0.0,1,0.5,0.5,1.0
0,2115,500,0,.01,1.0e-6
20,20
.005715,.005715,.005715,.005715,.005715,
.005715,.005715,.005715,.005715,.005715,
.005715,.005715,.005715,.005715,.005715,
.005715,.005715,.005715,.005715,.005715
.005715,.005715,.005715,.005715,.005715,
.005715,.005715,.005715,.005715,.005715,
.005715,.005715,.005715,.005715,.005715,
.005715,.005715,.005715,.005715,.005715
0,0.
21
1,1,1,1,1,1,1,1
22,1,1,1,1,1,1,1
43,1,1,1,1,1,1,1
64,1,1,1,1,1,1,1
85,1,1,1,1,1,1,1
106,1,1,1,1,1,1,1
127,1,1,1,1,1,1,1
148,1,1,1,1,1,1,1
169,1,1,1,1,1,1,1
190,1,1,1,1,1,1,1
211,1,1,1,1,1,1,1
232,1,1,1,1,1,1,1
253,1,1,1,1,1,1,1
274,1,1,1,1,1,1,1
295,1,1,1,1,1,1,1
316,1,1,1,1,1,1,1
337,1,1,1,1,1,1,1
358,1,1,1,1,1,1,1
379,1,1,1,1,1,1,1
400,1,1,1,1,1,1,1
421,1,1,1,1,1,1,1
0.,0.,0.,0.,0.,0.,0.,0.,0.,0.,
0.,0.,0.,0.,0.,0.,0.,0.,0.,0.,
0.,0.,0.,0.,0.,0.,0.,0.,0.,0.,
0.,0.,0.,0.,0.,0.,0.,0.,0.,0.,
0.,0.,0.,0.,0.,0.,0.,0.,0.,0.,
0.,0.,0.,0.,0.,0.,0.,0.,0.,0.,
0.,0.,0.,0.,0.,0.,0.,0.,0.,0.,
0.,0.,0.,0.,0.,0.,0.,0.,0.,0.,
0.,0.,0.,0.,0.,0.,0.,0.,0.,0.,
0.,0.,0.,0.,0.,0.,0.,0.,0.,0.,
0.,0.,0.,0.,0.,0.,0.,0.,0.,0.,
0.,0.,0.,0.,0.,0.,0.,0.,0.,0.,
0.,0.,0.,0.,0.,0.,0.,0.,0.,0.,
0.,0.,0.,0.,0.,0.,0.,0.,0.,0.,
0.,0.,0.,0.,0.,0.,0.
1
```

```
1543
1.000
1.14e11,.33,.001016
0,0,0
0
1
200
2,9.433962e-4,2,0.,0.
```

Square Titanium Plate, Linear, No Damping, 4 Noded, Von Karman

MASS DENSITY = 0.443000E+04
DAMPING COEFFICIENT = 0.000000E+00
METHOD = 1
NUMBER OF LOWEST MODES CALCULATED = 0
BETA PARAMETERS (USED IN BETA-M METHOD) = 0.500E+00 0.500E+00 0.100E+01

ELEMENT TYPE(1=PLATE, 2=CYL SHELL) = 1   NODES PER ELEMENT= 4
ORDER OF BETA-M METHOD = 2
NTIMES = 0
TIME INCREMENT = 0.4730000E-04

NUMBER OF ELEMENTS IN THE MESH =400
NUMBER OF NODES IN THE MESH = 441
DOF PER NODE = 7

DISPLACEMENT BOUNDARY CONDITIONS, 1=PRESCRIBED, 0=FREE

NODE	U	V	W	W-X	W-S	PSI-X	PSI-S
1	1	1	1	1	1	1	1
22	1	1	1	1	1	1	1
43	1	1	1	1	1	1	1
64	1	1	1	1	1	1	1
85	1	1	1	1	1	1	1
106	1	1	1	1	1	1	1
127	1	1	1	1	1	1	1
148	1	1	1	1	1	1	1
169	1	1	1	1	1	1	1
190	1	1	1	1	1	1	1
211	1	1	1	1	1	1	1
232	1	1	1	1	1	1	1
253	1	1	1	1	1	1	1
274	1	1	1	1	1	1	1
295	1	1	1	1	1	1	1
316	1	1	1	1	1	1	1
337	1	1	1	1	1	1	1
358	1	1	1	1	1	1	1
379	1	1	1	1	1	1	1
400	1	1	1	1	1	1	1
421	1	1	1	1	1	1	1

NUMBER OF PRESCRIBED DISPLACEMENTS= 147
SPECIFED DISPLACEMENT DOF AND THEIR VALUES FOLLOW:
1 2 3 4 5 6 7 148 149 150 151 152 153 154 295 296
297 298 299 300 301 442 443 444 445 446 447 448 589 590 591 592
593 594 595 736 737 738 739 740 741 742 883 884 885 886 887 888
889 1030 1031 1032 1033 1034 1035 1036 1177 1178 1179 1180 1181 1182 1183 1324
1325 1326 1327 1328 1329 1330 1471 1472 1473 1474 1475 1476 1477 1618 1619 1620
1621 1622 1623 1624 1765 1766 1767 1768 1769 1770 1771 1912 1913 1914 1915 1916
1917 1918 2059 2060 2061 2062 2063 2064 2065 2206 2207 2208 2209 2210 2211 2212
2353 2354 2355 2356 2357 2358 2359 2500 2501 2502 2503 2504 2505 2506 2647 2648
2649 2650 2651 2652 2653 2794 2795 2796 2797 2798 2799 2800 2941 2942 2943 2944
2945 2946 2947
0.00000D+00 0.00000D+00 0.00000D+00 0.00000D+00 0.00000D+00 0.00000D+00 0.00000D+00 0.00000D+00
0.00000D+00 0.00000D+00 0.00000D+00 0.00000D+00 0.00000D+00 0.00000D+00 0.00000D+00 0.00000D+00
0.00000D+00 0.00000D+00 0.00000D+00 0.00000D+00 0.00000D+00 0.00000D+00 0.00000D+00 0.00000D+00
0.00000D+00 0.00000D+00 0.00000D+00 0.00000D+00 0.00000D+00 0.00000D+00 0.00000D+00 0.00000D+00
0.00000D+00 0.00000D+00 0.00000D+00 0.00000D+00 0.00000D+00 0.00000D+00 0.00000D+00 0.00000D+00
0.00000D+00 0.00000D+00 0.00000D+00 0.00000D+00 0.00000D+00 0.00000D+00 0.00000D+00 0.00000D+00
0.00000D+00 0.00000D+00 0.00000D+00 0.00000D+00 0.00000D+00 0.00000D+00 0.00000D+00 0.00000D+00
0.00000D+00 0.00000D+00 0.00000D+00 0.00000D+00 0.00000D+00 0.00000D+00 0.00000D+00 0.00000D+00
0.00000D+00 0.00000D+00 0.00000D+00 0.00000D+00 0.00000D+00 0.00000D+00 0.00000D+00 0.00000D+00
0.00000D+00 0.00000D+00 0.00000D+00 0.00000D+00 0.00000D+00 0.00000D+00 0.00000D+00 0.00000D+00
0.00000D+00 0.00000D+00 0.00000D+00 0.00000D+00 0.00000D+00 0.00000D+00 0.00000D+00 0.00000D+00
0.00000D+00 0.00000D+00 0.00000D+00 0.00000D+00 0.00000D+00 0.00000D+00 0.00000D+00 0.00000D+00
0.00000D+00 0.00000D+00 0.00000D+00 0.00000D+00 0.00000D+00 0.00000D+00 0.00000D+00 0.00000D+00
0.00000D+00 0.00000D+00 0.00000D+00 0.00000D+00 0.00000D+00 0.00000D+00 0.00000D+00 0.00000D+00
0.00000D+00 0.00000D+00 0.00000D+00 0.00000D+00 0.00000D+00 0.00000D+00 0.00000D+00 0.00000D+00

0.00000D+00	0.00000D+00	0.00000D+00	0.00000D+00	0.00000D+00	0.00000D+00	0.00000D+00	0.00000D+00
0.00000D+00	0.00000D+00	0.00000D+00	0.00000D+00	0.00000D+00	0.00000D+00	0.00000D+00	0.00000D+00
0.00000D+00	0.00000D+00	0.00000D+00	0.00000D+00	0.00000D+00	0.00000D+00	0.00000D+00	0.00000D+00
0.00000D+00	0.00000D+00	0.00000D+00					

NUMBER OF SPECIFIED FORCES= 1
SPECIFIED FORCE DEGREES OF FREEDOM AND THEIR SPECIFIED VALUES FOLLOW:
1543
0.10000D+01

BOOLEAN (CONNECTIVITY) MATRIX-NOD(I,J)

1	1	2	23	22
2	2	3	24	23
3	3	4	25	24
4	4	5	26	25
5	5	6	27	26
6	6	7	28	27
7	7	8	29	28
8	8	9	30	29
9	9	10	31	30
10	10	11	32	31
11	11	12	33	32
12	12	13	34	33
13	13	14	35	34
14	14	15	36	35
15	15	16	37	36
16	16	17	38	37
17	17	18	39	38
18	18	19	40	39
19	19	20	41	40
20	20	21	42	41
21	22	23	44	43
22	23	24	45	44
23	24	25	46	45
24	25	26	47	46
25	26	27	48	47
26	27	28	49	48
27	28	29	50	49
28	29	30	51	50
29	30	31	52	51
30	31	32	53	52
31	32	33	54	53
32	33	34	55	54
33	34	35	56	55
34	35	36	57	56
35	36	37	58	57
36	37	38	59	58
37	38	39	60	59
38	39	40	61	60
39	40	41	62	61
40	41	42	63	62
41	43	44	65	64
42	44	45	66	65
43	45	46	67	66
44	46	47	68	67
45	47	48	69	68
46	48	49	70	69
47	49	50	71	70
48	50	51	72	71
49	51	52	73	72
50	52	53	74	73
51	53	54	75	74
52	54	55	76	75
53	55	56	77	76
54	56	57	78	77
55	57	58	79	78
56	58	59	80	79
57	59	60	81	80
58	60	61	82	81

59	61	62	83	82
60	62	63	84	83
61	64	65	86	85
62	65	66	87	86
63	66	67	88	87
64	67	68	89	88
65	68	69	90	89
66	69	70	91	90
67	70	71	92	91
68	71	72	93	92
69	72	73	94	93
70	73	74	95	94
71	74	75	96	95
72	75	76	97	96
73	76	77	98	97
74	77	78	99	98
75	78	79	100	99
76	79	80	101	100
77	80	81	102	101
78	81	82	103	102
79	82	83	104	103
80	83	84	105	104
81	85	86	107	106
82	86	87	108	107
83	87	88	109	108
84	88	89	110	109
85	89	90	111	110
86	90	91	112	111
87	91	92	113	112
88	92	93	114	113
89	93	94	115	114
90	94	95	116	115
91	95	96	117	116
92	96	97	118	117
93	97	98	119	118
94	98	99	120	119
95	99	100	121	120
96	100	101	122	121
97	101	102	123	122
98	102	103	124	123
99	103	104	125	124
100	104	105	126	125
101	106	107	128	127
102	107	108	129	128
103	108	109	130	129
104	109	110	131	130
105	110	111	132	131
106	111	112	133	132
107	112	113	134	133
108	113	114	135	134
109	114	115	136	135
110	115	116	137	136
111	116	117	138	137
112	117	118	139	138
113	118	119	140	139
114	119	120	141	140
115	120	121	142	141
116	121	122	143	142
117	122	123	144	143
118	123	124	145	144
119	124	125	146	145
120	125	126	147	146
121	127	128	149	148
122	128	129	150	149
123	129	130	151	150
124	130	131	152	151
125	131	132	153	152
126	132	133	154	153
127	133	134	155	154
128	134	135	156	155

129	135	136	157	156
130	136	137	158	157
131	137	138	159	158
132	138	139	160	159
133	139	140	161	160
134	140	141	162	161
135	141	142	163	162
136	142	143	164	163
137	143	144	165	164
138	144	145	166	165
139	145	146	167	166
140	146	147	168	167
141	148	149	170	169
142	149	150	171	170
143	150	151	172	171
144	151	152	173	172
145	152	153	174	173
146	153	154	175	174
147	154	155	176	175
148	155	156	177	176
149	156	157	178	177
150	157	158	179	178
151	158	159	180	179
152	159	160	181	180
153	160	161	182	181
154	161	162	183	182
155	162	163	184	183
156	163	164	185	184
157	164	165	186	185
158	165	166	187	186
159	166	167	188	187
160	167	168	189	188
161	169	170	191	190
162	170	171	192	191
163	171	172	193	192
164	172	173	194	193
165	173	174	195	194
166	174	175	196	195
167	175	176	197	196
168	176	177	198	197
169	177	178	199	198
170	178	179	200	199
171	179	180	201	200
172	180	181	202	201
173	181	182	203	202
174	182	183	204	203
175	183	184	205	204
176	184	185	206	205
177	185	186	207	206
178	186	187	208	207
179	187	188	209	208
180	188	189	210	209
181	190	191	212	211
182	191	192	213	212
183	192	193	214	213
184	193	194	215	214
185	194	195	216	215
186	195	196	217	216
187	196	197	218	217
188	197	198	219	218
189	198	199	220	219
190	199	200	221	220
191	200	201	222	221
192	201	202	223	222
193	202	203	224	223
194	203	204	225	224
195	204	205	226	225
196	205	206	227	226
197	206	207	228	227
198	207	208	229	228

199	208	209	230	229
200	209	210	231	230
201	211	212	233	232
202	212	213	234	233
203	213	214	235	234
204	214	215	236	235
205	215	216	237	236
206	216	217	238	237
207	217	218	239	238
208	218	219	240	239
209	219	220	241	240
210	220	221	242	241
211	221	222	243	242
212	222	223	244	243
213	223	224	245	244
214	224	225	246	245
215	225	226	247	246
216	226	227	248	247
217	227	228	249	248
218	228	229	250	249
219	229	230	251	250
220	230	231	252	251
221	232	233	254	253
222	233	234	255	254
223	234	235	256	255
224	235	236	257	256
225	236	237	258	257
226	237	238	259	258
227	238	239	260	259
228	239	240	261	260
229	240	241	262	261
230	241	242	263	262
231	242	243	264	263
232	243	244	265	264
233	244	245	266	265
234	245	246	267	266
235	246	247	268	267
236	247	248	269	268
237	248	249	270	269
238	249	250	271	270
239	250	251	272	271
240	251	252	273	272
241	253	254	275	274
242	254	255	276	275
243	255	256	277	276
244	256	257	278	277
245	257	258	279	278
246	258	259	280	279
247	259	260	281	280
248	260	261	282	281
249	261	262	283	282
250	262	263	284	283
251	263	264	285	284
252	264	265	286	285
253	265	266	287	286
254	266	267	288	287
255	267	268	289	288
256	268	269	290	289
257	269	270	291	290
258	270	271	292	291
259	271	272	293	292
260	272	273	294	293
261	274	275	296	295
262	275	276	297	296
263	276	277	298	297
264	277	278	299	298
265	278	279	300	299
266	279	280	301	300
267	280	281	302	301
268	281	282	303	302

269	282	283	304	303
270	283	284	305	304
271	284	285	306	305
272	285	286	307	306
273	286	287	308	307
274	287	288	309	308
275	288	289	310	309
276	289	290	311	310
277	290	291	312	311
278	291	292	313	312
279	292	293	314	313
280	293	294	315	314
281	295	296	317	316
282	296	297	318	317
283	297	298	319	318
284	298	299	320	319
285	299	300	321	320
286	300	301	322	321
287	301	302	323	322
288	302	303	324	323
289	303	304	325	324
290	304	305	326	325
291	305	306	327	326
292	306	307	328	327
293	307	308	329	328
294	308	309	330	329
295	309	310	331	330
296	310	311	332	331
297	311	312	333	332
298	312	313	334	333
299	313	314	335	334
300	314	315	336	335
301	316	317	338	337
302	317	318	339	338
303	318	319	340	339
304	319	320	341	340
305	320	321	342	341
306	321	322	343	342
307	322	323	344	343
308	323	324	345	344
309	324	325	346	345
310	325	326	347	346
311	326	327	348	347
312	327	328	349	348
313	328	329	350	349
314	329	330	351	350
315	330	331	352	351
316	331	332	353	352
317	332	333	354	353
318	333	334	355	354
319	334	335	356	355
320	335	336	357	356
321	337	338	359	358
322	338	339	360	359
323	339	340	361	360
324	340	341	362	361
325	341	342	363	362
326	342	343	364	363
327	343	344	365	364
328	344	345	366	365
329	345	346	367	366
330	346	347	368	367
331	347	348	369	368
332	348	349	370	369
333	349	350	371	370
334	350	351	372	371
335	351	352	373	372
336	352	353	374	373
337	353	354	375	374
338	354	355	376	375

339	355	356	377	376
340	356	357	378	377
341	358	359	380	379
342	359	360	381	380
343	360	361	382	381
344	361	362	383	382
345	362	363	384	383
346	363	364	385	384
347	364	365	386	385
348	365	366	387	386
349	366	367	388	387
350	367	368	389	388
351	368	369	390	389
352	369	370	391	390
353	370	371	392	391
354	371	372	393	392
355	372	373	394	393
356	373	374	395	394
357	374	375	396	395
358	375	376	397	396
359	376	377	398	397
360	377	378	399	398
361	379	380	401	400
362	380	381	402	401
363	381	382	403	402
364	382	383	404	403
365	383	384	405	404
366	384	385	406	405
367	385	386	407	406
368	386	387	408	407
369	387	388	409	408
370	388	389	410	409
371	389	390	411	410
372	390	391	412	411
373	391	392	413	412
374	392	393	414	413
375	393	394	415	414
376	394	395	416	415
377	395	396	417	416
378	396	397	418	417
379	397	398	419	418
380	398	399	420	419
381	400	401	422	421
382	401	402	423	422
383	402	403	424	423
384	403	404	425	424
385	404	405	426	425
386	405	406	427	426
387	406	407	428	427
388	407	408	429	428
389	408	409	430	429
390	409	410	431	430
391	410	411	432	431
392	411	412	433	432
393	412	413	434	433
394	413	414	435	434
395	414	415	436	435
396	415	416	437	436
397	416	417	438	437
398	417	418	439	438
399	418	419	440	439
400	419	420	441	440

CUTOUTS
THE FOLLOWING ELEMENT NUMBERS ARE CUTOUT

COORDINATES OF THE GLOBAL NODES:

1 0.00000D+00 0.00000D+00

2	0.57150D-02	0.00000D+00
3	0.11430D-01	0.00000D+00
4	0.17145D-01	0.00000D+00
5	0.22860D-01	0.00000D+00
6	0.28575D-01	0.00000D+00
7	0.34290D-01	0.00000D+00
8	0.40005D-01	0.00000D+00
9	0.45720D-01	0.00000D+00
10	0.51435D-01	0.00000D+00
11	0.57150D-01	0.00000D+00
12	0.62865D-01	0.00000D+00
13	0.68580D-01	0.00000D+00
14	0.74295D-01	0.00000D+00
15	0.80010D-01	0.00000D+00
16	0.85725D-01	0.00000D+00
17	0.91440D-01	0.00000D+00
18	0.97155D-01	0.00000D+00
19	0.10287D+00	0.00000D+00
20	0.10858D+00	0.00000D+00
21	0.11430D+00	0.00000D+00
22	0.00000D+00	0.57150D-02
23	0.57150D-02	0.57150D-02
24	0.11430D-01	0.57150D-02
25	0.17145D-01	0.57150D-02
26	0.22860D-01	0.57150D-02
27	0.28575D-01	0.57150D-02
28	0.34290D-01	0.57150D-02
29	0.40005D-01	0.57150D-02
30	0.45720D-01	0.57150D-02
31	0.51435D-01	0.57150D-02
32	0.57150D-01	0.57150D-02
33	0.62865D-01	0.57150D-02
34	0.68580D-01	0.57150D-02
35	0.74295D-01	0.57150D-02
36	0.80010D-01	0.57150D-02
37	0.85725D-01	0.57150D-02
38	0.91440D-01	0.57150D-02
39	0.97155D-01	0.57150D-02
40	0.10287D+00	0.57150D-02
41	0.10858D+00	0.57150D-02
42	0.11430D+00	0.57150D-02
43	0.00000D+00	0.11430D-01
44	0.57150D-02	0.11430D-01
45	0.11430D-01	0.11430D-01
46	0.17145D-01	0.11430D-01
47	0.22860D-01	0.11430D-01
48	0.28575D-01	0.11430D-01
49	0.34290D-01	0.11430D-01
50	0.40005D-01	0.11430D-01
51	0.45720D-01	0.11430D-01
52	0.51435D-01	0.11430D-01
53	0.57150D-01	0.11430D-01
54	0.62865D-01	0.11430D-01
55	0.68580D-01	0.11430D-01
56	0.74295D-01	0.11430D-01
57	0.80010D-01	0.11430D-01
58	0.85725D-01	0.11430D-01
59	0.91440D-01	0.11430D-01
60	0.97155D-01	0.11430D-01
61	0.10287D+00	0.11430D-01
62	0.10858D+00	0.11430D-01
63	0.11430D+00	0.11430D-01
64	0.00000D+00	0.17145D-01
65	0.57150D-02	0.17145D-01
66	0.11430D-01	0.17145D-01
67	0.17145D-01	0.17145D-01
68	0.22860D-01	0.17145D-01
69	0.28575D-01	0.17145D-01
70	0.34290D-01	0.17145D-01
71	0.40005D-01	0.17145D-01

72	0.45720D-01	0.17145D-01
73	0.51435D-01	0.17145D-01
74	0.57150D-01	0.17145D-01
75	0.62865D-01	0.17145D-01
76	0.68580D-01	0.17145D-01
77	0.74295D-01	0.17145D-01
78	0.80010D-01	0.17145D-01
79	0.85725D-01	0.17145D-01
80	0.91440D-01	0.17145D-01
81	0.97155D-01	0.17145D-01
82	0.10287D+00	0.17145D-01
83	0.10858D+00	0.17145D-01
84	0.11430D+00	0.17145D-01
85	0.00000D+00	0.22860D-01
86	0.57150D-02	0.22860D-01
87	0.11430D-01	0.22860D-01
88	0.17145D-01	0.22860D-01
89	0.22860D-01	0.22860D-01
90	0.28575D-01	0.22860D-01
91	0.34290D-01	0.22860D-01
92	0.40005D-01	0.22860D-01
93	0.45720D-01	0.22860D-01
94	0.51435D-01	0.22860D-01
95	0.57150D-01	0.22860D-01
96	0.62865D-01	0.22860D-01
97	0.68580D-01	0.22860D-01
98	0.74295D-01	0.22860D-01
99	0.80010D-01	0.22860D-01
100	0.85725D-01	0.22860D-01
101	0.91440D-01	0.22860D-01
102	0.97155D-01	0.22860D-01
103	0.10287D+00	0.22860D-01
104	0.10858D+00	0.22860D-01
105	0.11430D+00	0.22860D-01
106	0.00000D+00	0.28575D-01
107	0.57150D-02	0.28575D-01
108	0.11430D-01	0.28575D-01
109	0.17145D-01	0.28575D-01
110	0.22860D-01	0.28575D-01
111	0.28575D-01	0.28575D-01
112	0.34290D-01	0.28575D-01
113	0.40005D-01	0.28575D-01
114	0.45720D-01	0.28575D-01
115	0.51435D-01	0.28575D-01
116	0.57150D-01	0.28575D-01
117	0.62865D-01	0.28575D-01
118	0.68580D-01	0.28575D-01
119	0.74295D-01	0.28575D-01
120	0.80010D-01	0.28575D-01
121	0.85725D-01	0.28575D-01
122	0.91440D-01	0.28575D-01
123	0.97155D-01	0.28575D-01
124	0.10287D+00	0.28575D-01
125	0.10858D+00	0.28575D-01
126	0.11430D+00	0.28575D-01
127	0.00000D+00	0.34290D-01
128	0.57150D-02	0.34290D-01
129	0.11430D-01	0.34290D-01
130	0.17145D-01	0.34290D-01
131	0.22860D-01	0.34290D-01
132	0.28575D-01	0.34290D-01
133	0.34290D-01	0.34290D-01
134	0.40005D-01	0.34290D-01
135	0.45720D-01	0.34290D-01
136	0.51435D-01	0.34290D-01
137	0.57150D-01	0.34290D-01
138	0.62865D-01	0.34290D-01
139	0.68580D-01	0.34290D-01
140	0.74295D-01	0.34290D-01
141	0.80010D-01	0.34290D-01

142	0.85725D-01	0.34290D-01
143	0.91440D-01	0.34290D-01
144	0.97155D-01	0.34290D-01
145	0.10287D+00	0.34290D-01
146	0.10858D+00	0.34290D-01
147	0.11430D+00	0.34290D-01
148	0.00000D+00	0.40005D-01
149	0.57150D-02	0.40005D-01
150	0.11430D-01	0.40005D-01
151	0.17145D-01	0.40005D-01
152	0.22860D-01	0.40005D-01
153	0.28575D-01	0.40005D-01
154	0.34290D-01	0.40005D-01
155	0.40005D-01	0.40005D-01
156	0.45720D-01	0.40005D-01
157	0.51435D-01	0.40005D-01
158	0.57150D-01	0.40005D-01
159	0.62865D-01	0.40005D-01
160	0.68580D-01	0.40005D-01
161	0.74295D-01	0.40005D-01
162	0.80010D-01	0.40005D-01
163	0.85725D-01	0.40005D-01
164	0.91440D-01	0.40005D-01
165	0.97155D-01	0.40005D-01
166	0.10287D+00	0.40005D-01
167	0.10858D+00	0.40005D-01
168	0.11430D+00	0.40005D-01
169	0.00000D+00	0.45720D-01
170	0.57150D-02	0.45720D-01
171	0.11430D-01	0.45720D-01
172	0.17145D-01	0.45720D-01
173	0.22860D-01	0.45720D-01
174	0.28575D-01	0.45720D-01
175	0.34290D-01	0.45720D-01
176	0.40005D-01	0.45720D-01
177	0.45720D-01	0.45720D-01
178	0.51435D-01	0.45720D-01
179	0.57150D-01	0.45720D-01
180	0.62865D-01	0.45720D-01
181	0.68580D-01	0.45720D-01
182	0.74295D-01	0.45720D-01
183	0.80010D-01	0.45720D-01
184	0.85725D-01	0.45720D-01
185	0.91440D-01	0.45720D-01
186	0.97155D-01	0.45720D-01
187	0.10287D+00	0.45720D-01
188	0.10858D+00	0.45720D-01
189	0.11430D+00	0.45720D-01
190	0.00000D+00	0.51435D-01
191	0.57150D-02	0.51435D-01
192	0.11430D-01	0.51435D-01
193	0.17145D-01	0.51435D-01
194	0.22860D-01	0.51435D-01
195	0.28575D-01	0.51435D-01
196	0.34290D-01	0.51435D-01
197	0.40005D-01	0.51435D-01
198	0.45720D-01	0.51435D-01
199	0.51435D-01	0.51435D-01
200	0.57150D-01	0.51435D-01
201	0.62865D-01	0.51435D-01
202	0.68580D-01	0.51435D-01
203	0.74295D-01	0.51435D-01
204	0.80010D-01	0.51435D-01
205	0.85725D-01	0.51435D-01
206	0.91440D-01	0.51435D-01
207	0.97155D-01	0.51435D-01
208	0.10287D+00	0.51435D-01
209	0.10858D+00	0.51435D-01
210	0.11430D+00	0.51435D-01
211	0.00000D+00	0.57150D-01

212	0.57150D-02	0.57150D-01
213	0.11430D-01	0.57150D-01
214	0.17145D-01	0.57150D-01
215	0.22860D-01	0.57150D-01
216	0.28575D-01	0.57150D-01
217	0.34290D-01	0.57150D-01
218	0.40005D-01	0.57150D-01
219	0.45720D-01	0.57150D-01
220	0.51435D-01	0.57150D-01
221	0.57150D-01	0.57150D-01
222	0.62865D-01	0.57150D-01
223	0.68580D-01	0.57150D-01
224	0.74295D-01	0.57150D-01
225	0.80010D-01	0.57150D-01
226	0.85725D-01	0.57150D-01
227	0.91440D-01	0.57150D-01
228	0.97155D-01	0.57150D-01
229	0.10287D+00	0.57150D-01
230	0.10858D+00	0.57150D-01
231	0.11430D+00	0.57150D-01
232	0.00000D+00	0.62865D-01
233	0.57150D-02	0.62865D-01
234	0.11430D-01	0.62865D-01
235	0.17145D-01	0.62865D-01
236	0.22860D-01	0.62865D-01
237	0.28575D-01	0.62865D-01
238	0.34290D-01	0.62865D-01
239	0.40005D-01	0.62865D-01
240	0.45720D-01	0.62865D-01
241	0.51435D-01	0.62865D-01
242	0.57150D-01	0.62865D-01
243	0.62865D-01	0.62865D-01
244	0.68580D-01	0.62865D-01
245	0.74295D-01	0.62865D-01
246	0.80010D-01	0.62865D-01
247	0.85725D-01	0.62865D-01
248	0.91440D-01	0.62865D-01
249	0.97155D-01	0.62865D-01
250	0.10287D+00	0.62865D-01
251	0.10858D+00	0.62865D-01
252	0.11430D+00	0.62865D-01
253	0.00000D+00	0.68580D-01
254	0.57150D-02	0.68580D-01
255	0.11430D-01	0.68580D-01
256	0.17145D-01	0.68580D-01
257	0.22860D-01	0.68580D-01
258	0.28575D-01	0.68580D-01
259	0.34290D-01	0.68580D-01
260	0.40005D-01	0.68580D-01
261	0.45720D-01	0.68580D-01
262	0.51435D-01	0.68580D-01
263	0.57150D-01	0.68580D-01
264	0.62865D-01	0.68580D-01
265	0.68580D-01	0.68580D-01
266	0.74295D-01	0.68580D-01
267	0.80010D-01	0.68580D-01
268	0.85725D-01	0.68580D-01
269	0.91440D-01	0.68580D-01
270	0.97155D-01	0.68580D-01
271	0.10287D+00	0.68580D-01
272	0.10858D+00	0.68580D-01
273	0.11430D+00	0.68580D-01
274	0.00000D+00	0.74295D-01
275	0.57150D-02	0.74295D-01
276	0.11430D-01	0.74295D-01
277	0.17145D-01	0.74295D-01
278	0.22860D-01	0.74295D-01
279	0.28575D-01	0.74295D-01
280	0.34290D-01	0.74295D-01
281	0.40005D-01	0.74295D-01

282	0.45720D-01	0.74295D-01
283	0.51435D-01	0.74295D-01
284	0.57150D-01	0.74295D-01
285	0.62865D-01	0.74295D-01
286	0.68580D-01	0.74295D-01
287	0.74295D-01	0.74295D-01
288	0.80010D-01	0.74295D-01
289	0.85725D-01	0.74295D-01
290	0.91440D-01	0.74295D-01
291	0.97155D-01	0.74295D-01
292	0.10287D+00	0.74295D-01
293	0.10858D+00	0.74295D-01
294	0.11430D+00	0.74295D-01
295	0.00000D+00	0.80010D-01
296	0.57150D-02	0.80010D-01
297	0.11430D-01	0.80010D-01
298	0.17145D-01	0.80010D-01
299	0.22860D-01	0.80010D-01
300	0.28575D-01	0.80010D-01
301	0.34290D-01	0.80010D-01
302	0.40005D-01	0.80010D-01
303	0.45720D-01	0.80010D-01
304	0.51435D-01	0.80010D-01
305	0.57150D-01	0.80010D-01
306	0.62865D-01	0.80010D-01
307	0.68580D-01	0.80010D-01
308	0.74295D-01	0.80010D-01
309	0.80010D-01	0.80010D-01
310	0.85725D-01	0.80010D-01
311	0.91440D-01	0.80010D-01
312	0.97155D-01	0.80010D-01
313	0.10287D+00	0.80010D-01
314	0.10858D+00	0.80010D-01
315	0.11430D+00	0.80010D-01
316	0.00000D+00	0.85725D-01
317	0.57150D-02	0.85725D-01
318	0.11430D-01	0.85725D-01
319	0.17145D-01	0.85725D-01
320	0.22860D-01	0.85725D-01
321	0.28575D-01	0.85725D-01
322	0.34290D-01	0.85725D-01
323	0.40005D-01	0.85725D-01
324	0.45720D-01	0.85725D-01
325	0.51435D-01	0.85725D-01
326	0.57150D-01	0.85725D-01
327	0.62865D-01	0.85725D-01
328	0.68580D-01	0.85725D-01
329	0.74295D-01	0.85725D-01
330	0.80010D-01	0.85725D-01
331	0.85725D-01	0.85725D-01
332	0.91440D-01	0.85725D-01
333	0.97155D-01	0.85725D-01
334	0.10287D+00	0.85725D-01
335	0.10858D+00	0.85725D-01
336	0.11430D+00	0.85725D-01
337	0.00000D+00	0.91440D-01
338	0.57150D-02	0.91440D-01
339	0.11430D-01	0.91440D-01
340	0.17145D-01	0.91440D-01
341	0.22860D-01	0.91440D-01
342	0.28575D-01	0.91440D-01
343	0.34290D-01	0.91440D-01
344	0.40005D-01	0.91440D-01
345	0.45720D-01	0.91440D-01
346	0.51435D-01	0.91440D-01
347	0.57150D-01	0.91440D-01
348	0.62865D-01	0.91440D-01
349	0.68580D-01	0.91440D-01
350	0.74295D-01	0.91440D-01
351	0.80010D-01	0.91440D-01

352	0.85725D-01	0.91440D-01
353	0.91440D-01	0.91440D-01
354	0.97155D-01	0.91440D-01
355	0.10287D+00	0.91440D-01
356	0.10858D+00	0.91440D-01
357	0.11430D+00	0.91440D-01
358	0.00000D+00	0.97155D-01
359	0.57150D-02	0.97155D-01
360	0.11430D-01	0.97155D-01
361	0.17145D-01	0.97155D-01
362	0.22860D-01	0.97155D-01
363	0.28575D-01	0.97155D-01
364	0.34290D-01	0.97155D-01
365	0.40005D-01	0.97155D-01
366	0.45720D-01	0.97155D-01
367	0.51435D-01	0.97155D-01
368	0.57150D-01	0.97155D-01
369	0.62865D-01	0.97155D-01
370	0.68580D-01	0.97155D-01
371	0.74295D-01	0.97155D-01
372	0.80010D-01	0.97155D-01
373	0.85725D-01	0.97155D-01
374	0.91440D-01	0.97155D-01
375	0.97155D-01	0.97155D-01
376	0.10287D+00	0.97155D-01
377	0.10858D+00	0.97155D-01
378	0.11430D+00	0.97155D-01
379	0.00000D+00	0.10287D+00
380	0.57150D-02	0.10287D+00
381	0.11430D-01	0.10287D+00
382	0.17145D-01	0.10287D+00
383	0.22860D-01	0.10287D+00
384	0.28575D-01	0.10287D+00
385	0.34290D-01	0.10287D+00
386	0.40005D-01	0.10287D+00
387	0.45720D-01	0.10287D+00
388	0.51435D-01	0.10287D+00
389	0.57150D-01	0.10287D+00
390	0.62865D-01	0.10287D+00
391	0.68580D-01	0.10287D+00
392	0.74295D-01	0.10287D+00
393	0.80010D-01	0.10287D+00
394	0.85725D-01	0.10287D+00
395	0.91440D-01	0.10287D+00
396	0.97155D-01	0.10287D+00
397	0.10287D+00	0.10287D+00
398	0.10858D+00	0.10287D+00
399	0.11430D+00	0.10287D+00
400	0.00000D+00	0.10858D+00
401	0.57150D-02	0.10858D+00
402	0.11430D-01	0.10858D+00
403	0.17145D-01	0.10858D+00
404	0.22860D-01	0.10858D+00
405	0.28575D-01	0.10858D+00
406	0.34290D-01	0.10858D+00
407	0.40005D-01	0.10858D+00
408	0.45720D-01	0.10858D+00
409	0.51435D-01	0.10858D+00
410	0.57150D-01	0.10858D+00
411	0.62865D-01	0.10858D+00
412	0.68580D-01	0.10858D+00
413	0.74295D-01	0.10858D+00
414	0.80010D-01	0.10858D+00
415	0.85725D-01	0.10858D+00
416	0.91440D-01	0.10858D+00
417	0.97155D-01	0.10858D+00
418	0.10287D+00	0.10858D+00
419	0.10858D+00	0.10858D+00
420	0.11430D+00	0.10858D+00
421	0.00000D+00	0.11430D+00

422	0.57150D-02	0.11430D+00
423	0.11430D-01	0.11430D+00
424	0.17145D-01	0.11430D+00
425	0.22860D-01	0.11430D+00
426	0.28575D-01	0.11430D+00
427	0.34290D-01	0.11430D+00
428	0.40005D-01	0.11430D+00
429	0.45720D-01	0.11430D+00
430	0.51435D-01	0.11430D+00
431	0.57150D-01	0.11430D+00
432	0.62865D-01	0.11430D+00
433	0.68580D-01	0.11430D+00
434	0.74295D-01	0.11430D+00
435	0.80010D-01	0.11430D+00
436	0.85725D-01	0.11430D+00
437	0.91440D-01	0.11430D+00
438	0.97155D-01	0.11430D+00
439	0.10287D+00	0.11430D+00
440	0.10858D+00	0.11430D+00
441	0.11430D+00	0.11430D+00

LOAD PARAMETER=1,2,3,4; NORMAL,DEADWT,AXIAL,SHEAR

LOAD PARAMETER = 0 INTENSITY = 0.00000D+00

NUMBER OF NODES WITH IN-PLANE LOADING= 0
NODE NUMBERS:

NANAL(1)=0,1,2 FOR NONLINEAR,LINEAR,EIGENVALUES
NANAL(2)=0,1,2 FOR ARBITRARY LAMINATE,ISOTROPICSYMMETRIC LAMINATE
NANAL(3)=1 FOR VON KARMAN PLATE OR DONNELL SHELL EQNS
NANAL(1)= 1 NANAL(2)= 1 NANAL(3)= 1

THE FOLLOWING PROPERTIES WERE INPUT (E,NU,THICK)
0.1140000000000D+12
0.3300000000000D+00
0.1016000000000D-02

INITIAL CONDITION INFORMATION :
IREST = 0 INDIS = 0 INVEL = 0

HALF BAND WIDTH OF GLOBAL STIFFNESS MATRIX - 161

NCOUNT = 1

ELASTIC SOLUTION AT TTIME = 0.0 DUE TO INITIAL CONDITIONS, IF THERE IS ANY

NCOUNT = 2

NCON= 0 RATIO= 0.000000D+00 RINIT= 0.674297D-09 RCURR= 0.674297D-09
NCON= 1 RATIO= 0.241383D-11 RINIT= 0.674297D-09 RCURR= 0.674297D-09

RESULTS OF LINEAR ANALYSIS
INCREMENT NUMBER = 2 ITERATION = 2

NODE	U	V	W	W-X	W-S	PSI-X	PSI-S
231	0.00000D+00	0.00000D+00	0.12970D-09	0.13365D-07	0.37210D-21	-0.13395D-07	-0.37962D-21
231	0.00000D+00	0.00000D+00	0.14448D-08	0.25340D-06	0.14580D-20	-0.25448D-06	-0.15539D-20
231	0.00000D+00	0.00000D+00	0.46869D-08	0.14276D-05	0.70520D-20	-0.14339D-05	-0.72122D-20
231	0.00000D+00	0.00000D+00	-0.27170D-08	0.32087D-05	0.45754D-19	-0.32188D-05	-0.43758D-19
231	0.00000D+00	0.00000D+00	-0.58616D-07	0.10586D-05	0.11554D-18	-0.10454D-05	-0.10366D-18
231	0.00000D+00	0.00000D+00	-0.19310D-06	-0.10102D-04	0.37114D-18	0.10169D-04	-0.33799D-18
231	0.00000D+00	0.00000D+00	-0.38936D-06	-0.28266D-04	0.29302D-18	0.28372D-04	-0.22445D-18
231	0.00000D+00	0.00000D+00	-0.62214D-06	-0.50200D-04	0.12481D-17	0.50334D-04	-0.11685D-17
231	0.00000D+00	0.00000D+00	-0.88050D-06	-0.76981D-04	0.76178D-18	0.77182D-04	-0.66620D-18
231	0.00000D+00	0.00000D+00	-0.11116D-05	-0.10575D-03	-0.52134D-17	0.10604D-03	0.52901D-17
231	0.00000D+00	0.00000D+00	-0.12247D-05	-0.13122D-03	-0.58994D-17	0.13158D-03	0.60171D-17
231	0.00000D+00	0.00000D+00	-0.11622D-05	-0.15101D-03	-0.54915D-17	0.15134D-03	0.55982D-17
231	0.00000D+00	0.00000D+00	-0.93805D-06	-0.16582D-03	-0.92965D-17	0.16609D-03	0.93867D-17
231	0.00000D+00	0.00000D+00	-0.59729D-06	-0.18036D-03	-0.64632D-17	0.18062D-03	0.65180D-17
231	0.00000D+00	0.00000D+00	-0.14229D-06	-0.19472D-03	-0.12484D-16	0.19496D-03	0.12498D-16
231	0.00000D+00	0.00000D+00	0.44483D-06	-0.20409D-03	-0.27330D-16	0.20428D-03	0.27207D-16
231	0.00000D+00	0.00000D+00	0.11534D-05	-0.20628D-03	-0.26991D-16	0.20638D-03	0.26851D-16
231	0.00000D+00	0.00000D+00	0.19489D-05	-0.20309D-03	-0.31413D-16	0.20305D-03	0.31146D-16
231	0.00000D+00	0.00000D+00	0.28005D-05	-0.19716D-03	-0.50544D-16	0.19705D-03	0.49946D-16
231	0.00000D+00	0.00000D+00	0.37145D-05	-0.18583D-03	-0.67842D-16	0.18565D-03	0.67089D-16
231	0.00000D+00	0.00000D+00	0.46858D-05	-0.16796D-03	-0.10018D-15	0.16765D-03	0.99813D-16
231	0.00000D+00	0.00000D+00	0.56729D-05	-0.14518D-03	-0.16351D-15	0.14477D-03	0.16203D-15
231	0.00000D+00	0.00000D+00	0.66412D-05	-0.11654D-03	-0.27716D-15	0.11604D-03	0.27542D-15
231	0.00000D+00	0.00000D+00	0.75311D-05	-0.83442D-04	-0.32596D-15	0.82812D-04	0.32368D-15
231	0.00000D+00	0.00000D+00	0.82543D-05	-0.49927D-04	-0.32413D-15	0.49254D-04	0.32251D-15
231	0.00000D+00	0.00000D+00	0.87584D-05	-0.19224D-04	-0.44554D-15	0.18548D-04	0.44332D-15
231	0.00000D+00	0.00000D+00	0.90313D-05	0.67223D-05	-0.47207D-15	-0.73716D-05	0.46985D-15
231	0.00000D+00	0.00000D+00	0.91019D-05	0.27755D-04	-0.43894D-15	-0.28268D-04	0.43716D-15
231	0.00000D+00	0.00000D+00	0.90528D-05	0.47196D-04	-0.53439D-15	-0.47551D-04	0.53266D-15
231	0.00000D+00	0.00000D+00	0.89708D-05	0.69104D-04	-0.50074D-15	-0.69324D-04	0.49736D-15
231	0.00000D+00	0.00000D+00	0.89199D-05	0.97348D-04	-0.44620D-15	-0.97444D-04	0.44450D-15
231	0.00000D+00	0.00000D+00	0.89370D-05	0.13319D-03	-0.56032D-15	-0.13319D-03	0.55827D-15
231	0.00000D+00	0.00000D+00	0.90160D-05	0.17335D-03	-0.75170D-15	-0.17326D-03	0.74600D-15
231	0.00000D+00	0.00000D+00	0.91370D-05	0.21455D-03	-0.86712D-15	-0.21432D-03	0.86113D-15
231	0.00000D+00	0.00000D+00	0.93198D-05	0.25547D-03	-0.73754D-15	-0.25508D-03	0.73323D-15
231	0.00000D+00	0.00000D+00	0.96187D-05	0.29576D-03	-0.54334D-15	-0.29525D-03	0.53906D-15
231	0.00000D+00	0.00000D+00	0.10084D-04	0.33647D-03	-0.45343D-15	-0.33587D-03	0.44908D-15
231	0.00000D+00	0.00000D+00	0.10748D-04	0.37973D-03	-0.33323D-15	-0.37909D-03	0.32917D-15
231	0.00000D+00	0.00000D+00	0.11616D-04	0.42518D-03	-0.10089D-15	-0.42449D-03	0.96426D-16
231	0.00000D+00	0.00000D+00	0.12702D-04	0.47529D-03	0.16127D-15	-0.47457D-03	-0.16505D-15
231	0.00000D+00	0.00000D+00	0.13984D-04	0.52874D-03	0.77720D-15	-0.52813D-03	-0.77709D-15
231	0.00000D+00	0.00000D+00	0.15341D-04	0.57503D-03	0.16342D-14	-0.57449D-03	-0.16309D-14
231	0.00000D+00	0.00000D+00	0.16675D-04	0.60956D-03	0.20118D-14	-0.60906D-03	-0.20065D-14
231	0.00000D+00	0.00000D+00	0.17958D-04	0.63309D-03	0.23283D-14	-0.63259D-03	-0.23244D-14
231	0.00000D+00	0.00000D+00	0.19192D-04	0.64582D-03	0.30155D-14	-0.64534D-03	-0.30085D-14
231	0.00000D+00	0.00000D+00	0.20373D-04	0.64836D-03	0.34048D-14	-0.64797D-03	-0.33972D-14
231	0.00000D+00	0.00000D+00	0.21473D-04	0.64094D-03	0.36720D-14	-0.64064D-03	-0.36629D-14

ELEMENT 200

Z-COORD	X-COORD	S-COORD	SIGMA11	SIGMA22	SIGMA12	SIGMA23	SIGMA13
0.5080E-03	0.1139E+00	0.5675E-01	0.4297E+02	0.2840E+02	-0.2747E+01	0.0000E+00	0.0000E+00
0.5080E-03	0.1139E+00	0.5675E-01	0.3400E+03	0.1760E+03	-0.3411E+02	0.0000E+00	0.0000E+00
0.5080E-03	0.1139E+00	0.5675E-01	0.3635E+03	-0.2632E+03	-0.1150E+03	0.0000E+00	0.0000E+00
0.5080E-03	0.1139E+00	0.5675E-01	-0.2805E+04	-0.4302E+04	0.1011E+01	0.0000E+00	0.0000E+00
0.5080E-03	0.1139E+00	0.5675E-01	-0.9530E+04	-0.1305E+05	0.7810E+03	0.0000E+00	0.0000E+00
0.5080E-03	0.1139E+00	0.5675E-01	-0.1333E+05	-0.1916E+05	0.1913E+04	0.0000E+00	0.0000E+00
0.5080E-03	0.1139E+00	0.5675E-01	-0.1416E+05	-0.1710E+05	0.2541E+04	0.0000E+00	0.0000E+00
0.5080E-03	0.1139E+00	0.5675E-01	-0.1774E+05	-0.1659E+05	0.3108E+04	0.0000E+00	0.0000E+00
0.5080E-03	0.1139E+00	0.5675E-01	-0.2192E+05	-0.3307E+05	0.4618E+04	0.0000E+00	0.0000E+00
0.5080E-03	0.1139E+00	0.5675E-01	-0.2864E+05	-0.6449E+05	0.6911E+04	0.0000E+00	0.0000E+00
0.5080E-03	0.1139E+00	0.5675E-01	-0.3410E+05	-0.7203E+05	0.8421E+04	0.0000E+00	0.0000E+00
0.5080E-03	0.1139E+00	0.5675E-01	-0.2951E+05	-0.2367E+05	0.7543E+04	0.0000E+00	0.0000E+00
0.5080E-03	0.1139E+00	0.5675E-01	-0.2560E+05	0.5029E+05	0.6020E+04	0.0000E+00	0.0000E+00
0.5080E-03	0.1139E+00	0.5675E-01	-0.2334E+05	0.1258E+06	0.5610E+04	0.0000E+00	0.0000E+00
0.5080E-03	0.1139E+00	0.5675E-01	-0.1571E+05	0.2247E+06	0.4517E+04	0.0000E+00	0.0000E+00
0.5080E-03	0.1139E+00	0.5675E-01	-0.5747E+04	0.3409E+06	0.2492E+04	0.0000E+00	0.0000E+00
0.5080E-03	0.1139E+00	0.5675E-01	0.5001E+04	0.4486E+06	0.7324E+02	0.0000E+00	0.0000E+00
0.5080E-03	0.1139E+00	0.5675E-01	0.1617E+05	0.5437E+06	-0.2831E+04	0.0000E+00	0.0000E+00
0.5080E-03	0.1139E+00	0.5675E-01	0.2800E+05	0.6218E+06	-0.4857E+04	0.0000E+00	0.0000E+00
0.5080E-03	0.1139E+00	0.5675E-01	0.3718E+05	0.6956E+06	-0.6760E+04	0.0000E+00	0.0000E+00
0.5080E-03	0.1139E+00	0.5675E-01	0.4949E+05	0.7799E+06	-0.9850E+04	0.0000E+00	0.0000E+00
0.5080E-03	0.1139E+00	0.5675E-01	0.6147E+05	0.8498E+06	-0.1234E+05	0.0000E+00	0.0000E+00
0.5080E-03	0.1139E+00	0.5675E-01	0.7105E+05	0.9060E+06	-0.1477E+05	0.0000E+00	0.0000E+00
0.5080E-03	0.1139E+00	0.5675E-01	0.8220E+05	0.9413E+06	-0.1788E+05	0.0000E+00	0.0000E+00
0.5080E-03	0.1139E+00	0.5675E-01	0.8381E+05	0.9044E+06	-0.1877E+05	0.0000E+00	0.0000E+00
0.5080E-03	0.1139E+00	0.5675E-01	0.8103E+05	0.7993E+06	-0.1829E+05	0.0000E+00	0.0000E+00
0.5080E-03	0.1139E+00	0.5675E-01	0.7451E+05	0.6358E+06	-0.1690E+05	0.0000E+00	0.0000E+00
0.5080E-03	0.1139E+00	0.5675E-01	0.5973E+05	0.4149E+06	-0.1308E+05	0.0000E+00	0.0000E+00
0.5080E-03	0.1139E+00	0.5675E-01	0.4304E+05	0.1809E+06	-0.8904E+04	0.0000E+00	0.0000E+00
0.5080E-03	0.1139E+00	0.5675E-01	0.2928E+05	-0.4645E+05	-0.5415E+04	0.0000E+00	0.0000E+00
0.5080E-03	0.1139E+00	0.5675E-01	0.1447E+05	-0.2768E+06	-0.1951E+04	0.0000E+00	0.0000E+00
0.5080E-03	0.1139E+00	0.5675E-01	-0.1902E+04	-0.5012E+06	0.1129E+04	0.0000E+00	0.0000E+00
0.5080E-03	0.1139E+00	0.5675E-01	-0.1569E+05	-0.7172E+06	0.3666E+04	0.0000E+00	0.0000E+00
0.5080E-03	0.1139E+00	0.5675E-01	-0.3438E+05	-0.9550E+06	0.7567E+04	0.0000E+00	0.0000E+00
0.5080E-03	0.1139E+00	0.5675E-01	-0.5574E+05	-0.1202E+07	0.1228E+05	0.0000E+00	0.0000E+00
0.5080E-03	0.1139E+00	0.5675E-01	-0.7193E+05	-0.1407E+07	0.1586E+05	0.0000E+00	0.0000E+00
0.5080E-03	0.1139E+00	0.5675E-01	-0.8169E+05	-0.1558E+07	0.1842E+05	0.0000E+00	0.0000E+00
0.5080E-03	0.1139E+00	0.5675E-01	-0.8809E+05	-0.1651E+07	0.1941E+05	0.0000E+00	0.0000E+00
0.5080E-03	0.1139E+00	0.5675E-01	-0.9367E+05	-0.1706E+07	0.2089E+05	0.0000E+00	0.0000E+00
0.5080E-03	0.1139E+00	0.5675E-01	-0.9887E+05	-0.1715E+07	0.2192E+05	0.0000E+00	0.0000E+00
0.5080E-03	0.1139E+00	0.5675E-01	-0.9733E+05	-0.1641E+07	0.1976E+05	0.0000E+00	0.0000E+00
0.5080E-03	0.1139E+00	0.5675E-01	-0.9009E+05	-0.1519E+07	0.1756E+05	0.0000E+00	0.0000E+00
0.5080E-03	0.1139E+00	0.5675E-01	-0.8620E+05	-0.1390E+07	0.1660E+05	0.0000E+00	0.0000E+00
0.5080E-03	0.1139E+00	0.5675E-01	-0.8548E+05	-0.1250E+07	0.1636E+05	0.0000E+00	0.0000E+00
0.5080E-03	0.1139E+00	0.5675E-01	-0.8087E+05	-0.1072E+07	0.1544E+05	0.0000E+00	0.0000E+00
0.5080E-03	0.1139E+00	0.5675E-01	-0.6957E+05	-0.8399E+06	0.1281E+05	0.0000E+00	0.0000E+00
0.5080E-03	0.1139E+00	0.5675E-01	-0.5583E+05	-0.5810E+06	0.9962E+04	0.0000E+00	0.0000E+00
0.5080E-03	0.1139E+00	0.5675E-01	-0.4526E+05	-0.3133E+06	0.7597E+04	0.0000E+00	0.0000E+00
0.5080E-03	0.1139E+00	0.5675E-01	-0.3632E+05	-0.2284E+05	0.5099E+04	0.0000E+00	0.0000E+00
0.5080E-03	0.1139E+00	0.5675E-01	-0.1889E+05	0.3048E+06	0.1261E+04	0.0000E+00	0.0000E+00
0.5080E-03	0.1139E+00	0.5675E-01	-0.3421E+04	0.6238E+06	-0.1496E+04	0.0000E+00	0.0000E+00

1. Morrissey, R.J., McDowell, D.L., Nicholas, T. Frequency and Stress Ratio Effects in HCF of Ti-6AL-4V. *International Journal of Fatigue*. 21: 679-685, 1999.

2. Shigley and Mischke. *Mechanical Engineering Design*. McGraw-Hill. 1989.

3. Larsen, J.M., Worth, B.D. Annis, C.G. Jr., Hoake, F.K. An Assessment of the Role of Near-Threshold Crack Growth in High Cycle Fatigue: Life Prediction of Aerospace Titanium Alloys Under Turbine Engine Spectra. *International Journal of Fracture*. 80:237-255, 1996.

4. Shen, H. Reliabilty Assessment of High Cycle Fatigue Design of Gas Turbine Blades Using the Probabilistic Goodman Diagram. *International Journal of Fatigue*. 21:699-708, 1999.

5. McDowell, D.L. Basic Issues in the Mechanics of Metal High Cycle Fatigue. *International Journal of Fracture*. 80:103-145, 1996.

6. Cowles, B.A. High Cycle Fatigue in Aircraft Gas Turbines – An Industry Perspective. *International Journal of Fracture*. 80:147-163, 1996.

7. Nicholas, T. and Zuiker, J,R. On the Use of the Goodman Diagram for High Cycle Fatigue Design. *International Journal of Fracture*. 80:219-235, 1996.

8. Ritchie, R.O., Boyce, B.L., Campbell, J.P., Roder, O., Thompson, A.W., and Milligan, W.W. Thresholds for High Cycle Fatigue in a Turbine Engine Ti-6AL-4V Alloy. *International Journal of Fatigue*. 21:653-662, 1999.

9. Sadeghi, M. and Liu, F. Computation of Mistuning Effects on Cascade Flutter. *AIAA Journal*. 39:22-28, 2001.

10. McDowell, D.L. Foreword: Re-Visiting the Mechanics of High Cycle Fatigue. *International Journal of Fracture*. 80:101-102, 1996.

11. Ravichandran, K.S. Near Threshold Fatigue Crack Growth Behavior of a Titanium alloy: Ti-6Al-4V. *Acta Metall. Mater*. 39:401-410, 1991.

12. Saada, A.S. *Elasticity, Theory and Applications*. Krieger Publishing Company, Malabar, Florida, USA, 1993.

13. Timoshenko, S. and Woinowsky-Krieger, S. *Theory of Plates and Shells*. McGraw-Hill Book Company, New Yory, New York, USA, 1959.

14. Reddy, J.N. A Refined Nonlinear Theory of Plates with Transverse Shear Deformation. *International Journal of Solids Structures*. 20(9/10):881-896, 1984.

15. Cook, R.D., Malkus, D.S., and Plesha, M.E. *Concepts and Applications of Finite Element Analysis*. John Wiley and Sons, New York, New York, USA, 1989.

16. Panc, V. *Theories of Elastic Plates*. Noordhoff International Publishing, Leyden, The Netherlands, 1975.

17. Zienkiewicz, O.C., Taylor, R.L., and Too, J.M. Reduced Integration Technique in General Analysis of Plates and Shells. *International Journal for Numerical Methods in Engineering*. 3:275-290, 1971.

18. Ashwell, D.G. The Equilibrium Equations of the Inextensional Theory for Thin Flat Plates. *Quarterly Journal Mech. And Applied Math*. 10:169-182, 1957.

19. Mansfield, E.H. The Inextensional Theory for Thin Flat Plates. *Quarterly Journal Mech. And Applied Math*. 8:338-352, 1955.

20. Kui, L.X., Liu, G.Q., and Zienkiewicz, O.C. A Generalized Displacement Method for the Finite Element Analysis of Shells. *Internation Journal for Numerical Methods in Engineering*. 21:2145-2155, 1985.

21. Srinivas, S., Joga Rao, C.V., and Rao, A.K. An Exact Analysis for Vibrations of Simply-Supported Homogeneous and Laminated Thick Rectangular Plates. *Journal of Sound Vibrations*. 12:187-199, 1970.

22. Lo, K.H., Christensen, R.M., and Wu, E.M. A Higher-Order Theory of Plate Deformation Part 1: Homogeneous Plates. *Journal of Applied Mechanics*. 663-668, 1977.

23. Chien, L.S., and Palazotto, A.N. Nonlinear Snapping Considerations for Laminated Cylindrical Panels. *Composites Engineering*. 2(8):631-639, 1992.

24. Gummadi, L.N.B., and Palazotto, A.N. Nonlinear Dynamic Finite Element Analysis of Composite Cylindrical Shells Considering Large Rotations. *AIAA Journal*. 37(11):1489-1494, 1999.

25. Hughes, T.J.R., and Hinton, E. *Finite Element Methods for Plate and Shell Structures Volume 2: Formulations and Algorithms*. Pineridge Press International, Mumbles, Swansea, United Kingdom, 1986.

26. Meroueh, K.A. On a Formulation of a Nonlinear Theory of Plates and Shells with Applications. *Computers and Structures*. 24(5):691-705, 1986.

27. Saigal, S. and Yang, T.Y. Nonlinear Dynamic Analysis with a 48 Degree of Freedom Curved Thin Shell element. *International Journal for Nonlinear Methods in Engineering*. 21:1115-1128, 1985.

28. Stein, M. Nonlinear Theory for Plates and Shells Including the Effects of Transverse Shearing. *AIAA Journal.* 24(9):1537-1544, 1986.

29. Palazotto, A.N. and Dennis, S.T. *Nonlinear Analysis Shell Structures.* AIAA, INC. Washington D.C., USA, 1992.

30. Dennis, S.T. and Palazotto, A.N. Large Displacement and Rotational Formulation for Laminated Shells including Parabolic Transverse Shear. *International Journal of Non-Linear Mechanics.* 25(1): 67-85, 1990.

31. Belytschko, T. and Marchertas, A.H. Nonlinear Finite Element Method for Plates and its Application to Dynamic Response of Reactor Fuel Subassemblies. *Journal of Pressure Vessel Technology.* 251-257, 1974.

32. Clough, W. and Wilson, E.L. Dynamic Finite Elemenmt Analysis of Arbitrary Shells. *Comput. Struct.* 1:33-56, 1971.

33. Katona, M.G. and Zienkiewicz, O.C. A Unified Set of Single-Step Algorithms. Part 3: The Beta-m Method, a Generalization of the Newmark Scheme. *International Journal for Numerical Methods in Engineering.* 21:1345-1359, 1985.

34. Tsai, C.T. and Palazotto, A.N. On the Finite Element Analysis of Non-Linear Vibration for Cylindrical Shells with High-Order Shear Deformation Theory. *International Journal of Nonlinear Mechanics.* 26(1-4):379-388, 1991.

35. Petyt, M. *Introduction to Finite Element Vibration Analysis.* Cambridge University Press, New York, New York, USA, 1990.

36. Leissa, A. *Vibration of Plates.* Acoustical Society of America through the American Institute of Physics, 1993.

37. Bathe, K.J. *Finite Element Procedures.* Prentice-Hall, New Jersey, USA, 1996.

38. Palazotto, A.N., Chien, L.S., and Taylor, W.W. Stability Characteristics of Laminated Cylindrical Panels Under Transverse Loading. *AIAA Journal.* 30(6):1649-1653, 1992.

39. Szilard, R. *Theory and Analysis of Plates. Classical and Numerical Methods.* Prentice-Hall, New Jersey, USA, 1974.

Vita

Lieutenant William "Billy" Shipman graduated from San Angelo Central High School in San Angelo, Texas in May 1993. He entered undergraduate studies at the United States Air Force Academy, Colorado where he graduated with a Bachelor of Science degree in Engineering Mechanics in May 1997. He was then commissioned as a Second Lieutenant in the United States Air Force.

His first assignment was at Kelly AFB as a Program Manager for the F100 engines in August 1997. In May 1998, he switched jobs to become an engineer in support of the F100 engines and the SA-ALC Depot. Billy married his wife in November 1998 in San Antonio Texas. In August 1999, he entered the Graduate School of Engineering and Management, Air Force Institute of Technology. Upon graduation, he will be assigned to the Air Vehicles Directorate, Air Force Research Labs, Wright-Patterson AFB, Ohio.

REPORT DOCUMENTATION PAGE	*Form Approved* *OMB No. 074-0188*

1. REPORT DATE *(DD-MM-YYYY)*
20-03-2001

2. REPORT TYPE
Master's Thesis

3. DATES COVERED *(From – To)*
Oct 1999 – Mar 2001

4. TITLE AND SUBTITLE

THE DEVELOPMENT OF A FINITE ELEMENT PROGRAM TO MODEL HIGH CYCLE FATIGUE IN ISOTROPIC PLATES

5a. CONTRACT NUMBER

5b. GRANT NUMBER

5c. PROGRAM ELEMENT NUMBER

6. AUTHOR(S)

Shipman, William C., 1st Lieutenant, USAF

5d. PROJECT NUMBER

5e. TASK NUMBER

5f. WORK UNIT NUMBER

7. PERFORMING ORGANIZATION NAMES(S) AND ADDRESS(S)

Air Force Institute of Technology
Graduate School of Engineering and Management (AFIT/EN)
2950 P Street, Building 640
WPAFB OH 45433-7765

8. PERFORMING ORGANIZATION REPORT NUMBER

AFIT/GAE/ENY/01M-08

9. SPONSORING/MONITORING AGENCY NAME(S) AND ADDRESS(ES)

Dr M-H. Herman Shen
Ohio State University, Department of Aerospace Engineering and Aviation
328 Bolz Hall
2036 Neil Ave
Columbus, Ohio 43210
(614) 292-2280

10. SPONSOR/MONITOR'S ACRONYM(S)

11. SPONSOR/MONITOR'S REPORT NUMBER(S)

12. DISTRIBUTION/AVAILABILITY STATEMENT

APPROVED FOR PUBLIC RELEASE; DISTRIBUTION UNLIMITED.

13. SUPPLEMENTARY NOTES

14. ABSTRACT

As part of a joint AFRL/DAGSI turbine blade research effort, a computer program has been developed that uses a von Karman large-deflection two-dimensional finite element approximation to determine stress levels and patterns in isotropic thin plates. The dynamic loading of various plates has been carried out in order to model a high cycle fatigue situation. The research considered the various effects of mode shapes, resident frequency, non-linear cyclic effect, endurance limits, and stress variations within a high cycle fatigue environment.

Two main initiatives were taken. First, a transient analysis tool was developed that calculates stress and displacement patterns over a period of time. This analysis also included the effects of damping. The second initiative developed a tool to calculate the eigenvalues (natural frequencies) and eigenvectors of a plate with a given geometry. The results indicated that it is possible to model fatigue at high frequencies using FE analysis and compare these findings with experimentation incorporating a shaker table.

In this research, different geometries of plates were investigated to represent turbine blade configurations. One square plate and three trapezoidal plates were investigated. It was found that a linear relationship could be found between the loading amplitude and the resulting maximum stress. This relationship allows for the prediction of the needed loading amplitude to cause high cycle fatigue. It was also determined that by altering the geometry of the plate, the needed loading frequency or loading amplitude to reach a stress level that would initiate cracks could be minimized.

15. SUBJECT TERMS

Finite Element Analysis, Numerical Analysis, Nonlinear Analysis, Flat Plate Models, Fatigue Life, Fatigue Tests

16. SECURITY CLASSIFICATION OF: a. REPORT	b. ABSTRACT	c. THIS PAGE	17. LIMITATION OF ABSTRACT	18. NUMBER OF PAGES	19a. NAME OF RESPONSIBLE PERSON / 19b. TELEPHONE NUMBER *(Include area code)*
U	U	U	UU	111	Prof A. N. Palazotto, ENY, Anthony.Palazotto@afit.edu (937) 255-3636, ext 4599

Standard Form 298 (Rev. 8-98)
Prescribed by ANSI Std. Z39-18

	Form Approved *OMB No. 074-0188*